

Structural determination of membrane mimics using
small-angle X-ray and neutron scattering

Ryan Chadwick Oliver
Charlotte, North Carolina

B.S. Chemistry, University of N. Carolina at Chapel Hill, 2005
M.S. Chemistry, University of N. Carolina at Charlotte, 2010

A Dissertation presented to the Graduate Faculty
of the University of Virginia in Candidacy for the Degree of
Doctor of Philosophy

Department of Chemistry

University of Virginia
May, 2014

© Copyright by
Ryan Chadwick Oliver
All rights reserved.
May 2014

To my family for their support throughout the years.

Curriculum Vitae

Ryan C. Oliver

University of Virginia
Department of Chemistry

Phone: (704) 776 – 8279
ryan.oliver@virginia.edu

Education

2010-2014 Ph.D., Chemistry, *The University of Virginia*
2007-2010 M.S., Chemistry, *The University of North Carolina at Charlotte*
2001-2005 B.S., Chemistry, *The University of North Carolina at Chapel Hill*

Honors and Awards

2012 12th Annual Robert J. Huskey Research Exhibition Award, *The University of Virginia*
2011 13th Annual National School on Neutron and X-ray Scattering, *Oak Ridge and Argonne National Labs*
2010 NCNR Summer School on Fundamentals of Neutron Scattering, *NIST*
2007-2009 Thomas Walsh Tuition Fellowship, *The University of N. Carolina at Charlotte*
2003-2005 Dreyfus Foundation Scholarship for Excellence in Chemistry, *The University of N. Carolina at Chapel Hill*

Research Experience

Graduate Research Assistant, *The University of Virginia*

Advisor: Linda Columbus

Interests: Bacterial pathogen-host interactions mediated by membrane proteins; protein structural biology; protein folding; protein-ligand binding

Graduate Research Assistant, *The University of N. Carolina at Charlotte*

Advisor: Joanna Krueger

Interests: Calcium-dependent actin binding proteins and filament nucleation; protein structural biology; small angle X-ray and neutron scattering

Undergraduate Research Assistant, *The University of N. Carolina at Chapel Hill*

Advisor: Howard Weinberg, Dept. of Environmental Sciences and Engineering

Interests: Detection and analysis methods for disinfection byproducts from drinking water; mass spectrometry

Teaching Experience

Graduate Teaching Assistant, *The University of Virginia*

Biochemistry Laboratory, 2010-2012

Graduate Teaching Assistant, *The University of N. Carolina at Charlotte*

General Chemistry Laboratory, 2007-2009

Publications

RC Oliver, J Lipfert, DA Fox, RH Lo, S Doniach, L Columbus (2013). Dependence of Micelle Size and Shape on Detergent Alkyl Chain Length and Head group. *PLoS ONE*. 8(5): e62488.

MK Thompson, S Franzen, MF Davis, RC Oliver, JK Krueger (2011). Dehaloperoxidase-Hemoglobin from Amphitrite ornata is Primarily a Monomer in Solution. *J. Phys. Chem. B.* 115: 4266-4272.

Selected Talks

RC Oliver. (2013) Modulating the physical properties of micelles for membrane protein investigations. 57th Annual Biophysical Society Meeting. Philadelphia, PA.

RC Oliver, L Columbus. (2012) From model membranes to pathogenesis: Investigations of membrane protein structure and dynamics. UNC-Charlotte visit. Charlotte, NC.

RC Oliver. (2012) Detergent micelles as membrane mimics: Implications for membrane protein structure and dynamics. Southeast Regional ACS Meeting. Raleigh, NC.

Selected Posters

RC Oliver, J. Lipfert, J. Kim, L. Columbus. (2013) Modulating the Physical Properties of Micelles Using Binary Detergent Mixtures for Future Membrane Protein Investigations. *Chemistry Department 3rd Year Grad Student Poster Session* poster, Charlottesville, VA.

RC Oliver, J. Lipfert, J. Kim, L. Columbus. (2013) Modulating the Physical Properties of Micelles Using Binary Detergent Mixtures for Future Membrane Protein Investigations. *Huskey Graduate Research Exhibition* poster, Charlottesville, VA.

RC Oliver, D. Fox, R. Lo, J. Lipfert, and L. Columbus. (2012) Modulating the Physical Properties of Micelles Using Binary Detergent Mixtures for Future Membrane Protein Investigations. *FASEB:SRC Meeting* poster, Snowmass, CO.

RC Oliver, D. Fox, R. Lo, J. Lipfert, and L. Columbus. (2012) Investigating the Relationship Between Physical Properties of Detergents and Membrane Protein Structure Determination. *Huskey Graduate Research Exhibition* poster, Charlottesville, VA.

RC Oliver, R. Lo, J. Kim, and L. Columbus. (2011) Investigating the Relationship Between Physical Properties of Detergents and Membrane Protein Structure Determination. *Biophysical Society Meeting* poster, Baltimore, MD.

Abstract

The challenge of finding a suitable membrane mimic that produces a stable and functionally active membrane protein is one of the primary obstacles faced in membrane protein investigations. Not only is there a lack of understanding about the properties of the surrounding environment that produce such a stable complex, but many physical properties, such as size and shape, of the membrane mimics themselves remain uncharacterized. This dissertation presents the determination of such physical properties from small-angle scattering detergent-based membrane mimics to serve as a baseline for investigating how certain factors of the membrane mimic might influence membrane protein stability. First, the dependence of micelle size and shape on detergent monomer structure, such as head group chemistry and alkyl chain length, was determined using systematic variations in detergent structures and measuring properties of the resulting micelles formed. Next, detergent mixtures were investigated to determine the dependence of mixed micelle properties on detergent composition. Finally, aggregate structures of lipid-detergent mixtures expected to form bicelles were characterized in the detergent-rich regime. Contrast variation experiments performed on aggregates formed by these mixtures are expected to reveal internal organization and distribution of lipid and detergent molecules between the bicelle core and rim regions.

Table of Contents

Copyright page.....	I
Dedication.....	II
Curriculum Vitae	III
Abstract.....	V
Table of Contents.....	VI
List of Figures.....	X
List of Tables	XIII
Acknowledgements.....	XIV
Chapter 1: Membrane proteins and their environment.....	1
1.1 The native membrane	5
1.2 Membrane proteins.....	14
1.3 Membrane protein solubilization and stabilization	21
1.4 Applications of membrane mimics	25
1.4.1 Commonly used detergents in membrane protein studies	26
1.4.2 Bicelles.....	31
1.4.3 Nanodiscs.....	33
1.4.4 Liposomes.....	34
1.5 Summary and outline of dissertation	34
1.6 References.....	35
Chapter 2: Small-angle scattering.....	43
2.1 Theory and principles of SAS.....	45

2.1.1	Small-angle X-ray scattering	53
2.1.2	Small-angle neutron scattering	56
2.1.3	Sample requirements and instrument setup	59
2.2	Applications and experimental approaches.....	62
2.2.1	Zero-angle scattering and Guinier analysis.....	62
2.2.2	Form-factor models.....	63
2.2.3	Contrast variation experiments using SANS	66
2.3	Scattering and detergent micelles.....	67
2.3.1	Micelle aggregation numbers.....	67
2.3.2	Micelle core-shell models.....	68
2.3.3	Micelle hydrophobic core thicknesses	71
2.4	Scattering and protein-detergent complexes	71
2.5	References.....	73
Chapter 3:	Physical determinants of micelle assembly	80
3.1	Overview	80
3.2	Introduction.....	81
3.2.1	Detergent monomer properties	82
3.2.2	Micelle self-assembly	87
3.2.3	Implications for protein-detergent complexes	87
3.3	Results and discussion	88
3.3.1	Validation of core-shell model approach.....	88
3.3.2	Effects of alkyl chain length	90
3.3.3	Effects of head group steric bulk or electrostatics	95

3.3.4	Dependence of head group packing	96
3.4	Concluding remarks	97
3.5	Materials and methods	97
3.5.1	Preparation of detergent micelles.....	98
3.5.2	Micelle size and shape by SAXS	98
3.5.3	Core-shell model fitting	99
3.6	References	99
Chapter 4: Manipulating micelle dimensions and properties with detergent mixtures		
.....		106
4.1	Overview	106
4.2	Introduction.....	107
4.2.1	Solutions of mixed detergents.....	109
4.2.2	Mixed micelle size and shape	112
4.2.3	Surface potential	115
4.3	Results and discussion	116
4.3.1	Ideal mixing of detergents	116
4.3.2	Modulating micelle size.....	120
4.3.3	Modulating micelle shape.....	128
4.3.4	Modulating micelle surface properties.....	129
4.4	Concluding remarks	131
4.5	Materials and methods	134
4.5.1	Sample preparation	134
4.5.2	Critical micelle concentrations of mixed micelles.....	135

4.5.3 SAXS data collection and core-shell model fits	136
4.6 References	137
Chapter 5: Contrast variation studies of bicelle organization	141
5.1 Overview	141
5.2 Introduction	144
5.2.1 The ideal bicelle model	144
5.2.2 Scattering studies of lipid-detergent mixtures	146
5.2.3 Evidence of internal bicelle organization	146
5.3 Results and discussion	147
5.3.1 X-ray scattering of DMPC and DHPC mixtures.....	147
5.3.2 Comparison of lipid:detergent composition.....	153
5.3.3 Effects of temperature	159
5.3.4 Effects of concentration	163
5.4 Concluding remarks and future directions	167
5.5 Materials and methods	169
5.5.1 Sample preparation	169
5.5.2 SAXS data collection	170
5.5.3 SANS data collection	170
5.5.4 Contrast variation experiments	171
5.6 References	171
Appendix I	175

List of Figures

Chapter 1

1.1	Comparison of progress in soluble vs. membrane protein structure determination	3
1.2	Fluid mosaic model for biological membranes.....	8
1.3	Chemical structures of common membrane lipids.....	11
1.4	Examples of membrane proteins with α - or β - transmembrane domains ..	17
1.5	Functional roles of membrane proteins.....	19
1.6	General scheme for detergent-mediated solubilization of membrane proteins.....	24
1.7	Schematic of bicelle cross-section formed at intermediate lipid:detergent ratios.....	32

Chapter 2

2.1	Small-angle scattering experiment setup	47
2.2	Observed scattering is the result of constructive interference	49
2.3	Data reduction and buffer subtraction.....	51
2.4	Regions of scattering profiles used for different analysis approaches.....	55
2.5	Comparison of benchtop and synchrotron SAXS data	61
2.6	Expected scattering profiles and corresponding distance distributions for various geometric model form factors	65
2.7	Examples of core-shell geometric models and simulated SAXS profiles ..	70

Chapter 3

3.1	Chemical structures of detergents investigated by SAXS	86
-----	--	----

3.2	Correlation plots of model dependent vs. independent parameters	89
3.3	Dependence of aggregation number and micelle thickness on alkyl chain length.....	91
Chapter 4		
4.1	Ideal mixing for binary combinations of micelle-forming detergents	111
4.2	CMC of detergent mixtures measured by ITC.....	118
4.3	Scattering of mixed micelles versus individual and sum components	119
4.4	Model-independent micelle thicknesses from maltoside mixtures.....	121
4.5	Model-independent micelle thicknesses from mixtures of maltosides, phosphocholines, and LMPG.....	122
4.6	Model-dependent measurements of micelle size and shape from mixtures of maltosides with FC12	124
4.7	Aggregation numbers for detergent mixtures	126
4.8	Dependence of mixed micelle R_g on mole fraction of detergent in a binary mixed micelle.....	127
4.9	Modulation of micelle surface potential with binary mixtures.....	130
Chapter 5		
5.1	Comparison of ideal and mixed bicelle models.....	145
5.2	SAXS profiles of mixtures with different ratios of lipid and detergent...	149
5.3	Observed contrast in neutron scattering using deuterated and natural alkyl chain tails with and without lipid-detergent mixing	154
5.4	Contrast variation series for DMPC-D54:DHPC bicelles at $Q = 0.7$ or $Q = 0.3$ and 6% w/v at 25°C	155

- 5.5 Contrast variation data for bicelles at increased temperature (40°C)161
- 5.6 Contrast variation data for bicelles at dilute concentration (1.5% w/v) ..165

List of Tables

Chapter 1		
1.1	Examples of common detergents used in membrane protein studies	27
Chapter 2		
2.1	Neutron and X-ray scattering lengths for common elements in biological studies	58
Chapter 3		
3.1	Physical properties of pure detergents	84
3.2	SAXS-determined parameters of detergent micelle size and shape	92-93
Chapter 4		
4.1	Properties of detergents used to form mixed micelles	108
Chapter 5		
5.1	Physical properties of amphiphiles used to prepare bicelles for scattering experiments	143
5.2	Radii of gyration and dominant lengths of separation (thicknesses) for bicelles at different mole ratios of lipid:detergent from Guinier analysis of SAXS profiles	151
5.3	Measured $I(0)$ and R_g from Guinier analysis of contrast series data (6% w/v and 25°C)	157
5.4	Measured $I(0)$ and R_g from Guinier analysis of contrast series data at increased temperature (40°C)	162
5.5	Measured $I(0)$ and R_g from Guinier analysis of contrast series data at dilute conditions (1.5 % w/v)	166

Acknowledgements

The research presented herein would not have been possible without the continuous support from many people and institutions. Linda Columbus and members of the Columbus lab deserve recognition for much time and effort assisting in preparing experiments, collecting data, and interpreting results.

A large effort is required to operate and maintain guest user facilities, and as such, the people of Argonne National Laboratory's Advanced Photon Source and Oak Ridge National Laboratory's Center for Neutron Scattering deserve a special recognition for making this work, and others like it, possible. Finally, I would like to acknowledge the National Science Foundation for its financial support in funding this research.

1. Membrane proteins and their environment

“We’re lost, but we’re making great time.”

Proteins are polypeptide chains of amino acids that are involved in essentially every biological process. Each protein is defined by its amino acid sequence, and folds into a three-dimensional structure dependent upon this sequence. The functional role of a protein must be performed by this final folded structure, thus protein function is a result of the protein’s structure. Protein functions commonly require conformational changes, or correlated domain movements within the protein, which can be influenced by neighboring molecules and the surrounding environment. These amplitudes and rates of motion in conformational changes describe the protein dynamics, which along with structure and function, form a trifecta of biophysical knowledge about proteins.

Structural knowledge about proteins has grown exponentially since the publishing of the first high-resolution (2Å), three-dimensional protein structure from myoglobin via X-ray crystallography in 1960 (1). Structures at near-atomic resolution have revealed insights to functional mechanisms that have led to the development of novel pharmaceuticals and antibiotics, and spawned active areas of research. Prior to the availability of this information, chemical compounds were empirically screened for physiological responses and potential uses as treatment. With atomistic details and an understanding of protein structure-function relationships, entire libraries of compounds can be screened *in silico* for potential interactions with a target protein system, which has greatly accelerated modern structure-based drug discovery (2). However, despite a plethora of available structural knowledge, many types and classes of proteins remain

uncharacterized (structurally and/or functionally). These include a variety of bacterial proteins, intrinsically-disordered proteins, and membrane proteins, among others.

Membrane proteins are associated with cellular membranes, poised at interfaces between a cell and its environment or between cellular compartments, and include a variety of known structures and functions. Unfortunately, progress in membrane protein research is hindered by many challenges associated with this surrounding membrane environment as compared to soluble proteins. The significance of these challenges is realized when comparing structural determination progress with that of soluble proteins. The RCSB Protein Data Bank (PDB; <http://www.rcsb.org>), a repository for protein and other biological macromolecular structures, currently contains over 55,000 non-redundant entries (based on 100% sequence similarity) for searchable protein structures (3). However, since the determination of the first membrane protein crystal structure in 1985 of the bacterial photosynthetic reaction center complex (4), only ~285 unique PDB entries for transmembrane proteins have been deposited. A catalog by S. White of protein structures deposited annually by type, soluble or membrane, and adjusted to the first 18 years since the first structure of each type (Figure 1.1a), indicates a significant lag in the growth of deposited membrane protein structures compared to soluble proteins (5). Reassessment in 2013 (Figure 1.1b) revealed further declines in the exponential growth of membrane protein structures as compared to the predicted trend continuing from 2005 (6). Despite all of the technological advances in protein research since 1960, the membrane environment and unique properties of membrane proteins pose persistent hurdles to progress in membrane protein structure determination.

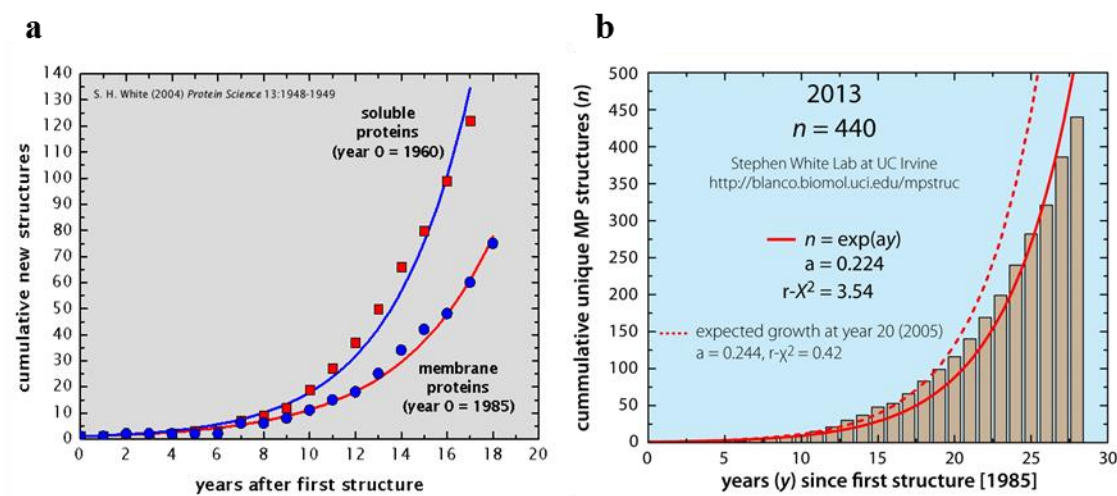


Figure 1.1 Comparison of progress in soluble vs. membrane protein structure determination. *Used with permission from (6).* **a.** This plot provides a comparison between soluble and membrane proteins throughout the first 18 years of progress in structure determination. Cumulative numbers of structures by type (soluble, red squares; membrane, blue circles) are plotted as a function of years since the first structure with lines indicating exponential fits to the data. Membrane protein structure determination progress lags significantly behind that of soluble proteins, and only 2,200 unique membrane protein structures are predicted by 2025. **b.** A similar plot includes progress up to 2013 for membrane protein structure determination with exponential fit indicated by red line. For comparison, a dashed red line indicates the previously measured trend for membrane protein structure determination from 2005 (red line in panel a).

These hurdles exist throughout the characterization of membrane proteins, from initial genesis of the peptide to interpretation of the final data. Since large yields of the protein of interest are generally desired, the protein is typically over-expressed using *E. coli* cells. However, chaperone proteins and machinery which assist in protein folding and insertion into the membrane are maintained at basal levels, thus much of the protein product may aggregate in inclusion bodies. Additionally, the increased concentration of folded protein may lead to destabilization of host membranes, and potential cell toxicity. If sufficient protein is obtained, the next challenge lies in preparing the membrane protein for analysis (structural and/or functional), and often involves stabilization of the protein in a soluble membrane mimic. The presence of these mimics, whose contributions must be evaluated and deviations from native membrane environment considered, form the final obstacle to interpreting results.

This chapter aims to address challenges associated with stabilizing a native membrane protein fold in a suitable mimic of the native membrane for *in vitro* investigations. During membrane protein purification, detergents are typically employed to solubilize membrane fractions and to isolate the protein of interest from other membrane components. Structural and functional knowledge can be gained directly from these protein-detergent complexes (PDCs), or the protein may be transferred to other membrane mimics, such as bicelles, liposomes, or nanodiscs. This initial purification process relies on empirical screening of many detergent conditions for production of a stable PDC. However, a suitable PDC is often not obtained and most conditions lead to protein aggregation and precipitation (as assessed via SDS-PAGE and visual inspection, for example). With specific focus on the potential factors of influence on protein-

detergent complex stability, the aim of this thesis research is to provide rationalization for the detergent selection process and accelerate membrane protein studies.

1.1 The native membrane

Membranes are a fundamental component of all cell-based life, and form semi-permeable, fluid barriers allowing compartmentalization within cells, as well as providing isolation of the cell from the surrounding environment. These barriers define living cells and confine their contents – ions, proteins, and other molecules – to regions where they are needed, preventing them from diffusing away. Membrane proteins comprise an essential part of native membranes, transporting molecules across membranes, among performing other vital cellular roles. This exchange of molecules and information across membranes includes import of nutrients, export of wastes, and initiation of cellular responses to external stimuli.

Cell membrane theory originated from seventeenth century microscopy observations, and has undergone many developments. Plant and animal tissue were generally accepted to be composed of individual cells, but only the barriers (cell walls) from plants were able to be identified surrounding each cell. By the turn of the 20th century, investigations of osmotic properties of cells and selective permeability of molecules and ions across membranes based on hydrophilic/hydrophobic properties led to a hypothesis that these thin semi-permeable barriers around cells had similar properties of oil and were composed of lipids and cholesterol (7, 8). However, the lipid bilayer structure was not proposed until 1925 (9, 10).

Lipids are amphiphilic molecules, and typically contain a hydrophilic, polar “head” group linked to two hydrophobic, nonpolar hydrocarbon “tails”. By comparing surface areas of various cells to the areas formed by monolayers from extracted lipids using a Langmuir film balance, Gorter and Grendel (10) found the monolayer area to be double that of the cell surface area, thus concluding the presence of two layers of lipids per cell. In order to minimize unfavorable interactions between hydrophobic lipid tails and aqueous surroundings, the two layers were proposed to be arranged in an opposing fashion with head groups pointing towards each aqueous surface, referred to as a lipid bilayer (10).

A decade later in 1935, a membrane model was proposed with a layer of globular proteins adsorbed to each lipid bilayer surface by Danielli and Davson (11). According to this model, the membrane possessed both lipophilic and hydrophilic properties with water-containing regions in the membrane allowing ion transport, and lipophilic parts transporting water-insoluble molecules. The late 1950s brought about advances in electron microscopy that allowed direct evidence of membrane structure to be obtained for the first time, and revealed a characteristic membrane thickness of 5-10 nm. In 1960, J. Robertson published a review supporting the models of Gorter and Grendel (10) and Danielli and Davson (11) with electron microscopy evidence from biological membranes of various organelles, establishing the concept of a “unit membrane” to be ubiquitously applied for describing common structure of all cell and organelle membranes (12).

Aforementioned models described proteins as being adsorbed to peripheral membrane surfaces; however increased structural knowledge from X-ray crystallography

and high α -helical content with hydrophobic amino acids observed in proteins near the membrane led Singer and Nicolson to propose that proteins may also span membranes, referred to as integral membrane proteins. Additional observations of lateral fluidity in membrane surfaces from the mixing of two cell populations with different membrane-bound, fluorescent tags (13) led Singer and Nicolson to propose the most recent fluid mosaic model (14). The fluid mosaic model accounts for membrane fluidity, membrane-spanning channels, heterogeneous and asymmetric protein and lipid distributions, and multiple modes of protein/bilayer association. Despite its few shortcomings, this model continues to form the basis for modern views of biological membranes (Figure 1.2).

Additional refinements have been proposed, and continue to address observations from additional biophysical characterizations of biological membranes. For example, the mattress model proposed by Mouritsen and Bloom accounts for hydrophobic mismatches between the protein's transmembrane domain and the bilayer thickness (15). In these cases, the distribution of lipids surrounding the protein may be altered, or aggregation and clustering of similarly mismatched proteins may be caused. Modern views of biological membranes must also account for lipid distributions which may form clusters, domains, or aggregates, and include the phase behavior of lipid and protein components.

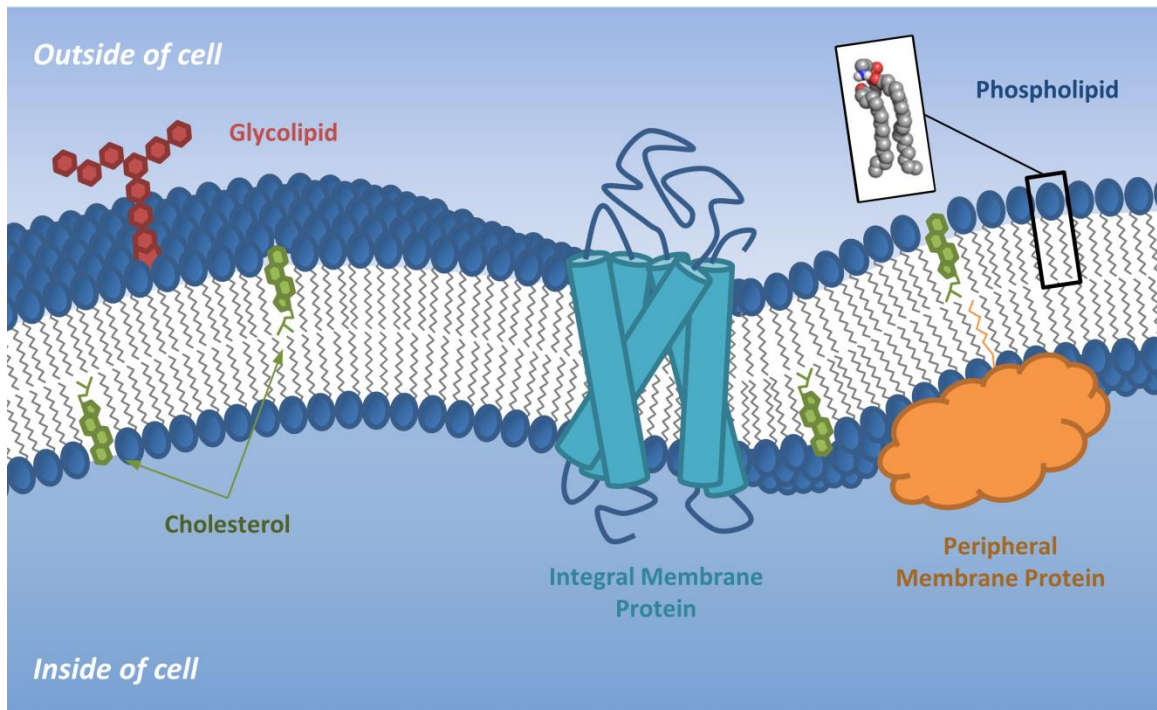


Figure 1.2 Fluid mosaic model for biological membranes. The native membrane is more crowded and complex than represented by the model, and contains a variety of macromolecules embedded in a lipid bilayer. The fluid mosaic model accounts for the presence of integral and peripheral membrane proteins, involved in the formation of ion channels and cytoskeletal anchors. Unfortunately, this model is a static representation, and does not reveal the dynamic and fluid-like motions of membranes, or distributions of lipid domains.

The overall membrane structure and properties, such as impermeability to ions and small molecules, result from the lipid bilayer properties: two opposing layers of lipids arranged with hydrophobic tails in the center sandwiched between hydrophilic head groups at each aqueous surface. Lipid bilayer formation is driven by the hydrophobic effect (16), similar to the coalescence of oil droplets in water and based on the inability of hydrocarbons to form hydrogen bonds with water. More specifically, at such interfaces with dissolved compounds, attractive forces between highly ordered water molecules must be distorted or broken. Although a favorable attraction exists between neighboring dissolved lipid molecules, lipid aggregation is mostly due to minimizing the entropic cost from the rearrangement of water. The lipid molecule has an overall cylindrical geometry (head group surface area to tail volume) that favors a planar bilayer organization. Similar amphiphiles with larger head group surface area to tail volume ratios have a more conical shape, thus have the propensity to form soluble, globular aggregates with highly curved surfaces (*e.g.* micelle-forming detergents).

Membrane lipids encompass three general types: phospholipids, glycolipids, and sterols (Figure 1.3). Phospholipids are the most abundant, and are typically composed of two long fatty acid chains linked via glycerol backbone to a phosphorylated alcohol, such as phosphatidylcholine (PC), phosphatidylethanolamine (PE), phosphatidylglycerol (PG), phosphatidylinositol (PI), and phosphatidylserine (PS) lipids. The lipids in Archaeal membranes are unique and contain ether linkages between the glycerol backbone and fatty acids, as opposed to ester linkages found in other domains of life. The fatty acid at the sn-1 position of the glycerol backbone is a saturated hydrocarbon chain with 16 or 18 carbon atoms, while the fatty acid at the sn-2 position is typically unsaturated containing

at least one *cis* double bond and at least 18 carbon atoms in chain length. Phospholipids may also consist of a sphingosine backbone in place of glycerol, and specifically referred to as sphingolipids to avoid confusion with glycerophospholipids. Sphingolipids contain one saturated fatty acid chain (up to 24 carbon atoms) amide-linked to the amino group of the sphingosine, which is often 2-hydroxylated due to the presence of a second hydrocarbon chain from the sphingosine backbone. The second tail is a hydrocarbon extension of the sphingosine backbone (17).

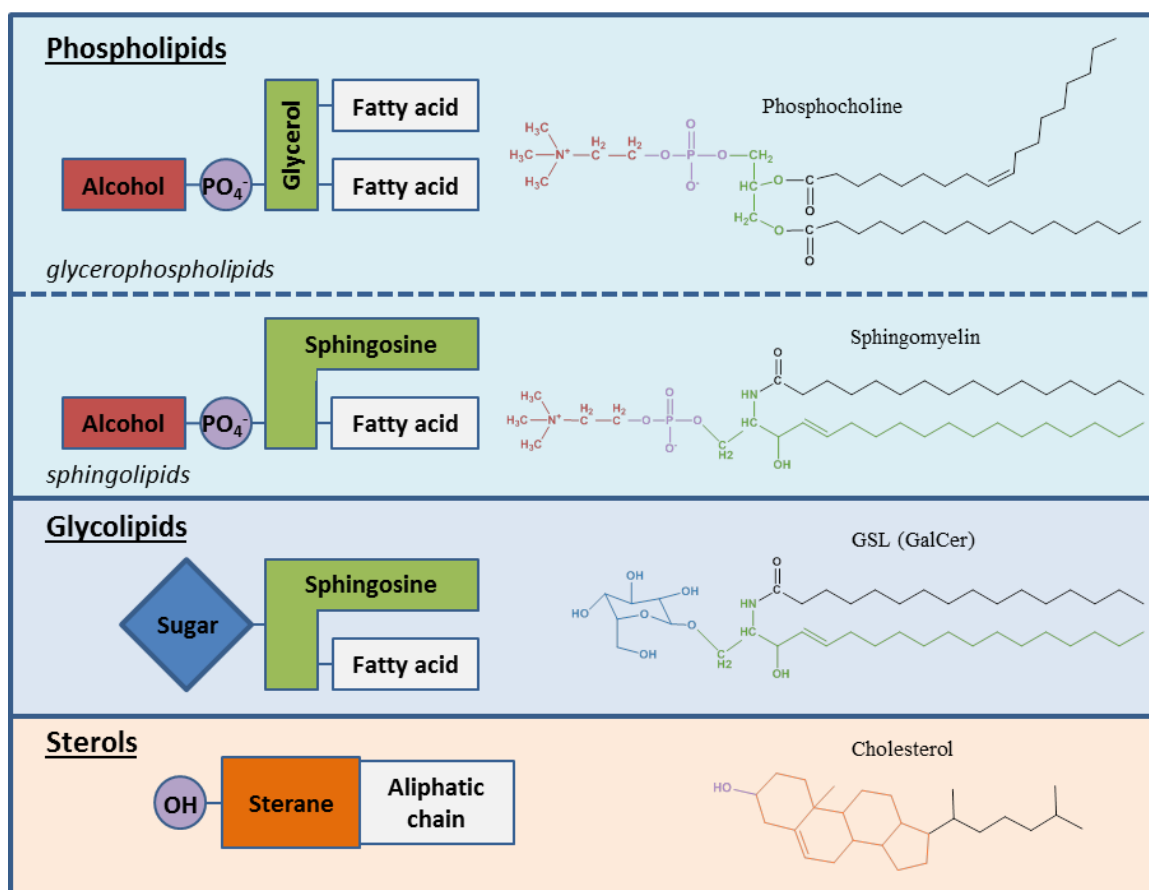


Figure 1.3 Chemical structures of common membrane lipids. Lipids can be categorized as glycerophospholipids, sphingolipids, and sterols, with glycolipid referring to glycosylated lipids or those containing a carbohydrate/polysaccharide chain as the lipid head group. Cartoon assemblies depict the overall organization of the head group and tail structure for each lipid type. Chemical structures of an example glycerophospholipid (16:0 18:1 PC), sphingolipid (sphingomyelin), glycolipid (galactosylceramide, GSL), and sterol (cholesterol) are also provided with components colored to match the corresponding cartoon assembly.

As the name suggests, glycolipids are sugar-containing lipids, with short, branched sugars typically less than 15 units. Examples include cerebroside and gangliosides. The carbohydrate chain most frequently occurs on the exterior surface of the cell membrane, and can be modified by glycosylhydrolase enzymes. These sugar components may act as recognition sites for specific molecules as well as maintaining the stability of the membrane and associating with other cells (18). The fatty acid chains in phospho- and glyco- lipids typically contain even numbers of carbon atom between 14 and 24, with 16 and 18 being the most common. Chains can vary in degree of saturation, but double bonds are nearly always arranged in the *cis* configuration.

Sterols occur in plants, animals, and fungi, and have a structure that is different than most lipids: a steroid alcohol of four linked hydrocarbon rings with a lone hydroxyl head group. The fused ring structure makes the molecule more rigid as compared to other lipids, and contains little hydrophilic character (a lone hydroxyl group). Cholesterol is present in most eukaryotic membranes, and has a significant impact on the rigidity of lipid bilayers. Cholesterol intercalates between lipids and its rigid ring structure decreases the mobility of neighboring lipid tails (19). These hydrophobic interactions decrease lateral lipid diffusion and increase lipid packing efficiency (20). As a consequence, the fluidity and permeability of the membrane is greatly reduced (21, 22). However, the presence of cholesterol also increases fluidity by interfering with close packing of lipid tails, raising their melting temperature and inhibiting transitions to a crystalline (rigid) state (20). Cholesterol has also been implicated in modulating overall membrane curvature (23). Yeast and fungi contain a different sterol, ergosterol, which performs similar functions.

Lipid composition in membranes is highly varied and directly influences bilayer properties. For example, an increase in saturation of lipid fatty acid chains decreases the interactions between neighboring tails, thus making membranes more fluid. Membrane fluidity can also be modulated by changing lipid tail length, as longer tails produce additional interactions between tails and decrease overall fluidity. Other membrane properties, such as bilayer thickness, are simultaneously affected by changes in lipid tail length. Transbilayer diffusion (“flip-flop”) of lipids across the membrane is thermodynamically unfavorable, allowing native membranes to adopt leaflet asymmetry, or different distributions of lipids found in each monolayer (24). These distributions are formed during membrane synthesis and maintained by enzymes that transport lipids between bilayer leaflets, such as flippases, floppases, and scramblases (25).

The inner leaflet of the plasma membrane is enriched in PS, PE and PI lipids, while PC lipids, sphingomyelin, and glycolipids are concentrated in the outer leaflet (26). The PS and PI lipids contain a net negative charge, and their localization to the inner leaflet imparts a negative surface charge on the cytosolic side of the membrane. This inner leaflet must also maintain a different degree of curvature (smaller head group area to tail volume ratio) than the outer leaflet to adopt the final spherical geometry of the cell. The association of peripheral membrane proteins on one side of the membrane and preferred orientations of integral proteins induces an additional asymmetry in the membrane that can be directly related to lipid asymmetry. For example, the negatively charged inner leaflet of lipids provides favorable electrostatic associations for positively charged amino acids in membrane proteins; referred to as the “positive inside” rule, and assists in orienting proteins in the membrane (27).

Membrane compositions (lipid and membrane protein components) are highly specialized to perform a given function. For example, a vertebrate retina rod cell contains a membrane specialized for light reception, thus the light-absorbing glycoprotein rhodopsin represents 90% of the total proteins in that membrane. Conversely, the average bacterial plasma membrane contains hundreds of different membrane proteins performing a wide variety of roles. Lipid composition must also be suited to maintain functionally active protein folds. Native membranes typically have mass ratios of protein to lipid ranging from 1:4 to 4:1 (28).

Environmental effects, such as local pH, temperature, and ionic strength, also have a direct influence on membrane properties such as fluidity, stability, and permeability. The membrane is fluid-like, but may contain regions of gel-like, ordered-chain lipids. These phase transitions in lipid bilayers are a function of the environmental variables, and alter the viscosity of membranes (29). Thus, taking into account all of the potential factors of influence, and variety in structural properties and components, the native membrane environment is certainly quite complex.

1.2 Membrane proteins

The fluid mosaic model for biological membranes recognized the existence of a class of proteins that were associated with membranes and distinct from soluble proteins, with broad diversity in structure and function. The fluid mosaic model, in addition to including an asymmetric bilayer, also demonstrates multiple modes of association between protein and membrane. Peripheral proteins associate with membrane surfaces or other membrane proteins, while integral membrane proteins traverse the bilayer.

Peripheral proteins may contain a glycosylphosphatidylinositol (GPI) anchor to the membrane surface from the C-terminus of the protein and/or prenylated (fatty acid substituted) side-chain residues for membrane docking. Integral membrane proteins span the bilayer, with soluble domains exposed on each surface, one surface, or neither. Membrane proteins are abundant, and account for ~50% of the total membrane by weight (30). Membrane proteins also account for about 30% of the typical coding genome (31), and 20-25% of the total proteins in an average cell. However, despite their relative abundance, the vast majority of membrane proteins remain uncharacterized, structurally or functionally.

In 1985, the first high-resolution structure of a membrane protein was published, the photosynthetic reaction center complex from the purple bacteria *Rhodospseudomonas viridis* (4). This structure consists of four subunits, two of which contain bundles of five membrane-spanning α -helices. Although some common challenges exist, the conditions that led to this structure provided certain advantages that are not afforded to most current studies. First, the protein was purified from its native source rather than via recombinant expression because the complex is found naturally at high concentrations in these bacterial membranes. Typical problems with recombinant approaches include achieving high-yields and potentially toxic effects on the host cell at higher concentrations. Secondly, the protein complex was expected to be part of a two-dimensional crystalline array already *in vivo*, and thus was believed to promote the *in vitro* formation of crystals needed for diffraction. Additionally, the complex contains chromophores in the active, folded state; loss of the chromophore indicates a loss of native fold and protein denaturation. Thus, the system contains an intrinsic assay for proper function and fold,

requiring minimal additional preparation. Despite advances in recombinant expression and structural determination methods, only 452 high-resolution structures of unique membrane proteins have been determined to date (6). One of the largest challenges yet to be overcome facing membrane protein structural determination is achieving an *in vitro* mimic of the native membrane that retains the functionally active fold of the membrane protein.

Membrane proteins are structurally divided by the organization of their membrane-spanning region, either α -helical or a β -stranded barrel (Figure 1.4). About 90% of membrane proteins are predicted to be α -helical (31). Some α -helical membrane proteins are monotopic (crossing the membrane once), while others occur as polytopic bundles of helices (spanning multiple times). Membrane proteins with α -helical transmembrane domains are abundant in cell membranes and inner membranes of gram-negative bacteria, whereas β -stranded barrels are localized specifically to outer membranes of gram-negative bacteria, mitochondria, and chloroplasts. Bundles of 7 transmembrane α -helices are common to the G-protein coupled receptor (GPCR) class of membrane proteins, but other size bundles have been found as well. β -barrels typically contain between 8 and 22 β -strands. Membrane proteins from eukaryotes typically form higher-order complexes, and often contain an assortment of post-translational modifications and glycosylations.

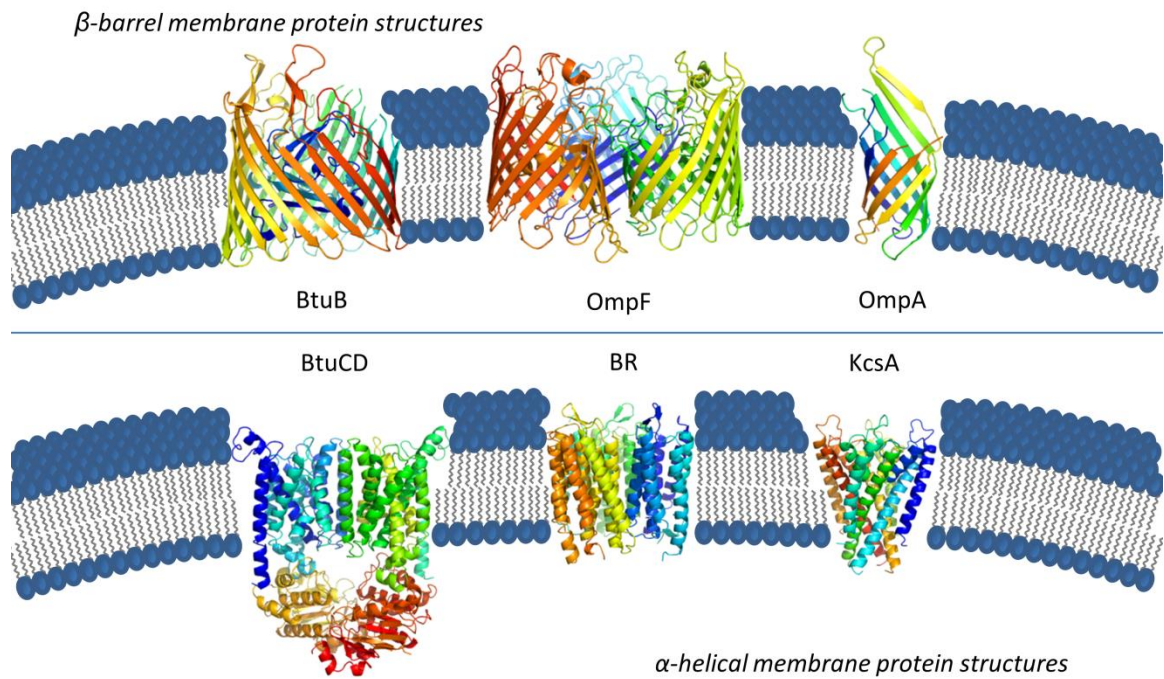


Figure 1.4 Examples of membrane proteins with α - or β - transmembrane domains. β -barrels (top) are composed of a large wrapped beta-sheets, containing 8-22 strands, that form a closed barrel structure across outer bacterial membranes. α -helical bundles (bottom) contain multiple α -helices in the transmembrane domain, and are located in inner bacterial or plasma membranes.

Membrane proteins are also classified according to four major functional roles, each vitally important to life at the cellular level (Figure 1.5). Structural proteins maintain the shape of the membrane, and are involved in cytoskeletal rearrangements and cellular motility. Transport proteins move ions and small molecules across the membrane barrier. In order to communicate extracellular signals from the surrounding environment, receptor proteins must be embedded in the membrane at the cell surface. Receptor proteins typically initiate a cascade of downstream events in response to extracellular signals. Additionally, membrane proteins may function as enzymes, converting local substrates to products. Each specific role requires the membrane protein to be localized at the membrane, and a variety of structures have evolved to suit these needs and perform these functions. Collectively, membrane proteins perform many cellular roles, such as nutrient and ion transport, establishing electrochemical gradients in respiratory and photosynthetic systems, and stimuli response and information processing; thus, they represent very desirable drug targets.

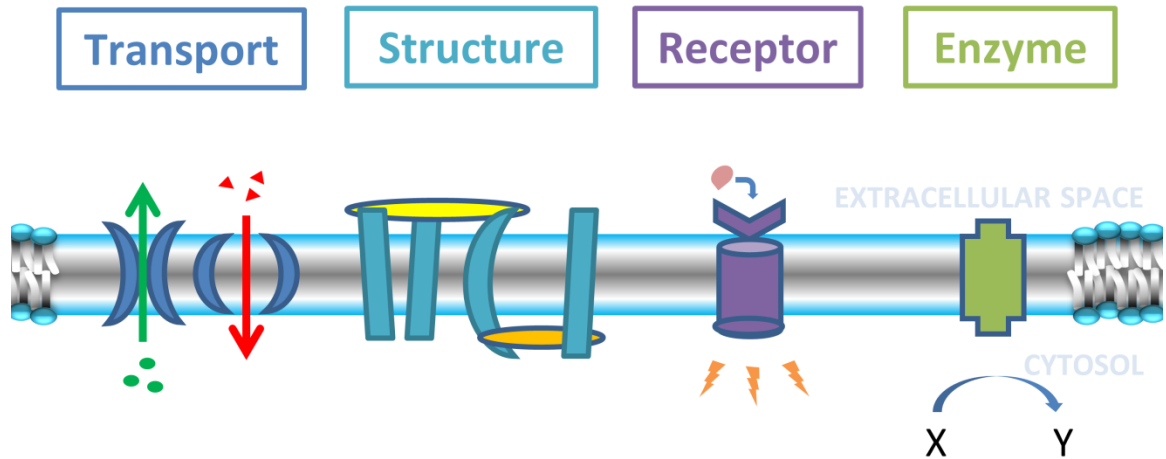


Figure 1.5 Functional roles of membrane proteins. Membrane proteins participate in vital cellular functions. These functions can be classified as: transport of molecules across the membrane; cytoskeletal anchors and structural components of the membrane; hormone and small molecule receptors; and enzymes.

Membrane proteins are translated from mRNA sequences similar to soluble proteins; however the amino acid sequence of a membrane protein must be targeted to a membrane, inserted, and folded before adopting its mature form (32). In eukaryotes, the same translocation machinery (Sec61 complex) is used for both nascent soluble and membrane proteins. Soluble proteins pass through the channel completely, but membrane proteins contain a signal sequence in the nascent peptide chain that allows hydrophobic transmembrane segments to exit laterally into the lipid bilayer. In prokaryotes, membrane protein synthesis and insertion occurs at the inner plasma membrane using similar translocation machinery (SecY complex). For outer membrane proteins of gram-negative bacteria, the nascent peptide chain must pass the SecY channel and cross the periplasmic space before associating with the outer membrane and inserting to form a folded β -barrel (33). This process is likely mediated by chaperone proteins, which assist in the insertion and folding of the nascent peptide, but many details remain unknown. Membrane proteins are expressed and targeted to specific membranes, and may even reside in special localized regions of membranes.

As such, membrane proteins have adopted various features to enhance their stability in membranes. First and foremost, transferring charged or highly polar compounds into the hydrophobic interior of membranes is strongly unfavorable in thermodynamic terms. Therefore, amino acid side chains must be mostly non-polar (*e.g.* Ala, Leu, Ile). Additionally, hydrogen bonds must be formed within the polar peptide backbone to compensate for energetic costs associated with its location in the hydrocarbon interior. Transmembrane segments found in membrane proteins (α -helices

and β -strands) provide optimum arrangement of the backbone for internal hydrogen bonding.

Membrane proteins may also exploit properties of different amino acids to enhance overall stability in membranes. Aromatic amino acid residues Trp and Tyr are commonly present in the transmembrane region located near the hydrophobic/hydrophilic interface. The hydrophobic rings of these residues extend laterally, buried in the hydrophobic portion of the membrane, but contain an amide functional group (Trp) or hydroxyl (Tyr) that orients toward the polar environment at the interface, and can participate in hydrogen bonding (34). Positively-charged amino acids Lys and Arg are also typically found near the hydrophobic/hydrophilic interface on the cytoplasmic face of membrane proteins. The aliphatic portions of these residues can interact favorably with hydrophobic lipid tails, while the positively-charged functional group at the end of the aliphatic chain is free to interact with the negatively-charged phospholipid head groups (27). This behavior is referred to as ‘snorkeling’. The *in vitro* preparation of membrane proteins aims to preserve these stabilizing features of membrane proteins.

1.3 Membrane protein solubilization and stabilization

Few methods exist for studying a membrane protein in its native state, and provide limited information due to complications from the many other surrounding proteins. The remainder of this chapter and thesis is focused on considerations for membrane proteins in non-native, but membrane-like, states. The two most common approaches for determining high-resolution protein structures – X-ray crystallography and nuclear magnetic resonance (NMR) – demand that the protein of interest be isolated

from other proteins and contaminants, and enriched to sufficient quantities. Functional assays have similar purification requirements, to ensure that the indicated activity originates from the isolated protein of interest and not from other factors in solution. The ease of manipulating solutions is an added benefit to working with solubilized membrane proteins. Following purification, the protein may be substituted into other membrane mimics to improve stability or as required per analytical method or technique.

Detergents are commonly employed to solubilize membranes and membrane proteins. Detergents are amphiphilic molecules similar to lipids, but typically have only one alkyl chain. The reduced tail volume and resulting ratio to head group surface area gives the molecule an overall conical shape, as compared to more cylindrical lipids. Thus, when sufficient detergent molecules are present in solution, monomers self-assemble into globular particles as opposed to bilayers, with alkyl chains facing inwards away from water, and hydrophilic head groups at the aqueous interface. The concentration of monomers required for self-assembly is the *critical micelle concentration* (CMC), and the soluble, higher-order assemblies are referred to as micelles.

Detergents and lipids are miscible, and the addition of detergent to membranes results in the intercalation of detergent to the lipid bilayer. The membrane is destabilized by the addition of detergent, and membrane fragments are formed at sufficient detergent concentrations (the *critical solubilization concentration*, CSC). These fragments retain membrane components and include detergent, but are sufficiently buoyant to remain suspended in solution. Complete exchange of native lipid with additional detergent may result in membrane proteins being encompassed by detergent micelles (Figure 1.6). In

practice, this lipid-detergent exchange process is performed by immobilizing the protein of interest using an affinity tagged protein and column, then eluting in the protein in the desired detergent conditions. The real challenge lies in determining the proper detergent conditions that lead to a stable, soluble protein-detergent complex (PDC) for a protein of interest. This process often entails empirically screening hundreds of detergent and solutions conditions in an extremely inefficient and costly process with no guarantee of success.

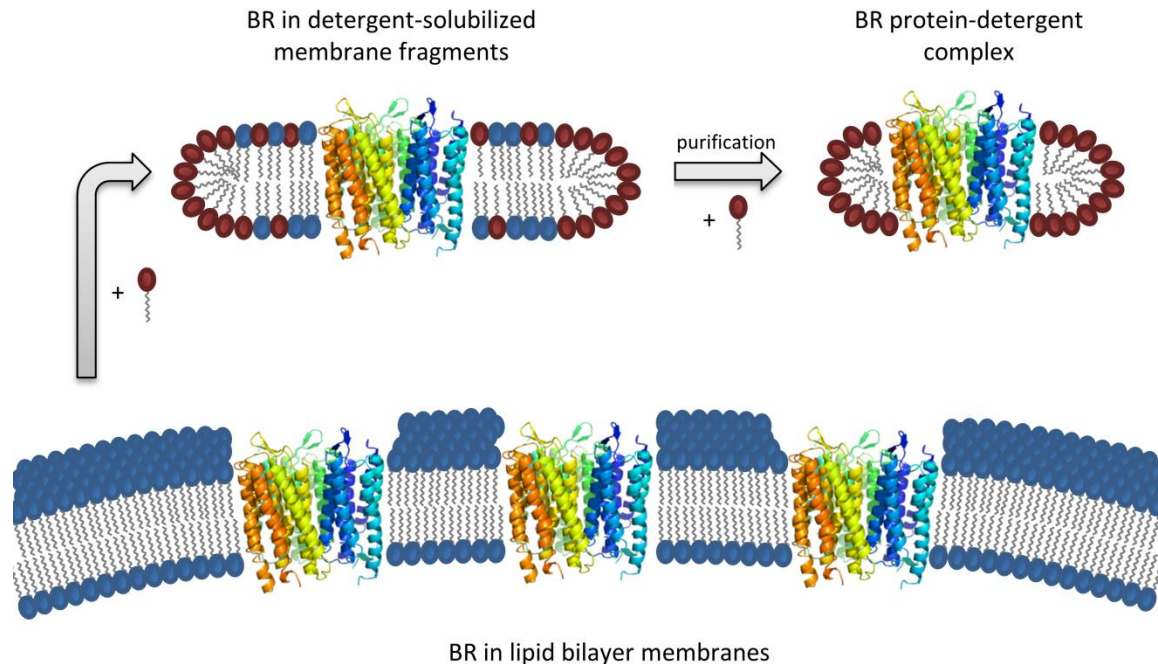


Figure 1.6 General scheme for detergent-mediated solubilization of membrane proteins. Bacteriorhodopsin (BR) membrane proteins reside in a lipid bilayer membrane environment. The addition of detergents results in destabilization of the membrane, and the formation of soluble membrane patches at the *critical solubilization concentration*. These soluble membrane fragments contain membrane proteins surrounded by lipid and detergent. Purification and complete exchange of lipids for detergents results in the formation of a protein-detergent complex.

Functionally-active, stable PDCs are rare because the membrane-spanning region of a membrane protein must adopt its final fold in a mimic environment quite different from the native membrane. For example, micelles are homogeneously mixed and thus contain no inner and outer leaflets or leaflet asymmetry. Additionally, dynamics of the hydrophobic core are expected to vary based upon the number and length of alkyl chain tails per detergent or lipid. The dependence of membrane protein stability on properties of the surrounding environment is not well-understood, yet a few considerations for successful PDC formation appear reasonable. First, the hydrophobic thickness of the mimic must be approximately equal to the protein's hydrophobic transmembrane domain distance, as in native membranes. This concept is called hydrophobic matching. Second, the volume of the mimic must be sufficient to accommodate the membrane protein, specifically the hydrophobic core and membrane spanning region. However, typically only one protein per micelle is desired, so the volume should also not be overly large such that multiple proteins are accommodated. Additionally, technique-specific restrictions may be imposed, such as upper limits in overall particle size from solution-based NMR techniques. Functional assays are valuable tools for assessing the successful fulfillment of all requirements for membrane protein reconstitution.

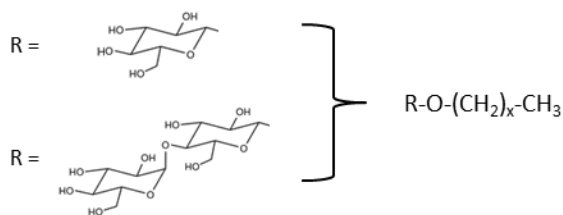
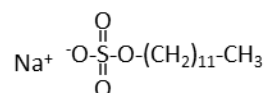
1.4 Applications of membrane mimics

A variety of methods have been presented in the past thirty years for extraction and solubilization of membrane proteins (35-41). Commonalities between approaches include the use of amphiphilic molecules to screen hydrophobic regions of protein from surrounding water. Most approaches also require the use of detergents for membrane

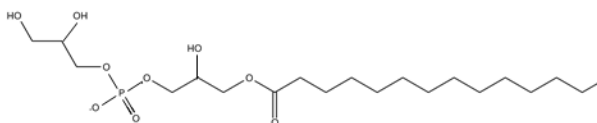
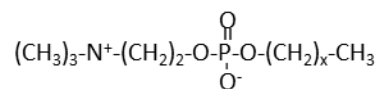
extraction and purification, prior to reconstitution in the final mimic. The largest obstacle facing membrane mimic design and optimization is a lack of understanding of the specific membrane protein requirements. An ordered and well-characterized system is highly desirable to aid in interpretation of final data. The ability to systematically manipulate properties of the membrane mimic is also beneficial for examining the influence of properties of surrounding environment on the protein.

1.4.1 Commonly used detergents in membrane protein studies

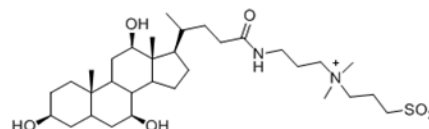
The use of detergents for membrane protein extraction and purification has been discussed previously (section 1.3). However, detergent micelles are also used as membrane mimics for structural and functional investigations of membrane proteins, and have demonstrated many successes. Unfortunately, membrane proteins in a detergent-solubilized state are prone to loss of function, denaturation, and/or aggregation. Detergents vary in alkyl chain length, head group structure, and chemistry (Table 1.1), resulting in a wide variety of available micelle sizes, shapes, and properties. The most commonly used detergents for membrane protein studies have between 8-14 carbons, and zwitterionic or nonionic head groups. In addition to a CMC, micelles can be described by a shape (*e.g.* spherical, cylindrical, and ellipsoidal) and an aggregation number, or number of detergent monomers forming the micelle.

Nonionic detergents***Glucosides***n-octyl- β -D-glucopyranoside ($x = 7$)***Maltosides***n-decyl- β -D-maltopyranoside ($x = 9$)n-dodecyl- β -D-maltopyranoside ($x = 11$)**Ionic detergents*****Sodium dodecyl sulfate (SDS)******Lyso-phosphatidylglycerol***

lyso-myristoyl-phosphatidylglycerol (LMPG)

**Zwitterionic detergents*****Phosphocholines***decyl-phosphocholine ($x = 9$)dodecyl-phosphocholine ($x = 11$)tetradecyl-phosphocholine ($x = 13$)***CHAPS***

3-[(3-Cholamidopropyl)dimethylammonio]-1-propanesulfonate (CHAPS)

**Table 1.1 Examples of common detergents used in membrane protein studies.**

The most commonly used nonionic detergents for membrane protein studies have a single alkyl chain attached to a simple carbohydrate head group: alkyl maltosides, and alkyl glucosides. Nonionic detergents are generally non-denaturing to proteins, and do not interfere with native structure or functional activity (38). This feature makes them likely candidates for the start of most membrane protein solubilization attempts at destabilizing the membrane and isolating membrane fragments. An alkyl maltoside with a 12-carbon chain, dodecylmaltoside (DDM), is routinely used to solubilize membranes, and has led to the successful determination of crystal structures, such as the secondary transporters from the major facilitator superfamily (42). However, additional “fine tuning” of the detergent system is often required for optimizing protein stability. For example, if initial screens indicate that a membrane protein is partially soluble, but insufficiently stable in a given detergent, attempts to improve protein stability might involve using a similar detergent with systematic variations in select properties.

Before continuing with optimization of the detergent environment, the end goal must be considered as well, since solution-state NMR and X-ray crystallography have very different requirements of the PDC. For NMR, the PDC is required to remain in solution, while minimizing interactions with neighboring PDCs, whereas crystallography requires the formation of crystals from the ordered arrangement of PDCs. The use of detergents for specific applications in membrane protein studies has been recently reviewed (40, 43, 44). For example, charged detergents forming lower molecular weight micelles have been considered ideal candidates for solution-state NMR studies where the size of the PDC is limited.

Zwitterionic detergents carry both a positive and negative charge in the head group. The most common example in membrane protein studies is dodecylphosphocholine (FC12). The phosphocholine head group is often mistaken to be the same as that of the phosphatidylcholine phospholipids, however the detergent lacks the glycerol backbone between lipid head and tail, and contains one alkyl chain attached to the phosphate group. Dihexanoylphosphatidylcholine (DHPC) forms micelles rather than bilayers and is classified as a detergent, although it is a short-chain phospholipid. Electrostatic repulsions between similar charges in zwitterionic head groups are assumed to increase the effective surface area per head group in the micelle assembly. This process may account for the decreased aggregation number observed in micelles from zwitterionic detergent compared with their nonionic counterparts. As previously mentioned, NMR investigations are limited by the overall complex size, and using low aggregation number detergents has been especially beneficial for minimizing the contributions from detergent (45).

Ionic detergents include those with either positively or negatively charged head groups, such as sodium dodecylsulfate (SDS) or lysophosphoglycerols (LPGs). SDS is well-known for its ability to bind and denature soluble proteins and some membrane proteins, but has been used for structural determination of membrane proteins such as glycophorin A (35), PagP (46), and others. Lysomyristoyl phosphatidylglycerol (LMPG) is one example of a lyso-lipid (single chain lipid) detergent, which has yielded quality solution NMR spectra for KCNE1 while sustaining protein activity (47).

Principles of the hydrophobic effect and applications to thermodynamics of micelle formation have been well described in *The Hydrophobic Effect: Formation of Micelles and Biological Membranes* by Charles Tanford (16). The underlying basis is that micelle formation is a balance of two opposing forces: attractive forces between detergent tails (including their exclusion from water via the hydrophobic effect) and repulsive forces between neighboring polar head groups. The sizes and shapes of micelles are strongly dependent on this balance of forces.

A thorough discussion regarding the effects of head group properties and alkyl chain length on micelle properties will be reserved for the focus of chapter three. It should be noted, however, that just as the final protein fold is encoded in and determined by its primary structure, so too, the final micelle structure is a direct result of the detergent's chemical structure. The focus of chapter four is the effect of detergent composition in mixed micelles on the resulting micelle size and shape, and has additional implications for fine tuning PDC systems to optimize protein stability. Detergent mixtures have demonstrated success in membrane protein structure determinations, and were shown to be critical for stabilization and functional activity of a G-protein coupled receptor (GPCR) (48). Steroid-based detergents, such as CHAPS, are often critical for maintaining function, and have found widespread use in detergent mixtures for studies of eukaryotic systems (49, 50).

Although most successes to date have involved “classical” detergents with simple polar head groups and linear hydrocarbon tails, novel detergents and features are under constant development. CYMAL® and CYCLOFOS™ detergents from Anatrace contain

cyclo-hexyl hydrocarbon rings in the tail portion (40). Tripod amphiphiles contain a branch-point for incorporation of a combination of up to three hydrophilic/hydrophobic functional groups (51). Detergents with fluorocarbon tails have also been developed (52). These novel detergents have provided a variety of options for systematic investigations and effects on membrane protein stability, although little is known about the aggregate structures formed.

1.4.2 *Bicelles*

Bicelles are intermediate formations of detergents and lipids between micelles and bilayers, and consist of a central lipid bilayer-like disc encircled by a belt of detergent (Figure 1.7). The detergent orients with its chains facing the outer disc edge, and serves to screen the outermost lipid tails from interactions with water. A key feature describing the bicelle system is the mole ratio of lipid to detergent, expressed as Q . Bicelles are formed when proportions of detergent and lipid are approximately equal at moderate temperatures (10-40 °C), existing as isotropic, or fast-tumbling bicelles at $0.20 < Q < 2.0$, exhibiting a liquid crystalline like phase at $2.0 < Q < 5.0$, and perforated Swiss cheese-like multi-lamellar sheets or vesicles with hole edges stabilized by detergent above $Q = \sim 7.0$ (53). Diameters range up to several hundred angstroms with a thickness of about forty angstroms. Bicelles containing protein are often prepared from the addition of detergent to solutions of liposomes (lipid bilayer vesicles) reconstituted with protein, similar to the detergent solubilization of native membranes. Bicelles are formed with a short chain and long chain amphiphile (commonly DMPC and DHPC), but other variations exist such as DMPC and CHAPSO (54).

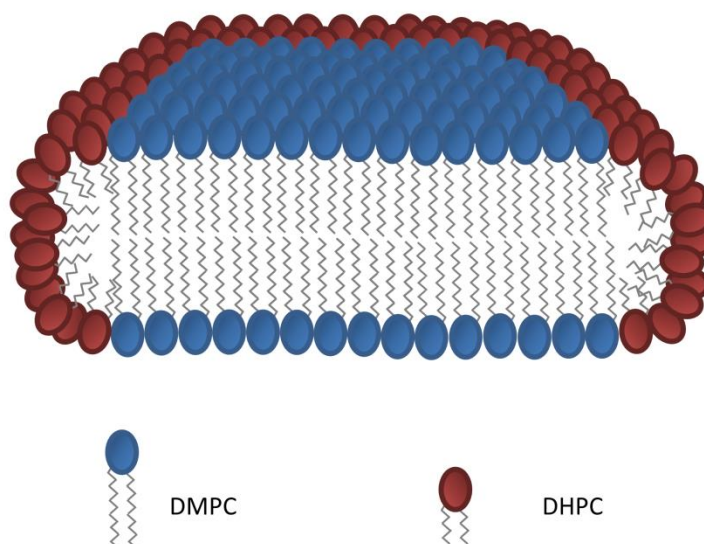


Figure 1.7 Schematic of bicelle cross-section formed at intermediate lipid:detergent ratios. The overall bicelle structure is proposed to contain a lipid bilayer-like disk surrounded at the edges by detergent. The most studied bicelle system employs DMPC as the lipid component and DHPC as the detergent. In this model, complete partitioning between detergent edge and lipid core components is illustrated.

One appealing attribute of bicelles as membrane mimics is that lipid bilayer architecture is maintained in the bicelle core, yet the particles remain soluble and can be easily mixed. Another particularly interesting feature of bicelles with $2.0 < Q < 3.5$ is their ability to be aligned in magnetic fields due to diamagnetic properties of the lipids in a liquid crystalline state (55). Advances in solid-state NMR structural determination have exploited this property by using aligned bicelles as a matrix to impart specific orientation to proteins, allowing orientations of bonds between neighboring atoms to be determined with respect to the rest of the molecule (56). This method was originally applied to align soluble and membrane-associated proteins, but has been adapted for use in membrane protein structure determination (57). Isotropic solutions of bicelles have also been used in solution-state NMR studies of membrane proteins (58). High-quality membrane protein crystals have been obtained using bicelle crystallization approaches as well (59).

1.4.3 *Nanodisks*

Similar to bicelles, nanodisks contain a central disk with lipid bilayer-like organization, but have hydrophobic edges encircled by long, amphipathic helical proteins (called membrane scaffold proteins, or MSPs) as opposed to a boundary of detergent (60). Unlike micelles and bicelles, in which size can be systematically varied through detergent mixing or altering lipid-to-detergent ratio respectively, the diameter of nanodisks is fixed by the length of apolipoprotein stabilizing the bilayer edge. Therefore, MSPs must be prepared at different lengths to create different nanodisk diameters (61). Reconstitution of membrane proteins in the central lipid bilayer region of nanodisks has

also been employed for biophysical investigations of membrane proteins (62). However, these strategies still rely on membrane protein purification using detergent solubilization.

1.4.4 Liposomes

Liposomes, particularly small unilamellar vesicles (15-30 nm in diameter), are another class of commonly used membrane mimics. Liposomes are fluid-filled synthetic lipid bilayer membranes, and have been used in a variety of membrane transport and fusion studies. These studies are made possible by the liposome's ability to carry an aqueous core with different contents or properties than the surrounding solution. Liposomal formulations have also been used as drug delivery systems (DOXIL® for example), using liposomes to carry active hydrophilic or hydrophobic compounds *in vivo*. Optimizing the stability, targeting of specific cells or tissues, uptake, and biocompatibility remain active areas of research, and have shown promising results.

1.5 Summary and outline of dissertation

Now that challenges associated with membrane proteins, particularly those related to its amphiphilic nature and finding a suitable mimic of the native membrane environment, have been presented, an introduction to small-angle scattering methods and their use in membrane protein and membrane mimic investigations will be provided in the next chapter. Following this discussion, these methods will be applied to study aggregate structures formed by single micelle-forming detergents, mixed detergents, and mixtures of lipid and detergent. First, the dependence of micelle size and shape on detergent monomer structure, such as head group chemistry and alkyl chain length, was

determined using systematic variations in detergent structures and measuring properties of the resulting micelles formed. Next, detergent mixtures were investigated to determine the dependence of mixed micelle properties on detergent composition. Finally, aggregate structures of lipid-detergent mixtures expected to form bicelles were characterized in the detergent-rich regime. Contrast variation experiments performed on aggregates formed by these mixtures are expected to reveal internal organization and distribution of lipid and detergent molecules between the bicelle core and rim regions.

1.6 References

1. Kendrew, J. C., R. E. Dickerson, B. Strandberg, R. G. Hart, D. R. Davies, D. C. Phillips, and V. C. Shore. 1960. Structure of myoglobin: A three-dimensional fourier synthesis at 2 Å. Resolution. *Nature* 185:422-427.
2. Jhoti, H., and A. R. Leach, eds. *Structure-based drug discovery*. 2007, Springer: Berlin. 249.
3. Berman, H. M. 2000. The protein data bank. *Nucleic Acids Research* 28:235-242.
4. Deisenhofer, J., O. Epp, K. Miki, R. Huber, and H. Michel. 1985. Structure of the protein subunits in the photosynthetic reaction centre of rhodospseudomonas viridis at 3Å resolution. *Nature* 318:618-624.
5. White, S. H. 2004. The progress of membrane protein structure determination. *Protein Science* 13:1948-1949.
6. White, S. H., *Membrane proteins of known 3d structure*, 2013.

7. Loeb, J. 1906. The dynamics of living matter. Columbia university biological series, Osborn, H. F., and E. B. Wilson, editors. Vol. VIII. Columbia University Press, New York.
8. Overton, E. 1895. Ueber die osmotischen eigenschaften der lebenden pflanzen und tierzelle. Vierteljahrsschr Naturforsch Ges Zuerich 40:159-201.
9. Fricke, H. 1925. The electric capacity of suspensions with special reference to blood. The Journal of general physiology 9:137-152.
10. Gorter, E., and F. Grendel. 1925. On bimolecular layers of lipoids on the chromocytes of the blood. The Journal of experimental medicine 41:439-43.
11. Danielli, J. F., and H. Davson. 1935. A contribution to the theory of permeability of thin films. Journal of Cellular and Comparative Physiology 5:495-508.
12. Robertson, J. D., *A molecular theory of cell membrane structure*, in *Verhandlungen band ii/biologisch-medizinischer teil*1960, Springer. p. 159-171.
13. Frye, L. D., and M. Edidin. 1970. The rapid intermixing of cell surface antigens after formation of mouse-human heterokaryons. Journal of Cell Science 7:319-335.
14. Singer, S. J., and G. L. Nicolson. 1972. The fluid mosaic model of the structure of cell membranes. Science 175:720-731.
15. Mouritsen, O. G., and M. Bloom. 1984. Mattress model of lipid-protein interactions in membranes. Biophysical Journal 46:141-153.
16. Tanford, C. 1980. The hydrophobic effect: Formation of micelles and biological membranes 2d ededitorsJ. Wiley.

17. Fantini, J., N. Garmy, R. Mahfoud, and N. Yahi. 2004. Lipid rafts: Structure, function and role in hiv, alzheimer's and prion diseases. *Expert Reviews in Molecular Medicine* 4.
18. Curatolo, W. 1987. Glycolipid function. *Biochimica et Biophysica Acta (BBA) - Reviews on Biomembranes* 906:137-160.
19. Bhattacharya, S., and S. Haldar. 2000. Interactions between cholesterol and lipids in bilayer membranes. Role of lipid headgroup and hydrocarbon chain-backbone linkage. *Biochimica et Biophysica Acta (BBA)-Biomembranes* 1467:39-53.
20. Rubenstein, J., B. A. Smith, and H. M. McConnell. 1979. Lateral diffusion in binary mixtures of cholesterol and phosphatidylcholines. *Proceedings of the National Academy of Sciences* 76:15-18.
21. Szabo, G. 1974. Dual mechanism for the action of cholesterol on membrane permeability. *Nature* 252:47-49.
22. Corvera, E., O. Mouritsen, M. Singer, and M. Zuckermann. 1992. The permeability and the effect of acyl-chain length for phospholipid bilayers containing cholesterol: Theory and experiment. *Biochimica et Biophysica Acta (BBA)-Biomembranes* 1107:261-270.
23. Kraft, M. L. 2013. Plasma membrane organization and function: Moving past lipid rafts. *Molecular Biology of the Cell* 24:2765-2768.
24. McConnell, H. M., and R. D. Kornberg. 1971. Inside-outside transitions of phospholipids in vesicle membranes. *Biochemistry* 10:1111-1120.

25. Rothman, J. E., and E. P. Kennedy. 1977. Rapid transmembrane movement of newly synthesized phospholipids during membrane assembly. *Proceedings of the National Academy of Sciences* 74:1821-1825.
26. Bretscher, M. S. 1972. Asymmetrical lipid bilayer structure for biological membranes. *Nature New Biology* 236:11-12.
27. von Heijne, G. 1992. Membrane protein structure prediction. *Journal of molecular biology* 225:487-494.
28. von Heijne, G., and D. Rees. 2008. Membranes: Reading between the lines. *Current Opinion in Structural Biology* 18:403-405.
29. Saxton, M. J., R. W. Breidenbach, and J. M. Lyons, *Membrane dynamics: Effects of environmental stress*, in *Genetic engineering of osmoregulation*, Rains, D. W., R. C. Valentine, and A. Hollaender, Editors. 1980, Springer US. p. 203-233.
30. Rosenberg, S. A., and G. Guidotti. 1968. The protein of human erythrocyte membranes i. Preparation, solubilization, and partial characterization. *Journal of Biological Chemistry* 243:1985-1992.
31. Almén, M., K. J. V. Nordström, R. Fredriksson, and H. B. Schiöth. 2009. Mapping the human membrane proteome: A majority of the human membrane proteins can be classified according to function and evolutionary origin. *BMC Biology* 7:50.
32. Rapoport, T. A. 2007. Protein translocation across the eukaryotic endoplasmic reticulum and bacterial plasma membranes. *Nature* 450:663-669.

33. Osborne, A. R., T. A. Rapoport, and B. van den Berg. 2005. Protein translocation by the sec61/secy channel. *Annual Review of Cell and Developmental Biology* 21:529-550.
34. Killian, J. A., and G. von Heijne. 2000. How proteins adapt to a membrane–water interface. *Trends in biochemical sciences* 25:429-434.
35. MacKenzie, K. R., J. H. Prestegard, and D. M. Engelman. 1997. A transmembrane helix dimer: Structure and implications. *Science* 276:131-133.
36. White, S. H., and W. C. Wimley. 1999. Membrane protein folding and stability: Physical principles. *Annual review of biophysics and biomolecular structure* 28:319-365.
37. Seddon, A. M., P. Curnow, and P. J. Booth. 2004. Membrane proteins, lipids and detergents: Not just a soap opera. *Biochimica et Biophysica Acta (BBA)-Biomembranes* 1666:105-117.
38. Garavito, R. M., and S. Ferguson-Miller. 2001. Detergents as tools in membrane biochemistry. *Journal of Biological Chemistry* 276:32403-32406.
39. le Maire, M., P. Champeil, and J. V. Møller. 2000. Interaction of membrane proteins and lipids with solubilizing detergents. *Biochimica et Biophysica Acta (BBA)-Biomembranes* 1508:86-111.
40. Privé, G. G. 2007. Detergents for the stabilization and crystallization of membrane proteins. *Methods* 41:388-397.
41. Sanders, C. R., A. Kuhn Hoffmann, D. N. Gray, M. H. Keyes, and C. D. Ellis. 2004. French swimwear for membrane proteins. *ChemBioChem* 5:423-426.

42. Lemieux, M. J., J. Song, M. J. Kim, Y. Huang, A. Villa, M. Auer, X.-D. Li, and D.-N. Wang. 2003. Three-dimensional crystallization of theescherichia coliglycerol-3-phosphate transporter: A member of the major facilitator superfamily. *Protein Science* 12:2748-2756.
43. Columbus, L., J. Lipfert, K. Jambunathan, D. A. Fox, A. Y. Sim, S. Doniach, and S. A. Lesley. 2009. Mixing and matching detergents for membrane protein nmr structure determination. *Journal of the American Chemical Society* 131:7320-7326.
44. Fernández, C., and K. Wüthrich. 2003. Nmr solution structure determination of membrane proteins reconstituted in detergent micelles. *FEBS Letters* 555:144-150.
45. Vinogradova, O., F. Sönnichsen, and C. Sanders, II. 1998. On choosing a detergent for solution nmr studies of membrane proteins. *Journal of Biomolecular NMR* 11:381-386.
46. Hwang, P. M., W. Y. Choy, E. I. Lo, L. Chen, J. D. Forman-Kay, C. R. H. Raetz, G. G. Prive, R. E. Bishop, and L. E. Kay. 2002. Solution structure and dynamics of the outer membrane enzyme pagp by nmr. *Proceedings of the National Academy of Sciences* 99:13560-13565.
47. Tian, C., C. G. Vanoye, C. Kang, R. C. Welch, H. J. Kim, A. L. George, and C. R. Sanders. 2007. Preparation, functional characterization, and nmr studies of human kcne1, a voltage-gated potassium channel accessory subunit associated with deafness and long qt syndrome†,‡. *Biochemistry* 46:11459-11472.

48. O'Malley, M. A., M. E. Helgeson, N. J. Wagner, and A. S. Robinson. 2011. The morphology and composition of cholesterol-rich micellar nanostructures determine transmembrane protein (gpcr) activity. *Biophysical Journal* 100:L11-L13.
49. Sloan, M. E., P. Rodis, and B. P. Wasserman. 1987. Chaps solubilization and functional reconstitution of β -glucan synthase from red beet root (*beta vulgaris* l.) storage tissue. *Plant physiology* 85:516-522.
50. Hjelmeland, L. M. 1980. A nondenaturing zwitterionic detergent for membrane biochemistry: Design and synthesis. *Proceedings of the National Academy of Sciences* 77:6368-6370.
51. SeokáChae, P. 2010. Tripod amphiphiles for membrane protein manipulation. *Molecular bioSystems* 6:89-94.
52. Chabaud, E., P. Barthelemy, N. Mora, J. Popot, and B. Pucci. 1998. Stabilization of integral membrane proteins in aqueous solution using fluorinated surfactants. *Biochimie* 80:515-530.
53. Luchette, P. A., T. N. Vetman, R. S. Prosser, R. E. W. Hancock, M.-P. Nieh, C. J. Glinka, S. Krueger, and J. Katsaras. 2001. Morphology of fast-tumbling bicelles: A small angle neutron scattering and nmr study. *Biochimica et Biophysica Acta (BBA) - Biomembranes* 1513:83-94.
54. Li, M., H. H. Morales, J. Katsaras, N. Kučerka, Y. Yang, P. M. Macdonald, and M.-P. Nieh. 2013. Morphological characterization of dmpc/chapso bicellar mixtures: A combined sans and nmr study. *Langmuir* 29:15943-15957.

55. Sanders, C. R., and J. P. Schwonek. 1992. Characterization of magnetically orientable bilayers in mixtures of dihexanoylphosphatidylcholine and dimyristoylphosphatidylcholine by solid-state nmr. *Biochemistry* 31:8898-8905.
56. Tjandra, N., and A. Bax. 1997. Direct measurement of distances and angles in biomolecules by nmr in a dilute liquid crystalline medium. *Science* 278:1111-1114.
57. Sanders, C. R., and R. S. Prosser. 1998. Bicelles: A model membrane system for all seasons? *Structure* 6:1227-1234.
58. Vold, R. R., R. S. Prosser, and A. J. Deese. 1997. Isotropic solutions of phospholipid bicelles: A new membrane mimetic for high-resolution nmr studies of polypeptides. *Journal of Biomolecular NMR* 9:329-335.
59. Faham, S., and J. U. Bowie. 2002. Bicelle crystallization: A new method for crystallizing membrane proteins yields a monomeric bacteriorhodopsin structure. *Journal of molecular biology* 316:1-6.
60. Bayburt, T. H., Y. V. Grinkova, and S. G. Sligar. 2002. Self-assembly of discoidal phospholipid bilayer nanoparticles with membrane scaffold proteins. *Nano Letters* 2:853-856.
61. Denisov, I., Y. Grinkova, A. Lazarides, and S. Sligar. 2004. Directed self-assembly of monodisperse phospholipid bilayer nanodiscs with controlled size. *Journal of the American Chemical Society* 126:3477-3487.
62. Bayburt, T. H., and S. G. Sligar. 2010. Membrane protein assembly into nanodiscs. *FEBS Letters* 584:1721-1727.

2. Small-angle scattering

Small-angle scattering methods are used to probe size, shape, and orientation of objects in a variety of media, and at length scales up to several orders of magnitude larger than the wavelength of incident radiation. Thus, applications are highly versatile and widely varied, including measurements of chemical aggregation (1), colloids (2), surfactants (3), material defects (4), and alloys (5). Additionally, small-angle X-ray scattering (SAXS) and small-angle neutron scattering (SANS) are complementary techniques often used to study the size and shape of biological macromolecules in dilute solutions (6-8). These techniques allow examination of overall macromolecular structure (size and shape) and/or complex associations in solution at near-physiological conditions and are not influenced by crystal-packing forces present in crystallization-based methods. Macromolecular sizes studied can also range from a few kilodaltons to several megadaltons, as opposed to the limited ceiling (~75-100 kDa) present in solution-state NMR investigations (9).

Scattering results from interactions between incident radiation and atoms in the sample solution (*e.g.*, electrons in the case of X-rays), and thus contains information about the atomic structure from the ensemble of molecules in solution. In a typical biological scattering experiment, the net scattering profile for a macromolecule of interest (protein, DNA, micelle assembly, etc.) is calculated by subtracting the measured scattering of matched buffer components from the scattering of a monodisperse solution of the macromolecule. This net scattering profile contains information about the macromolecular structure; specifically, a distribution of distances between correlated pairs of atoms within the macromolecule.

Due to the exposure of many randomly-oriented macromolecules in the sample, the observed scattering is equivalent to that of the macromolecule spherically averaged over all orientations. Thus, information about the relative atomic positions within the macromolecule is not retained using scattering methods, as opposed to X-ray crystallography, which results from regular, repeated molecules in an oriented crystal. This loss of relative positions and atomistic detail often causes scattering techniques to be referred to as “low resolution” ($\sim 15 \text{ \AA}$) structural techniques, yet interatomic distances are typically measured with the same degree of precision as their diffraction counterparts. One of the main difficulties and challenges associated with scattering experiments is reconstructing this three-dimensional structural information from the experimental data.

Many methods exist for extracting structural information from the observed scattering pattern, and provide additional information when combined with related structural data from other techniques, such as crystallography and NMR (10, 11). In these hybrid approaches, known as rigid-body refinements, high-resolution portions are positioned to fit the lower resolution SAXS envelope describing the overall shape. *Ab initio* methods are also used to reconstruct the overall macromolecular size and shape to match the observed scattering with very few assumptions about the macromolecule or additional constraints (12). Similarly, geometric models provide an added means of simulating the expected scattering profile, which can be refined to match the experimental data (13). Model-free approaches exist for direct determination of structural features from the scattering profile as well (14, 15). The methodologies used in this series of studies are described in more detail in section 2.2: Applications and interpretation of scattering data.

2.1 Theory and principles of SAS

The basic theory and principles of small-angle scattering apply to both SAXS and SANS, although the fundamental interactions of X-rays and neutrons with matter are very different. X-rays and neutrons exhibit similar wavelike properties, and are scattered at interfaces between regions with different scattering qualities. However, X-rays interact with electrons, and thus probe variations in electron density of the sample; Neutrons interact primarily with atomic nuclei, and are sensitive to atomic composition. Due to inherent differences in the interactions of neutrons with hydrogen and deuterium atoms, neutron scattering is often used in biophysics as a tool to resolve structural components of complex assemblies in solution that can be varied in hydrogen or deuterium content. Together, these complementary techniques provide information about the overall size, shape, and orientation of the macromolecular ensemble in solution.

In a typical biological scattering experiment, a dilute solution of macromolecules (>0.5 mg/mL) is exposed to a focused beam of X-rays ($\lambda \approx 1.5 \text{ \AA}$) or thermal neutrons ($\lambda \approx 5 \text{ \AA}$). Scattered intensities are recorded as a function of the magnitude of the scattering vector \mathbf{q} , defined as:

$$\mathbf{q} = \frac{4\pi \sin(\theta)}{\lambda} \quad (1)$$

where 2θ is the angle between the incident beam and scattered intensity, and λ is the wavelength of incident radiation. Since this definition normalizes the scattered angles by the wavelength (or energy) of incident radiation, a direct comparison of results can be easily performed between different experiments. This vector is also referred to as the

angular momentum transfer, as it represents the “perceived force” required to deflect incident radiation at the scattered angle ($\mathbf{q} = |\mathbf{k}_s - \mathbf{k}_i|$, Figure 2.1).

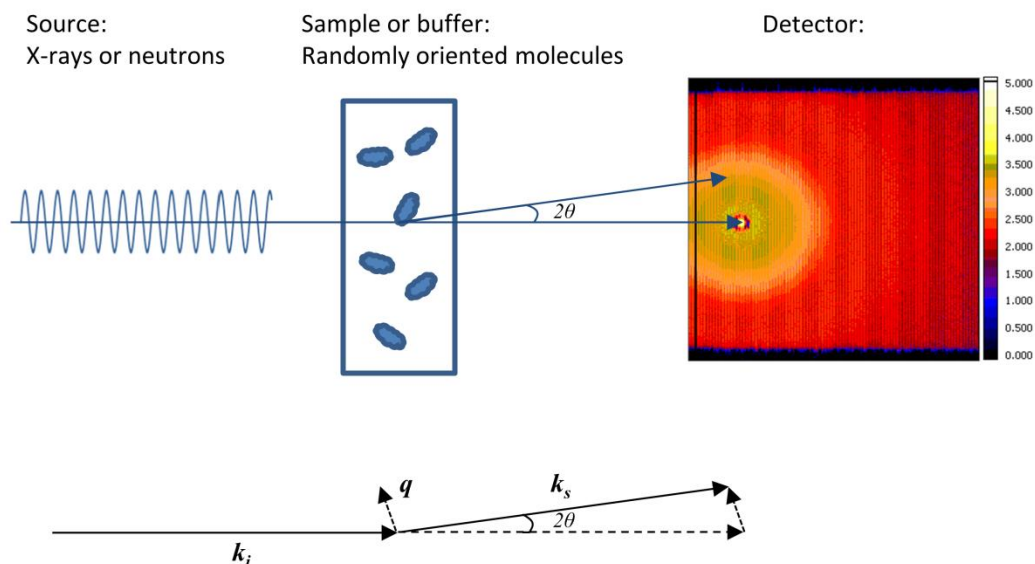


Figure 2.1 Small-angle scattering experiment setup. A collimated beam of X-rays or neutrons is focused on the sample or matched buffer. The scattered radiation is recorded by a detector. Long sample to detector distances are often required to measure scattering at small angles. To minimize incoherent and background scattering, the flight path between sample and detector is typically evacuated. The vertical lines observed in the detector image result from pixel efficiencies or instrument setup and are masked out during data reduction. The angular momentum transfer vector q is represented below as the component giving rise to the observed scattering angle.

Scattered intensities are the result of constructive interference between correlated scattering centers, or atoms within a molecule (Figure 2.2). The incident beam is scattered isotropically, and produces scattered radiation at the same frequency as the incident radiation. Conditions for constructive interference can also be related using an approximation from first-order Bragg diffraction (Eq. 2), *i.e.* the interatomic distances in the crystalline array that produce constructive interference and the observed crystallographic reflections, referred to as “diffraction spots”.

$$n \lambda = 2d \sin \theta \quad (n = 1) \quad (2)$$

Combining equations 1 and 2 yields the following relationship between the scattering vector and real-space interatomic distance:

$$\mathbf{q} = \frac{2\pi}{d} \quad (3)$$

Note that the units for \mathbf{q} are in reciprocal space (\AA^{-1}), and scattered intensities at larger angles result from structural separations at smaller distances in real space. Based on this relationship, to examine structures on the typical biological order of 20-500 \AA , a \mathbf{q} -range of 0.0125 – 0.314 \AA^{-1} is desired, and can be achieved by examining angles of 0.34 – 8.60° from the incident beam with a 1.5 \AA wavelength of incident radiation.

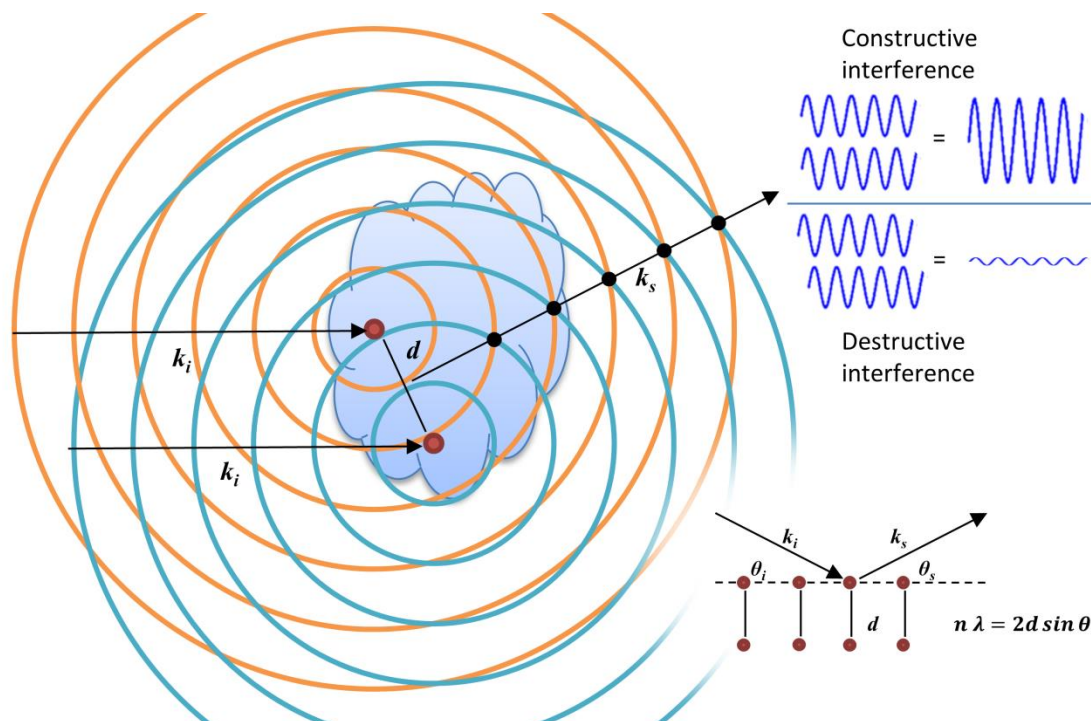


Figure 2.2 Observed scattering is the result of constructive interference. Incident radiation (blue) encounters atoms (red) separated by a distance d within a macromolecule (light blue). This interaction produces isotropic scattering of radiation in all directions (cross-sections of spherical waves represented as circles drawn at areas of maximum amplitude, and with same frequency as incident radiation). Constructive interference is observed by the detector and occurs along angles where this scattered radiation is in phase, indicated by overlapping circles and black dots. The interatomic spacing that gives rise to reflected radiation in diffraction methods is provided at bottom right for comparison.

The observed scattering pattern originates from many molecules with random positions and orientations in solution. Therefore, specific positions and atomic coordinates are indiscernible, and the two-dimensional scattering pattern can be reduced by circular averaging to a one-dimensional plot of scattered intensities $I(q)$ as a function of q . Scattering from matched buffer conditions is collected independently and subtracted from the sample scattering to yield the net macromolecular scattering profile (Figure 2.3).

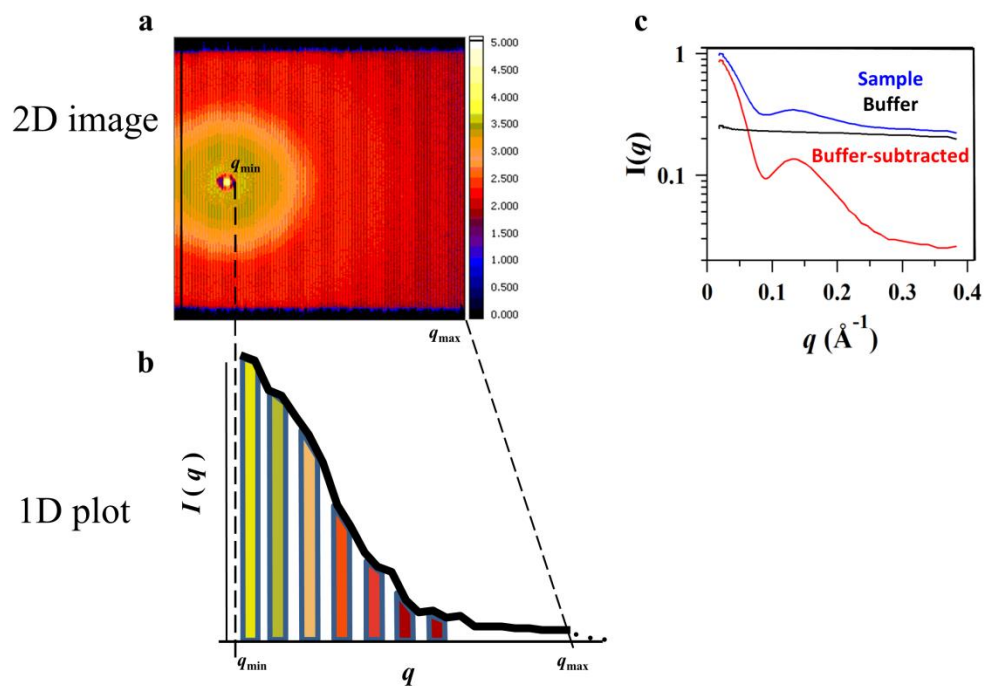


Figure 2.3 Data reduction and buffer subtraction. **a, b.** The two-dimensional detector image (**a**) is reduced to a one-dimensional plot of intensity as a function of q (**b**) by circularly averaging data around the incident beam. **c.** The scattering from a matched buffer solution (black) is similarly reduced and subtracted from the sample scattering (blue) to provide the net macromolecular scattering (red).

The scattering observed for a given macromolecule is dependent upon the squared difference in scattering length density (ρ ; electron density in the case of X-rays and nuclear/spin density for neutrons) between the macromolecule (ρ_1) and buffer (ρ_2) (Eq. 4). This difference ($\Delta\rho$) is referred to as the sample contrast.

$$I(\mathbf{q}) \propto (\rho_1 - \rho_2)^2 \quad (4)$$

The net macromolecular scattering is also proportional to the scattering from a single macromolecule averaged over all orientations. This macromolecular shape is defined by its arrangement of scattering centers, or atoms. Thus, the scattering intensity distribution for a given macromolecule can be expressed as:

$$I(\mathbf{q}) = \iint_V \Delta\rho(r_1)\Delta\rho(r_2) \frac{\sin \mathbf{q}|r_1-r_2|}{\mathbf{q}|r_1-r_2|} dr_1 dr_2 \quad (5)$$

where the volume is integrated over all pairs of scattering centers or atoms, r_1 and r_2 , located within the macromolecule.

The measured scattering pattern is the product of this macromolecular distribution, or form factor, and the solution's structure factor: $I(\mathbf{q}) = F(\mathbf{q}) * S(\mathbf{q})$. The form factor $F(\mathbf{q})$ describes the particle shape, while the structure factor $S(\mathbf{q})$ adjusts for any interparticle interference or matrix effects. If the system is considered to be dilute and non-interacting, the structure factor approximates 1, and the observed scattering is simply due to the macromolecular form factor. The form factor is also provided by a Fourier transform of the macromolecule's distance distribution function. The distance distribution function $g(r)$ describes the frequency (or probability) of certain distances of separation r within the macromolecule as:

$$g(r) = \frac{r^2}{2\pi^2} \int_0^\infty I(\mathbf{q}) \frac{\sin qr}{qr} \mathbf{q}^2 d\mathbf{q} \quad (6)$$

2.1.1 Small-angle X-ray scattering

Small-angle X-ray scattering experiments were first performed in the late 1930's by André Guinier, who demonstrated a relationship between particle size (radius of gyration, R_g) and intensities measured at very low scattering angles (14). Subsequent developments in the method came from Peter Debye (16), Otto Kratky (17-19), and Gunther Porod (20), among others (6, 8, 21). The discovery of synchrotron radiation in 1946, and further development and availability of stable, high flux, and high brilliance photon sources have greatly accelerated research in X-ray applications, including SAXS. In the 1990's, advances in data analysis and computation provided methods for *ab initio* modeling of biological macromolecular complexes (22, 23), and the use of rigid body refinement techniques (24, 25). SAXS remains a popular tool for biochemical investigations involving structural or conformational changes in solution (26), such as complex formation (27), ligand binding (28), or protein folding (29).

X-rays, first detected by Wilhelm Röntgen in 1895, are a form of electromagnetic radiation, classified by a wavelength in the range of 0.1-100 Å and energies in the range of 100 eV to 100 keV. The wavelength typically used for biological SAXS studies is ~1.5 Å (~8 keV), corresponding to the Cu- $K_{\alpha 1}$ emission used in traditional copper anode sources. At this wavelength and energy, X-rays are classified as “hard” X-rays and are highly penetrating to most matter. Although most of the X-rays pass through the sample unaffected, a small fraction (~1%) interact with electrons in the sample, and are scattered elastically (without change in energy) and isotropically (in all directions). Constructive

interference occurs between these scattered X-rays at an angle dependent on their distance of separation, as previously described.

The total, or absolute scale, of the scattered intensities contains no information about the macromolecule shape, and is only of interest for determining number densities (concentrations) or molecular weights (see 2.2.1 Zero-angle scattering). However, the scattering profile (intensity as a function of momentum transfer) contains a variety of information describing the macromolecular size and shape. A radius of gyration, or average distance between atoms in the macromolecule and the macromolecule's center of mass, can be determined using a Guinier approximation of the low- q data (see 2.2.1 Guinier analysis), which includes no prior assumption about the macromolecular shape (14). Information about the macromolecular size and shape can also be determined by reconstructing an *ab initio* model from the experimental data (30). Similarly, the particle's form factor (Eq. 5) can also be geometrically modeled and fit to the corresponding experimental data to establish the macromolecule's size and shape (15)(Figure 2.4).

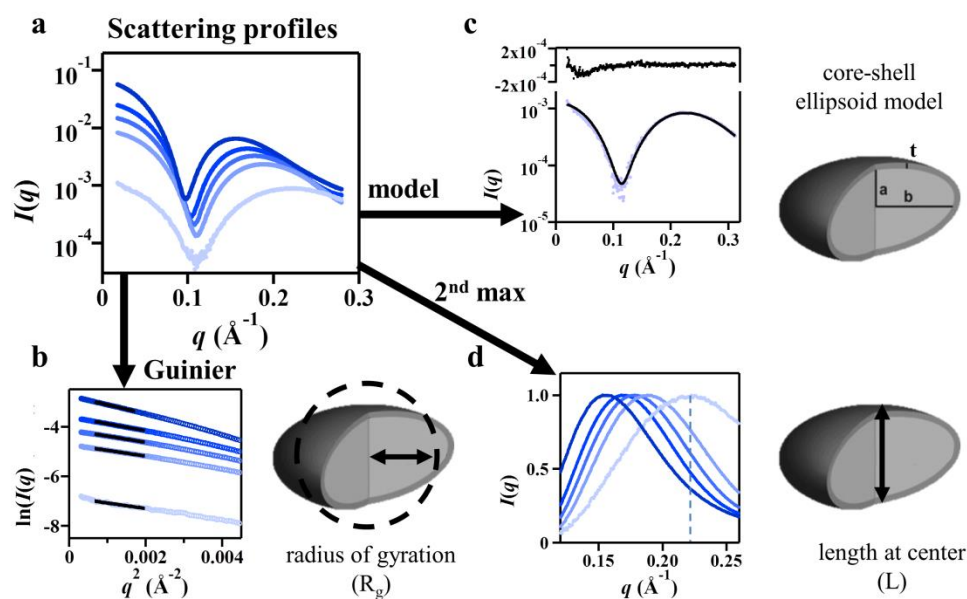


Figure 2.4 Regions of scattering profiles used for different analysis approaches. a. scattering profiles for core-shell ellipsoid-like macromolecules are used in this example. Three general approaches to gathering structural information about the macromolecule are presented. **b.** A Guinier plot is used to determine structural parameters, such as radius of gyration, directly from the slope of the scattering profile. **c.** The position of a second maximum is used to determine the most frequently occurring spacing across the core between shells, corresponding to a thickness near the ellipsoid center. **d.** The entire scattering profile can be used for model fitting. The approaches used depend on the system being studied and properties to be investigated.

2.1.2 *Small-angle neutron scattering*

Neutrons, discovered in 1932 by James Chadwick, are subatomic particles with no net charge. These particles can be produced from nuclear chain reactions at relatively high speeds and focused into beams having transverse wave properties (based on wave-particle duality) with wavelengths of $\sim 5 \text{ \AA}$ suitable for biological scattering experiments (31). Neutrons are electrically neutral, allowing them to penetrate the electronic shell and interact with atomic nuclei. Neutrons also have a mass, nuclear spin, and magnetic moment which interact with these same properties of target nuclei. Thus, their interactions with different elements are more complicated than X-rays.

Unlike X-ray interactions dependent on electron density, the neutron scattering lengths between each element, and even isotopes of the same element, vary quite randomly. That is, effective scattering power increases systematically with atomic number for X-ray interactions, but not in the case of neutrons. Table 2.1 depicts this variation among some common elements in biological studies, and a comparison to their X-ray counterparts (32). The distinction between hydrogen and deuterium isotopes in neutron scattering is particularly of interest in biological SANS studies. In most systems, hydrogen can be exchanged for deuterium with very little consequence on the chemical properties, but drastic effects on the observed neutron scattering. Additionally, hydrogen contains a large incoherent scattering cross-section as well, which is a significant source of noise and requires the path length of sample be kept to a minimum.

The information obtained from SANS experiments is complementary to that of SAXS, and both contain information about the correlated distances between atoms within

the macromolecule. Additionally, the difference in wavelengths used in SAXS and SANS is accounted for in q , thus, a direct comparison can be made between the arbitrarily scaled scattering profiles from SAXS and SANS experiments. Likewise, interpretations of the data and mathematical formalisms can be equally applied to both. The major consideration for SANS experiments is that the contrast originates from elemental composition, whereas SAXS is sensitive only to number of electrons, and indiscriminate of nuclear properties.

Element	Neutron scattering lengths (10^{-12} cm)	X-ray scattering lengths (10^{-12} cm)
Hydrogen	-0.374	0.282
Deuterium	0.667	0.282
Carbon	0.665	1.69
Nitrogen	0.940	1.97
Oxygen	0.580	2.16
Phosphorus	0.510	3.23
Sulfur	0.280	4.51

Table 2.1 Neutron and X-ray scattering lengths for common elements in biological studies.

2.1.3 Sample requirements and instrument setup

One critical requirement for collecting quality SAXS or SANS data is preparing a monodisperse sample with only the macromolecule of interest in buffered solution. The relatively large focal area of the beam irradiates numerous particles, and provides an average of all exposed particles. Polydispersity, or populations of similar-size molecules, will contribute to the net scattering and present a bias in the data. All solutions should be filtered (0.2 micron) and degassed to eliminate large contaminants, as well as air bubbles, as these can cause reflections of the X-ray beam into the scattering region. Likewise, the buffer used for background subtraction should be identical to the sample matrix and only lack the macromolecule of interest.

Mild polydispersity due to aggregation or interparticle effects may be evident by upward or downward inflections in the scattering profile as zero-scattering angle is approached. A concentration series of the macromolecule of interest is often prepared to determine any concentration-dependence of these effects. In cases where aggregation is suspected to be dependent on radiation exposure, a series of shorter exposures may be taken at intervals (to allow diffusion of aggregate from the exposed area) and averaged together. The use of a flow cell accelerates this replacement of exposed sample in the beam path with new sample between exposures (33). For additional considerations regarding the collection of quality scattering data for structural biology applications, a comprehensive review of the topic by D. Jacques and J. Trewhella is recommended (8).

The instrumental configuration is fairly straightforward, and designed to measure scattered radiation at angles near the incident beam. Small-angle scattering (SAS)

experiments commonly employ a two-dimensional CCD (charge-coupled device) detector downstream of the sample environment to record the incident and scattered radiation. The primary concern for instrument setup is distinguishing the scattered radiation from the incident beam at such low angles. This often requires a rather large distance of separation between the sample and detector. Additionally, the presence of molecules in the air contributes to incoherent background scattering, but can be minimized with evacuated chambers. The direct beam transmitted through the sample is also orders of magnitude greater in intensity than the scattered component. A material capable of blocking the direct beam is usually suspended between the sample and detector to prevent the direct beam from damaging the detector. For scaling purposes to compensate for variations in beam flux between samples, the intensity of the incident beam is measured using an attenuated beam or with a semi-transparent beam stop.

Although laboratory-size SAXS instruments using X-ray generators are available, the weak scattering from dilute solutions of biomolecules typically requires the much higher brilliance of a synchrotron radiation beam. The synchrotron beamline 12-ID-C,D at Argonne National Laboratory's Advanced Photon Source (ANL-APS) produces a flux of $\sim 1 \times 10^{13}$ photons/sec from an undulating source, which passes through a Si(111) monochromator, producing a 1 mm x 1 mm focused beam on the sample (34). By comparison, a rotating anode X-ray generator is only capable of producing $\sim 1 \times 10^{10}$ photons/sec/mm² (35). This reduced flux requires much longer exposure times for benchtop SAXS instruments, with increased incoherent and background scattering resulting in poorer signal-to-noise and statistics as well (Figure 2.5).

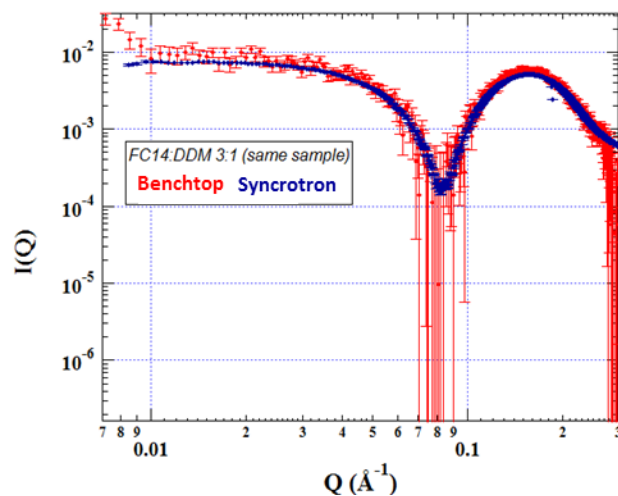


Figure 2.5 Comparison of benchtop and synchrotron SAXS data. This plot provides a comparison of data from the same sample collected on both a laboratory benchtop SAXS instrument (Rigaku) and at a synchrotron source (APS). While the overall shape of the profile is similar, and data is collected over a similar q -range, the statistical confidence for measured intensities from the benchtop SAXS is greatly reduced compared to the synchrotron source. Total exposure times for sample and buffer were 1 sec at the synchrotron, while benchtop data were collected over 8 hours.

2.2 Applications and interpretation of scattering data

SAS experiments provide many ways to extract useful information, typically involving global conformational changes in proteins, or other large macromolecules. Such information has been used to investigate ligand binding, protein-protein association, multisubunit oligomerization, and protein folding/unfolding. However, interpretation of the scattering data to determine the relevant structural details is not always a straightforward process, and presents many challenges to the investigator. The remainder of this section will outline some of the common approaches to extracting structural information from scattering data.

2.2.1 Zero-angle scattering and Guinier analysis

Two parameters, the zero-angle scattering $I(0)$ and macromolecular radius of gyration R_g , can be determined directly from the scattering profile using a Guinier analysis of the very low angle (typically $q < 0.05$) scattering data. The zero-angle scattering is the intensity of scattered radiation in parallel with the incident beam at $q = 0$. However, due to transmission of the direct beam through the sample, this component cannot be measured directly and must be extrapolated. The Guinier approximation is defined as:

$$I(q) \approx I(0) \cdot e^{\frac{-R_g^2 q^2}{3}} \quad (7)$$

with an upper limit defined as $q \cdot R_g \leq 1.3$. A plot of the natural log of scattered intensities versus q^2 (referred to as a Guinier plot) reveals a linear portion of the data below this limit, and is commonly used for extrapolation of the zero-angle component. In addition,

the slope of this linear region (rf. Figure 2.4) is used to calculate a radius of gyration for the macromolecule.

Recall that the value of the scattered intensity is typically in arbitrary units, but can be scaled using known standards and concentrations. Thus, a calibration curve can be constructed to determine unknown properties based on the relationship:

$$I(0) \propto \frac{N}{V} (\rho_p - \rho_s)^2 V_p^2 \quad (8)$$

where N is the number of macromolecules in an illuminated volume V , ρ_p is the scattering length density of the particle, ρ_s is the scattering length density of the solvent, and V_p is the volume of the macromolecule. This process is often used to determine the molecular weight of an unknown protein or complex using the formula

$$MW_P = I(0)_P / c_P \frac{MW_{Std}}{I(0)_{Std} / c_{Std}} \quad (9)$$

where MW_P and MW_{Std} are molecular weights of unknown and standard, respectively, $I(0)_P$ and $I(0)_{Std}$ are the scattering intensities at zero angle, and c_P and c_{Std} are the concentrations (36). The Guinier analysis does not require fitting to the scattering data and makes no assumptions about the shape or geometry of the macromolecule (*i.e.* model-free).

2.2.2 Form-factor models

Another approach to determining macromolecular size and shape from SAXS data is to apply geometric models, which can be fit either directly to the form factor of the scattering profile or to the corresponding distance distribution function (Eq. 6) (15, 32). If

electron densities (contrast) of components are known, unknown parameters such as axial dimensions and geometric constraints can be obtained through least-squares fitting to the experimental data. Figure 2.6 illustrates this relationship between model geometry and expected scattering profile, as well as corresponding distance distribution function $g(r)$ (Eq 6).

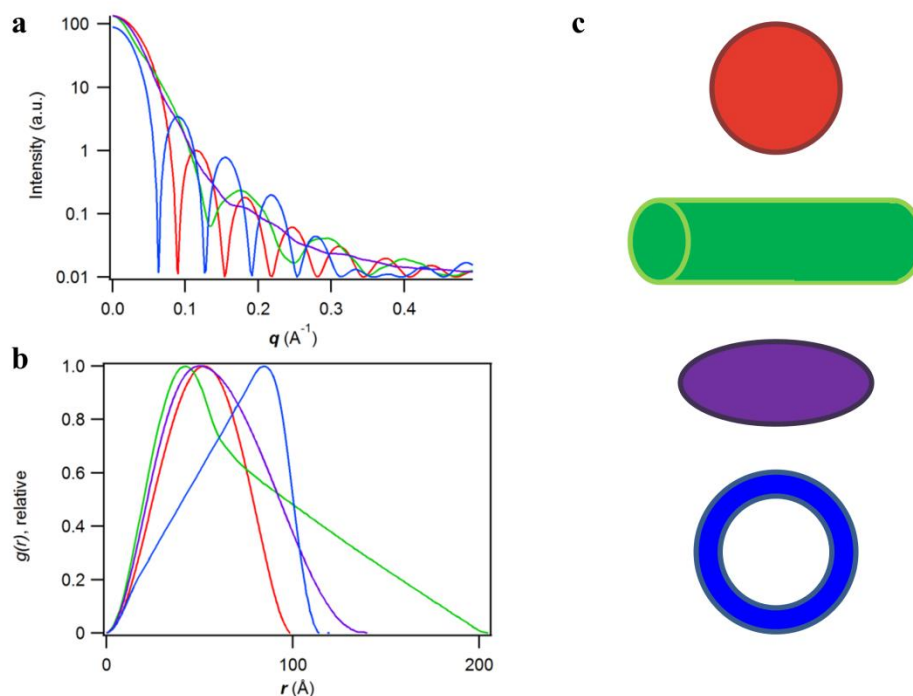


Figure 2.6 Expected scattering profiles and corresponding distance distributions for various geometric model form factors. **a.** Predicted scattering profiles of four geometric models: sphere (red), cylinder (green), oblate ellipsoid (purple), and hollow sphere (blue). The scattering profile corresponds to the form factor describing the model shape. **b.** Matching distance distribution functions $g(r)$ for each model shape describing the relative probabilities as a function of distance between two points within the model. The maximum particle dimension is indicated by the non-zero intersection with the x-axis. **c.** Schematics of geometric models used to generate scattering profiles and $g(r)$ for panels **a** and **b**. Particle scattering length density contrast was the same for each model, and a constant model volume was maintained. Additional descriptions of dimensions include: sphere, 50 \AA radius; cylinder, 28.9 \AA radius and 200 \AA length; oblate ellipsoid, 25.5 \AA rotational axis and 70 \AA elliptical axis; hollow sphere, 40 \AA inner radius and 57.4 \AA outer radius.

2.2.3 Contrast variation experiments using SANS

As previously described, hydrogen and deuterium have significantly different scattering lengths, which directly influence the contrast between buffer and macromolecule. Contrast variation experiments with neutron scattering exploit this difference, and are used to resolve the shape and relative position between deuterium-labelled and unlabeled components in a complex. Similar to other scattering experiments, scattering from buffer is collected and subtracted from that of the sample, but data are measured at multiple contrast points, or concentrations of D₂O in the buffer. If the sample contains two associated components forming a complex, and one component has been labelled with excess deuterium, then the scattering observed at each contrast point is defined as:

$$I(\mathbf{q}) = \Delta\rho_1^2 I_{11}(\mathbf{q}) + \Delta\rho_2^2 I_{22}(\mathbf{q}) + \Delta\rho_1 \Delta\rho_2 I_{12}(\mathbf{q}) \quad (9)$$

where $I_{11}(\mathbf{q})$ and $I_{22}(\mathbf{q})$ describe the basic scattering functions originating from each component, and $I_{12}(\mathbf{q})$ represents the cross-term scattering.

In the case of protein-protein complexes, the contrast between components is usually achieved by recombinantly expressing one of the proteins in a deuterium oxide growth media. Complete deuteration can only be achieved by using perdeuterated carbon sources as well (*i.e.* glucose or glycerol) (37). Deuteration level of the protein can be assessed via mass spectrometry and total solution levels by IR spectroscopy. DNA and protein have inherent differences in scattering length density which provide sufficient natural contrast for contrast variation experiments of these complexes (8). The commercial availability of deuterium-labeled lipids and detergents allows the contrast to

be manipulated in aggregate structures such as micelles and bicelles, as well as protein-detergent complexes.

2.3 Scattering and detergent micelles

Small-angle scattering experiments have been used to determine physical properties and structural characteristics of micelle-forming detergent solutions since the 1960s (38), and their use as membrane mimics in studies of membrane proteins has rekindled this interest (39). In addition to a radius of gyration, micelle aggregation numbers can be determined for micelles using known standards and a calibration curve in a manner similar to the molecular weight determination for an unknown protein. A characteristic second maximum in the scattering intensity (rf. Figure 2.4) also provides a direct measurement of the head group-head group spacing across the micelle core (15). Furthermore, geometric model fits to the experimental data provide micelle size and shape parameters.

2.3.1 *Micelle aggregation numbers*

The micelle's aggregation number can be determined from a series of protein standards, but the relationship must account for the difference in electron density and contrast between detergent and protein. By calculating the expected zero-angle scattering due to a single monomer and comparing that to the observed zero-angle scattering, the number of detergent monomers per micelle is provided. Therefore, the following relationship is used:

$$N = \frac{I(0)_{mic}}{I(0)_{mon}} = \frac{I(0)_{mic}}{K(c-cmc)(\rho_{mic}-\rho_s)^2V_{mon}^2} \quad (10)$$

where V_{mon} is the volume of a detergent monomer, $c - cmc$ represents the concentration of micelle-forming detergent, $\rho_{mic} - \rho_s$ is the contrast between micelle and solvent, and K is a proportionality constant determined from standards of known concentration, volume, and electron density.

2.3.2 *Micelle core-shell models*

Membrane mimics, such as bicelles and micelles, are described by hydrocarbon-like inner cores surrounded by an outer shell of the surfactant head groups. Therefore, geometric core-shell models can be constructed for interpretation of SAXS data having an electron density ρ_1 , corresponding to the hydrocarbon core, ρ_2 , corresponding to the head group shell, and ρ_s , corresponding to the solvent. The geometric properties of each model can be used to systematically investigate various shapes and dimensions of the macromolecule by fitting to its experimental scattering profile.

More specifically, a series of similar models may be used to determine the best-fit model that describes the shape of the macromolecule in solution using least-squares fitting of the predicted form factor to the experimental data. This process can be used to refine structural information about the macromolecule, and typically incorporates the entire range of scattered data. The sensitivity of different q -regimes and resulting form factors from examples of different core-shell model shapes, overall sizes, and shell thicknesses are demonstrated in Figure 2.7. In this figure, the core-shell shape models all contain equivalent volumes of core and shell with equal scattering length densities, thus overlap in the low- q Guinier region and have a similar $I(0)$. Discrepancies between the geometric shapes used become apparent in the higher- q data ($0.1 < q < 0.3$).

Macromolecular size is readily apparent by the slope of the Guinier region; larger particles produce a steeper slope at low- q . Features of the model can also be systematically varied, such as shell thickness of core-shell models.

The ellipsoid model contains a core having semi-axes a and b with an outer shell defined by the head group, having a uniform thickness t . Thus, the particle form factor for the ellipsoid micelle is given by

$$P(q) = \int_0^1 (3V_1(\rho_1 - \rho_2) \frac{j_1(u_1)}{u_1} + 3(V_1 + V_2)(\rho_2 - \rho_s) \frac{j_1(u_2)}{u_2})^2 \quad (11)$$

where $u_1 = q(a^2x^2 + b^2(1 - x^2))^{1/2}$, $u_2 = q(a + t)^2x^2 + (b + t)^2(1 - x^2))^{1/2}$, the core volume $V_1 = \frac{4}{3}\pi ab^2$, and the total volume $V_1 + V_2 = \frac{4}{3}\pi(a + t)(b + t)^2$. For $a < b$, the ellipsoid is oblate, and, for $a > b$, it is prolate. A nonlinear least-squares fitting routine implemented in Igor Pro (WaveMetrics) as part of the NCNR analysis toolkit (40) was used to fit two-component (core-shell) prolate and oblate ellipsoids (as well as spherical and cylindrical models) to the full scattering profiles. Best-fit models were chosen based on lowest residuals. Although designed for model fits to neutron scattering profiles, this procedure was readily adapted to produce SAXS profiles by replacing the nuclear scattering length densities with electron densities. If two models appear to fit the data equally well, potential steric violations in each model should be considered first. For example, a minor axis length corresponding to an alkyl chain length that is longer than the maximum possible extended chain length results in an invalid model. Additionally, the model-independent measurement of micelle parameters must agree with the model parameters to validate the best model choice.

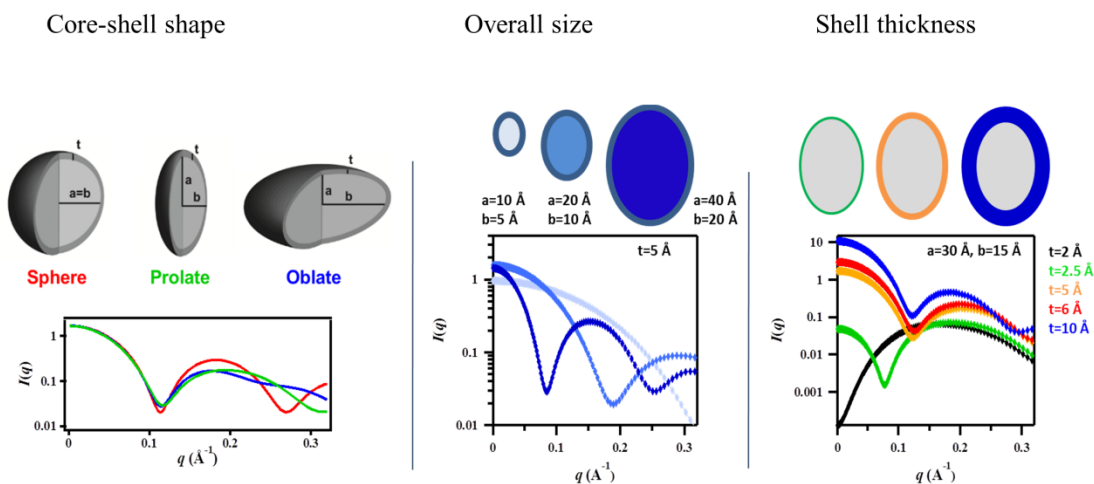


Figure 2.7 Examples of core-shell geometric models and simulated SAXS profiles.

Equivalent volumes and scattering densities were used to construct core-shell models of spherical (red), prolate ellipsoid (green), and oblate ellipsoid (blue) shapes. Using this prolate ellipsoid geometry, examples of the effects of overall size are demonstrated. A larger particle size results in a steeper slope at low- q . Effects of shell thickness in the core-shell model are also presented for five shell thicknesses.

2.3.3 *Micelle hydrophobic core thickness*

The hydrophobic core thickness (L) describes the length of the shortest elliptical dimension across the center of the micelle, occurring between opposing head groups (rf. Figure 2.4d). The more frequent occurrence of this head group spacing along this dimension (as opposed to the dimension containing the more highly curved surface of the ellipsoid) manifests as a maximum in the scattering profile in the mid- q ($0.1 < q < 0.3$) scattering region (15). Thus, this distance can be determined directly from the peak maximum position in the scattering profile (q_{max}) using the relationship $L_{expt} = 2\pi/q_{max}$. A similar measurement can be made from the core-shell models according to $L_{model} = 2*(a+t/2)$ for oblate and $2*(b+t/2)$ for prolate. This distance has interesting implications for the alkyl chain length of the detergent used, as it includes a reasonable estimate of the extended alkyl chain length. As such, this distance must not exceed a defined length given by a maximum extension of the alkyl chain. Descriptions of micelle size and shape, with specific attention to the impact of alkyl chain length and head group properties, will be the focus of the following chapter.

2.4 Scattering and protein-detergent complexes

In crystallography, the detergent domains surrounding the protein in the PDC crystal are usually too dynamic and therefore not resolved. However, low resolution (13-16 Å) neutron diffraction methods have been used to study the detergent domains in four membrane protein-crystal systems: the reaction center from *R. sphaeroides* in octyl glucoside (41), the reaction center from *R. viridis* in N,N-dimethyldodecylamine oxide, DDAO (42), a tetragonal crystal of OmpF porin trimers in octyl glucoside and N,N-

dimethyldecylamino oxide, C₁₀DAO (43), and a trigonal crystal of OmpF porin trimers in *n*-octyl-2-hydroxyethylsulfoxide and decaethylene glycol *n*-octyl ether, C₈E₁₀ (44). Except in the case of the trigonal crystal where protein-protein contacts appear to disrupt detergent packing, the detergent forms a continuous belt around the transmembrane portion of the membrane proteins and extends 15-20 Å from the protein/detergent interface. These results support the early hypothesis that detergents cover regions typically exposed to lipids in bilayers (45, 46).

Only a few scattering experiments have been performed on protein-detergent complexes, but have revealed unique insights about protein and detergent interactions (47, 48). Scattering methods are suitable for determining overall PDC size and shape in solution, and natural contrast between detergent and protein is an added benefit for contrast variation methods and attempts to resolve these individual components. Contrast variation experiments are often used to determine the extent of detergent binding in PDCs by measuring contrast match point of the complex and the expression:

$$x = \frac{(\rho_P - \rho_S)v_P}{(\rho_P - \rho_S)v_P - (\rho_D - \rho_S)v_D} \quad (12)$$

where x is the mass fraction of detergent in the complex; v_P and v_D are partial specific volumes of the protein and detergent, respectively; and ρ_P , ρ_D , and ρ_S are scattering length densities of the protein at the match point of the complex, the detergent at the match point of the complex, and the solvent, respectively. This method was applied to determine the oligomeric state of Photosystem I (PSI), as well as amount of associated detergent (49), and associated detergent with a porin from *E. coli* solubilized in C₈E₄ (50).

In addition to quantifying the associated detergent in PDCs, small-angle neutron scattering has also been used to examine PDC size and shape. These experiments require the use of contrast variation as well in order to resolve the detergent and protein components independently; however, contrasts exist between both protein and detergent, as well as each of these components with solvent, and may complicate preparation and interpretation of the results. In one example, complexes of rhodopsin and polyoxyethylene alcohol detergents were prepared in buffer with varying H₂O:D₂O ratios and with varying composition of deuterated-tail detergents (48). This process allowed the detergent component of the complex to be completely solvent matched, thus eliminating its contribution to the observed scattering and revealing information about the protein component alone, as well as the overall complex.

2.5 References

1. Gaboriaud, F., A. Nonat, D. Chaumont, and A. Craievich. 1999. Aggregation and gel formation in basic silico-calco-alkaline solutions studied: A saxs, sans, and els study. *The Journal of Physical Chemistry B* 103:5775-5781.
2. Ballauff, M. 2001. Saxs and sans studies of polymer colloids. *Current opinion in colloid & interface science* 6:132-139.
3. Nilsson, F., O. Söderman, and I. Johansson. 1996. Physical-chemical properties of the n-octyl β -d-glucoside/water system. A phase diagram, self-diffusion nmr, and saxs study. *Langmuir* 12:902-908.
4. Kostorz, G. 1991. Small-angle scattering studies of phase separation and defects in inorganic materials. *Journal of Applied Crystallography* 24:444-456.

5. Fratzl, P. 2003. Small-angle scattering in materials science-a short review of applications in alloys, ceramics and composite materials. *Journal of Applied Crystallography* 36:397-404.
6. Lipfert, J., and S. Doniach. 2007. Small-angle x-ray scattering from rna, proteins, and protein complexes. *Annu Rev Biophys Biomol Struct* 36:307-327.
7. Koch, M. H., P. Vachette, and D. I. Svergun. 2003. Small-angle scattering: A view on the properties, structures and structural changes of biological macromolecules in solution. *Quarterly reviews of biophysics* 36:147-227.
8. Jacques, D. A., and J. Trehwella. 2010. Small-angle scattering for structural biology-expanding the frontier while avoiding the pitfalls. *Protein Science* 19:642-657.
9. Cowieson, N. P., B. Kobe, and J. L. Martin. 2008. United we stand: Combining structural methods. *Current Opinion in Structural Biology* 18:617-622.
10. Grishaev, A., J. Wu, J. Trehwella, and A. Bax. 2005. Refinement of multidomain protein structures by combination of solution small-angle x-ray scattering and nmr data. *Journal of the American Chemical Society* 127:16621-16628.
11. Putnam, C. D., M. Hammel, G. L. Hura, and J. A. Tainer. 2007. X-ray solution scattering (saxs) combined with crystallography and computation: Defining accurate macromolecular structures, conformations and assemblies in solution. *Quarterly reviews of biophysics* 40:191-285.
12. Svergun, D. I., M. V. Petoukhov, and M. H. Koch. 2001. Determination of domain structure of proteins from x-ray solution scattering. *Biophysical Journal* 80:2946-2953.

13. Pedersen, J. S. 1997. Analysis of small-angle scattering data from colloids and polymer solutions: Modeling and least-squares fitting. *Advances in Colloid and Interface Science* 70:171-210.
14. Guinier, A. 1939. La diffraction des rayons x aux tres petits angles: Applications a l'etude de phenomenes ultramicroscopiques. *Annales de physique* 11.Sér. 12.1939:161-237.
15. Lipfert, J., L. Columbus, V. B. Chu, S. A. Lesley, and S. Doniach. 2007. Size and shape of detergent micelles determined by small-angle x-ray scattering. *The Journal of Physical Chemistry B* 111:12427-12438.
16. Debye, P. 1949. Light scattering in soap solutions. *Annals of the New York Academy of Sciences* 51:575-592.
17. Kratky, O., I. Pilz, and P. Schmitz. 1966. Absolute intensity measurement of small angle x-ray scattering by means of a standard sample. *Journal of colloid and interface science* 21:24-34.
18. Glatter, O., and O. Kratky. 1982. Small angle x-ray scattering editors. Vol. 102. Academic press London.
19. Kratky, O. 1963. X-ray small angle scattering with substances of biological interest in diluted solutions. *Progress in biophysics and molecular biology* 13:105-IN1.
20. Porod, G. 1953. X-ray and light scattering by chain molecules in solution. *Journal of Polymer Science* 10:157-166.
21. Feigin, L., D. I. Svergun, and G. W. Taylor. 1987. Structure analysis by small-angle x-ray and neutron scattering editors Springer.

22. Svergun, D. I. 1999. Restoring low resolution structure of biological macromolecules from solution scattering using simulated annealing. *Biophysical Journal* 76:2879-2886.
23. Svergun, D. I., M. V. Petoukhov, and M. H. Koch. 2001. Determination of domain structure of proteins from x-ray solution scattering. *Biophysical Journal* 80:2946-53.
24. Konarev, P. V., M. V. Petoukhov, and D. I. Svergun. 2001. Massha– a graphics system for rigid-body modelling of macromolecular complexes against solution scattering data. *Journal of Applied Crystallography* 34:527-532.
25. Petoukhov, M. V., and D. I. Svergun. 2005. Global rigid body modeling of macromolecular complexes against small-angle scattering data. *Biophysical Journal* 89:1237-1250.
26. Doniach, S. 2001. Changes in biomolecular conformation seen by small angle x-ray scattering. *Chemical Reviews* 101:1763-1778.
27. Rambo, R. P., and J. A. Tainer. 2010. Bridging the solution divide: Comprehensive structural analyses of dynamic rna, DNA, and protein assemblies by small-angle x-ray scattering. *Current Opinion in Structural Biology* 20:128-137.
28. Dumas, C., and J. Janin. 1983. Conformational changes in arginine kinase upon ligand binding seen by small-angle x-ray scattering. *FEBS Letters* 153:128-130.
29. Millett, I. S., S. Doniach, and K. W. Plaxco. 2002. Toward a taxonomy of the denatured state: Small angle scattering studies of unfolded proteins. *Advances in protein chemistry* 62:241-262.

30. Volkov, V. V., and D. I. Svergun. 2003. Uniqueness of ab initio shape determination in small-angle scattering. *Journal of Applied Crystallography* 36:860-864.
31. Jacrot, B. 1976. The study of biological structures by neutron scattering from solution. *Reports on Progress in Physics* 39:911-953.
32. Svergun, D. I., and M. H. J. Koch. 2003. Small-angle scattering studies of biological macromolecules in solution. *Reports on Progress in Physics* 66:1735-1782.
33. Lipfert, J., I. S. Millett, S. n. Seifert, and S. Doniach. 2006. Sample holder for small-angle x-ray scattering static and flow cell measurements. *Review of Scientific Instruments* 77:046108.
34. Argonne. Available from:
http://www.aps.anl.gov/Beamlines/Directory/beamline.php?beamline_id=19.
35. Rigaku. Available from: <http://www.rigaku.com/products/sources>.
36. Mylonas, E., and D. I. Svergun. 2007. Accuracy of molecular mass determination of proteins in solution by small-angle x-ray scattering. *Journal of Applied Crystallography* 40:s245-s249.
37. Leiting, B., F. Marsilio, and J. F. O'Connell. 1998. Predictable deuteration of recombinant proteins expressed in *Escherichia coli*. *Analytical Biochemistry* 265:351-355.
38. Reiss-Husson, F., and V. Luzzati. 1966. Small-angle x-ray scattering study of the structure of soap and detergent micelles. *Journal of colloid and interface science* 21:534-546.

39. Thiagarajan, P., and D. Tiede. 1994. Detergent micelle structure and micelle-micelle interactions determined by small-angle neutron scattering under solution conditions used for membrane protein crystallization. *The Journal of Physical Chemistry* 98:10343-10351.
40. Kline, S. R. 2006. Reduction and analysis of sabs and usabs data using igor pro. *Journal of Applied Crystallography* 39:895-900.
41. Roth, M., B. Arnoux, A. Ducruix, and F. Reiss-Husson. 1991. Structure of the detergent phase and protein-detergent interactions in crystals of the wild-type (strain y) rhodobacter sphaeroides photochemical reaction center. *Biochemistry* 30:9403-9413.
42. Roth, M., A. Lewit-Bentley, H. Michel, J. Deisenhofer, R. Huber, and D. Oesterhelt. 1989. Detergent structure in crystals of a bacterial photosynthetic reaction centre.
43. Pebay-Peyroula, E., R. Garavito, J. Rosenbusch, M. Zulauf, and P. Timmins. 1995. Detergent structure in tetragonal crystals of ompf porin. *Structure* 3:1051-1059.
44. Penel, S., E. Pebay-Peyroula, J. Rosenbusch, G. Rummel, T. Schirmer, and P. Timmins. 1998. Detergent binding in trigonal crystals of ompf porin from *Escherichia coli*. *Biochimie* 80:543-551.
45. Helenius, A., and K. Simons. 1975. Solubilization of membranes by detergents. *Biochimica et Biophysica Acta (BBA)-Reviews on Biomembranes* 415:29-79.

46. Tanford, C., and J. A. Reynolds. 1976. Characterization of membrane proteins in detergent solutions. *Biochimica et Biophysica Acta (BBA)-Reviews on Biomembranes* 457:133-170.
47. Timmins, P., E. Pebay-Peyroula, and W. Welte. 1994. Detergent organisation in solutions and in crystals of membrane proteins. *Biophysical chemistry* 53:27-36.
48. Osborne, H. B., C. Sardet, M. Michel-Villaz, and M. Chabre. 1978. Structural study of rhodopsin in detergent micelles by small-angle neutron scattering. *Journal of molecular biology* 123:177-206.
49. Schafheutle, M. E., E. Setlikova, P. A. Timmins, H. Johner, P. Gutgesell, W. Welte, and I. Setlik. 1990. Molecular weight determination of an active photosystem i preparation from a thermophilic cyanobacterium, *synechococcus elongatus*. *Biochemistry* 29:1216-1225.
50. Zulauf, M., V. Degiorgio, and M. Corti, *Physics of amphiphiles: Micelles, vesicles and microemulsions*, 1985, Academic Press: New York.

3. Physical determinants of micelle assembly

A brief introduction to the uses of detergents in studies of membrane proteins, and principles of micelle formation, were presented in chapter 1. The scattering methods outlined in chapter 2 are applied in this chapter to systematically examine the dependence of micelle size and shape on detergent alkyl chain length and head group. This work was published on May 8, 2013, in Plos One by R. Oliver, *et al.* (1). At time of publication, few experimental studies had systematically investigated the effects of detergent structure on micelle geometry. In addition, a limited number of detergents and alkyl chain lengths had been investigated and inconsistencies in buffer conditions and methodologies between studies complicated comparison of detergent micelle properties. This study experimentally correlated the detergent monomer structure with micelle physical properties so that micelle shapes and sizes can be more accurately predicted, in particular with a view towards assessment of PDC structure and function.

3.1 Overview

Detergent micelles provide an amphipathic environment similar to lipid bilayers (hydrophobic alkyl chains surrounded by hydrophilic head groups), particularly at the micelle center where detergents are arranged in an opposing tail-to-tail fashion with hydrophobic thicknesses similar to lipid bilayers. As such, detergents are important tools for solubilizing membrane proteins in functional and structural investigations *in vitro*. However, a stable and functional protein-detergent complex (PDC) is difficult to obtain, as protein denaturation and aggregation present continuous challenges. Thus, the

formation of a soluble PDC currently relies on empirical screening of many detergent conditions to minimize these detrimental effects.

To provide a basis for understanding the relationship between detergent micelle and resulting PDC, a comprehensive set of detergents commonly used for membrane proteins studies were systematically investigated. Using small-angle X-ray scattering (SAXS), micelles shapes and sizes were determined for phosphocholines with 10, 12, and 14 alkyl carbons, glucosides with 8, 9 and 10 carbons, maltosides with 8, 10 , and 12 alkyl carbons, and lysophosphatidyl glycerols with 14 and 16 alkyl carbons. The SAXS profiles are well described using two-component ellipsoid models, with an electron rich outer shell corresponding to the detergent head groups and a less electron dense hydrophobic core composed of the alkyl chains. The minor axis of the elliptical micelle core from these models is constrained by alkyl chain length, and increases by 1.2-1.5 Å per methylene addition to the alkyl chain. The major elliptical axis also increases with chain length; however, the ellipticity remains approximately constant throughout each detergent series. In addition, the aggregation number of these detergent increases by ~16 monomers per micelle for each methylene added. These results provided a comprehensive view of the determinants of micelle shape and size and provided a baseline for correlating micelle properties with protein-detergent interactions.

3.2 Introduction

Detergents have played a significant role in advancing our understanding of membrane protein structure and function; however, additional information about detergent micelle properties is needed to overcome barriers in membrane protein

research. Detergent monomers self-assemble to form micelles in solution when the detergent monomer concentration is above the critical micelle concentration (CMC), and this concentration of monomer remains in equilibrium with the formed micelles. Micelles adopt globular shapes (e.g. spheres, ellipsoids, and cylinders) of various sizes, determined by the head group chemistry and alkyl chain length (2). The hydrophilic head groups of the detergents comprise a solvent-exposed outer shell, while the hydrophobic alkyl chains are sequestered from water and form the micelle core.

Consequently, micelles are often employed as mimics of lipid bilayers to solubilize and stabilize integral membrane proteins for structural and functional *in vitro* studies (3-6). Although other lipid bilayer mimics, such as nanodiscs (7) and bicelles (8), are used in membrane protein studies, detergents have been more successful in high-resolution structure determination of membrane proteins. Nonetheless, stable, functional protein-detergent complexes (PDCs) are difficult to obtain because protein denaturation and aggregation often occur. Determining the optimal conditions that yield a functionally-active, folded membrane protein relies heavily on exhaustive screening of detergent conditions (detergent type, concentration, additives, etc.) (9-12). This need for empirical detergent screening stems from a lack of understanding of the physical relationships between the detergent micelle and membrane protein.

3.2.1 *Detergent monomer properties*

The sizes and shapes of micelles formed by four classes of detergents (phosphocholines, maltosides, glucosides, and lysophosphatidyl glycerols – Table 3.1 and Figure 3.1) are investigated using small-angle X-ray scattering (SAXS) in this chapter.

The detergents were selected based on their relevance to membrane protein structural biology. Approximately 40% of the ~115 membrane protein structures determined by NMR were prepared in dodecyl phosphocholine (FC12) micelles while nearly 40% of the ~1200 membrane protein structures determined by X-ray crystallography were in octyl glucoside (OG), decyl maltoside (DM), or dodecyl maltoside (DDM) micelles (13). Lysophosphatidyl glycerols (LPGs) have also demonstrated success in NMR investigations of membrane proteins (14). Multiple alkyl chain lengths for each class were studied and compared to address structural similarities within the class. Trends amongst all classes were also assessed and compared to identify common determinants of micelle structure that could be extended to predict micelle size and shape from detergent monomer properties.

Detergent (abbreviation)	FW (Da)	CMC ^a (mM)	$V_{\text{mon}}^{\text{b}}$ (\AA^3)	$\rho_{\text{det}}^{\text{c}}$ ($\text{e}/\text{\AA}^3$)	$N_{\text{lit.}}^{\text{a}}$
<i>n</i> -decylphosphocholine (FC10)	323	11	494	0.360	24, 45-53 (15)
<i>n</i> -dodecylphosphocholine (FC12)	351	1.5	548	0.354	54, 60-80 (15)
<i>n</i> -tetradecylphosphocholine (FC14)	380	0.12	602	0.348	108
<i>n</i> -octyl- β -D-glucopyranoside (OG)	292	18-20 (16)	419	0.382	87 (17), 27-100 (16)
<i>n</i> -nonyl- β -D-glucopyranoside (NG)	306	6.5 ^c	446	0.377	133
<i>n</i> -decyl- β -D-glucopyranoside (DG)	320	2.2 (18)	472	0.373	200-400 (19)
<i>n</i> -octyl- β -D-maltopyranoside (OM)	454	19.5	590	0.416	6, 26 (20)
<i>n</i> -decyl- β -D-maltopyranoside (DM)	483	1.8	644	0.407	69, 82-90 (15)
<i>n</i> -dodecyl- β -D-maltopyranoside (DDM)	511	0.17	698	0.398	132 (21), 78- 149 (22), 135- 145 (15, 23)
1-myristoyl-2-hydroxy- <i>sn</i> -glycero- 3-phosphor-(1'- <i>rac</i> -glycerol) (LMPG)	478	0.16 (24)	639	0.404	90 ^d
1-palmityl-2-hydroxy- <i>sn</i> -glycero- 3-phosphor-(1'- <i>rac</i> -glycerol) (LPPG)	507	0.018 (24)	693	0.395	160-170 (15)

Table 3.1 Physical properties of pure detergents. ^aMeasurements performed by Anatrache except where noted. CMCs are reported for conditions of detergent in H₂O, except for the CMC of OM which is reported in 20 mM HEPES, pH 7.5 with 100 mM NaCl. Aggregation numbers from ref. (15) are reported in the same buffer used in this study. ^bMonomer volumes were calculated from published specific densities, using the Tanford formula ($V_{\text{tail}} = N*(24.7 + 26.9n_c)$) for alkyl chain volumes to adjust for different chain lengths. ^cThe detergent electron density values were computed by summing the number of electrons from the chemical composition and dividing by the molecular volume. ^dA measured value was not found in the literature; although many studies report

this aggregation number. However, an estimate can be made from the PDC molecular weight reported by Tian *et al.* of ~60 kD (25) (detergent contribution of 44 kD), which yields an aggregation number of ~90.

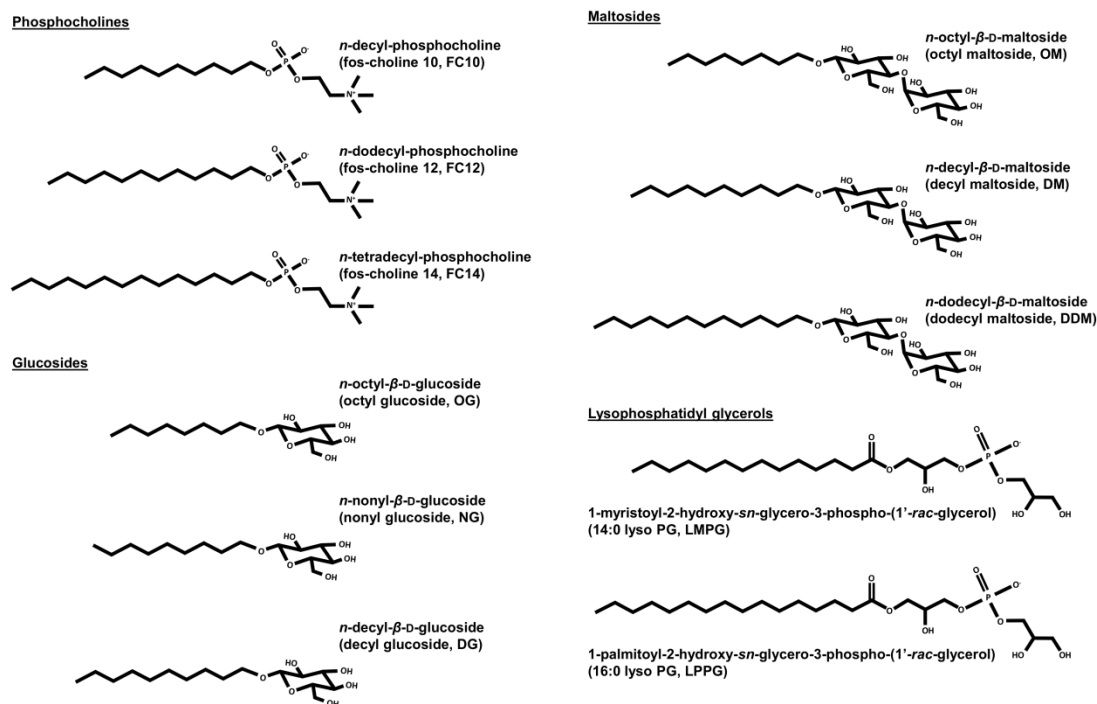


Figure 3.1 Chemical structures of detergents investigated by SAXS. Chemical structures of detergent types investigated in this study. A total of seven detergents were components of binary mixtures: phosphocholines with 10, 12, and 14 carbons in the alkyl chain (FC10/FC12/FC14), glucosides with 8, 9, and 10 carbons in the alkyl chain (OG/NG/DG), maltosides with 8, 10, and 12 carbons in the alkyl chain (OM/DM/DDM), and lysophosphatidyl glycerols with 14 and 16 carbons in the alkyl chain (LMPG/LPPG).

3.2.2 *Micelle self-assembly*

Shapes and sizes of micelles formed by the eleven detergents (Table 3.1) were collected under the same experimental conditions and in identically buffered solutions. Model independent and dependent parameters were analyzed to establish trends in micelle size and shape resulting from changes in either detergent monomer head group, alkyl chain, or both. With an increase in the alkyl chain by a single methylene group, the aggregation number (monomers per micelle) increases by 16 ± 3 detergent monomers. The shorter ellipsoid axis of the micelles increases with a distance expected for an additional alkyl carbon, while the aspect ratio (ratio of axial lengths) is maintained. These results establish ellipsoid micelle models that are consistent throughout a detergent series, which provides predictive measures for other detergent micelle sizes and shapes.

3.2.3 *Implications for protein-detergent complexes*

Micelle size, shape, and detergent concentration should be considered when evaluating a PDC for structural and biochemical studies. Evidence suggests that the micelle hydrophobic thickness must match that of the membrane protein to maintain proper fold and function (26-28) (similar to the hydrophobic match proposed for membrane proteins in bilayers (29-33)). The micelle volume must be sufficient to accommodate the membrane protein of interest as well. Therefore, a systematic investigation of the size and shape determinants of pure micelles will provide a baseline and foundation for a further understanding of micelle-protein interactions. The concentration of detergent must also be considered, as free detergent monomers exist in solution up to concentrations equal to the CMC. Thus, detergent concentration must be

sufficient to form micelles, but it can affect PDC stability by influencing micelle size and shape.

3.3 Results and discussion

3.3.1 Validation of core-shell models

Comparisons between parameters determined from both geometric models and the scattering profile (model-independent) validate the core-shell ellipsoid models. Agreement between the models and the model-independent values for radius of gyration (R_g), aggregation number (N), and dominant head group to head group length (L) strongly support the proposed ellipsoid models (Figure 3.2).

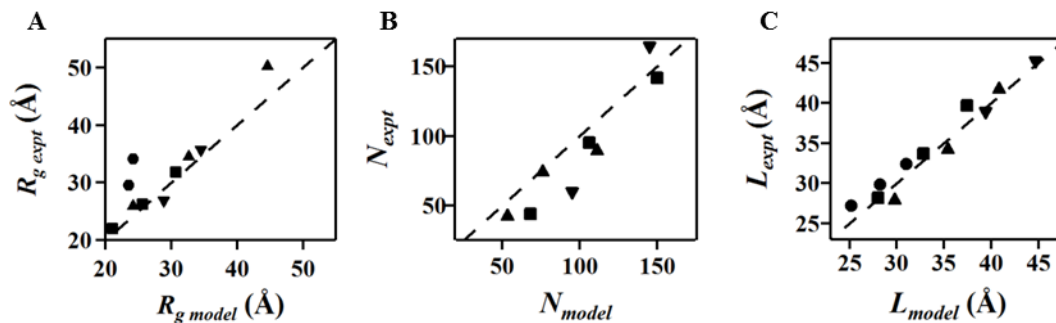


Figure 3.2 Correlation plots of model dependent vs. independent parameters.

Relationships between measurements from the core-shell model fit to the SAXS profile and model-independent measurements are shown for phosphocholine (▲), maltoside (■), glucoside (●), and lysophosphatidyl glycerol (▼) head groups. These comparisons were performed for radii of gyration (A), aggregation number (B), and head group distance across the micelle (C) to verify that the model results were consistent with features of the SAXS profile. Dashed lines indicate absolute correlation between values.

3.3.2 Effects of alkyl chain length

The dependence of micelle physical parameters on chain length and head group was investigated using data from different detergent types with systematic variations in alkyl chain length. The dominant head group – head group distances calculated from the best fit models for each detergent micelle studied (L_{model}) are plotted as a function of alkyl chain length in Figure 3.3B. The dominant distance between head groups across the micelle increases by 2.5 – 3.0 Å with each methylene added to the alkyl chain in each class of detergents studied (this distance corresponds to two opposing alkyl chains in the micelle, and thus the contributions from two methylene groups). The short ellipsoid axis dimension increases by ~2.5 Å for every two carbons added to the alkyl chain for the phosphocholines, ~2.4 Å for every two carbons added to the alkyl chain for the maltosides, ~1.5 Å for each carbon added to the alkyl chain for the glucosides, and ~2.5 Å for the two carbon increase in the LPG tail length (Table 3.2). The average increase in alkyl chain length per added carbon unit for all micelles in this study is approximately 1.31 ± 0.13 Å (length of shorter elliptical axis (a or b) divided by the number of alkyl chain carbons), which agrees with the length expected from Tanford's formula (34) for the addition of each methylene group: 1.265 Å for the maximum extension of the alkyl chain ($l_c = 1.5 + 1.265 n_c$).

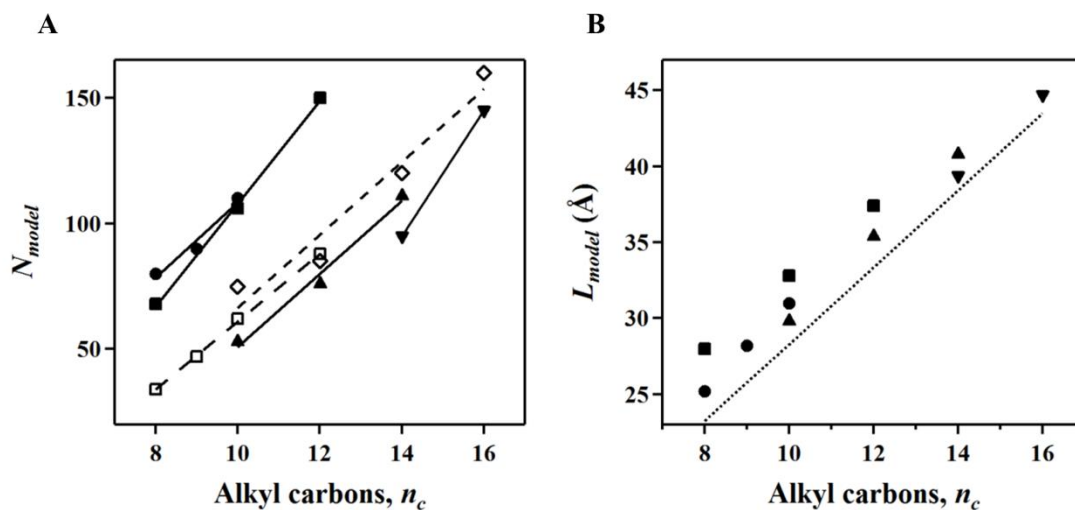


Figure 3.3 Dependence of aggregation number and micelle thickness on alkyl chain length. (A) The aggregation numbers determined from the hydrophobic core volume (N_{model}) are plotted against the number of carbons comprising the alkyl chain (n_c) for phosphocholine (▲), maltoside (■), glucoside (●), and lysophosphatidyl glycerol (▼) detergents measured in this study, as well as (N-alkylamino)-1-deoxylactitol (35) (□), and sucrose ester (36) (◇) head groups from other studies. Equations and quality of fit for each linear series are as follows: (▲), $N = 14.5 n_c - 94$, $R^2 = 0.986$; (■), $N = 20.5 n_c - 97$, $R^2 = 0.998$; (●), $N = 15.0 n_c - 42$, $R^2 = 0.964$; (□), $N = 13.5 n_c - 75$, $R^2 = 0.999$; (◇), $N = 14.5 n_c - 79$, $R^2 = 0.944$. Lysophosphatidyl glycerol fits are not reported since there are only two data points in the series. (B) The dominant distances between head groups across the micelle determined from the best model fit for each detergent (L_{model}) are plotted as a function of the number of carbons in the alkyl chain. The dotted line represents the distance of two alkyl chains having a fully extended hydrocarbon chain according to Tanford's formula for alkyl chain length (34).

detergent	shape	ρ_1 ($e/\text{\AA}^3$)	ρ_2 ($e/\text{\AA}^3$)	a (\AA)	b (\AA)	t (\AA)	a/b	R_g^{expt} (\AA)	R_g^{model} (\AA)	L^{expt} (\AA)	L^{model} (\AA)	N^{expt}	N^{model}
FC10 (59 mM)	prolate	0.273	0.490	20.4- 20.9	13.3- 13.6	2.7- 3.0	1.52- 1.55	25.9 ± 0.2	24.2 ± 0.5	27.6- 28.2	29.3- 30.2	39- 45	50- 56
FC12 (77 mM)	prolate	0.277	0.490	24.3- 24.8	16.1- 16.4	2.7- 3.0	1.49- 1.52	34.5 ± 0.8	32.6 ± 0.5	33.9- 34.5	34.9- 35.8	68- 80	72- 80
FC14 (97 mM)	prolate	0.280	0.490	29.6- 30.1	18.8- 19.1	2.7- 3.0	1.57- 1.60	50.2 ^a ± 3.7	44.6 ± 0.5	41.4- 42.0	40.3- 41.2	88- 91	106- 116
OG (50 mM)	oblate	0.268	0.540	10.6- 11.4	20.6- 21.4	2.9- 3.5	0.51- 0.55	29.6 ^b ± 2.2	23.5 ± 0.5	26.9- 27.5	24.1- 26.3	n.d. ^b	70- 90
NG (50 mM)	oblate	0.271	0.540	12.1- 12.9	20.7- 21.5	2.9- 3.5	0.58- 0.62	34.2 ^b ± 2.3	24.2 ± 0.5	29.6- 30.2	27.1- 29.3	n.d. ^b	80- 100
DG (50 mM)	oblate	0.273	0.540	13.5- 14.3	22.6- 23.4	2.9- 3.5	0.60- 0.64	n.d. ^b	27.5 ± 0.5	32.1- 32.7	29.9- 32.1	n.d. ^b	100- 120
OM (56 mM)	oblate	0.268	0.520	11.0- 11.4	18.4- 18.8	5.4- 5.8	0.59- 0.61	22.0 ± 0.1	21.1 ± 0.5	27.9- 28.5	27.4- 28.6	35- 47	65- 71
DM (80 mM)	oblate	0.273	0.520	13.4- 13.8	22.7- 23.1	5.4- 5.8	0.59- 0.61	26.2 ± 0.1	25.6 ± 0.5	33.4- 34.0	32.2- 33.4	86- 103	98- 104
DDM (94 mM)	oblate	0.277	0.520	15.7- 16.1	27.9- 28.3	5.4- 5.8	0.56- 0.58	31.8 ± 0.1	30.7 ± 0.5	39.4- 40.0	36.8- 38.0	135- 149	145- 155
LMPG (16 mM)	oblate	0.280	0.470	16.6- 17.6	23.5- 24.5	5.3- 6.1	0.70- 0.73	26.9 ± 2.4	28.8 ± 0.5	38.7- 39.3	38.5- 41.3	63- 69	90- 100
LPPG (25 mM)	oblate	0.281	0.470	19.0- 20.0	28.4- 29.4	5.3- 6.1	0.67- 0.70	35.7 ± 2.5	34.5 ± 0.5	45.2- 45.8	43.3- 46.1	160- 170	140- 150

Table 3.2 SAXS-determined parameters of detergent micelle size and shape. Total concentrations of detergent for the condition measured are given in parentheses. ^aFor FC14, an average $R_{g\text{ expt}}$ from the lower concentration data (<150 mM) was used because deviation from linearity in the Guinier region was observed; ^bThe Guinier regions for the glucosides are mostly nonlinear in the range that $q \cdot R_g < 1.3$, however estimation were made from the lower concentration data where possible. In addition, the rise in intensity as q tends toward 0 precluded the determination of forward scattering intensities and thus N_{expt} could not be determined. Parameters were obtained from optimal core-shell ellipsoid model fits to the experimental SAXS data at given total concentrations of detergent in solution.

The aggregation numbers determined from the model for each detergent micelle are plotted as a function of detergent alkyl chain length in Figure 3.3A, with corresponding values listed in Table 3.2. The average increase for all detergent micelles in this study indicates that micelle aggregation numbers increase linearly by approximately 16 ± 3 monomers per micelle with the addition of each carbon atom to the alkyl chain. This steady increase in aggregation number highlights the significant contributions to the increased hydrophobic interactions between adjacent monomers made by the addition to alkyl chain length.

Maximum micelle aggregation numbers have been predicted from geometric packing of the alkyl chains in the hydrocarbon core for spherical and ellipsoidal micelles over a given range of micelle ellipticities and detergent chain lengths (37). The detergent monomers are assumed to have maximally extended alkyl chains, which will result in overestimation of the aggregation number (38). The best-fit model parameters for the phosphocholine data indicate a prolate ellipsoid geometry with a ratio a/b of ~ 1.5 , which corresponds to a predicted increase of ~ 14 monomers per micelle with each added carbon in the alkyl chain, which is in agreement with the observed 12–15 monomers (Table 3.2 and Figure 3.3A). The oblate maltosides have a relative a/b of ~ 0.57 corresponding to a predicted increase of ~ 28 monomers per micelle with each increased carbon in the alkyl chain (37) and in reasonable agreement with the observed 20–25 monomers. The oblate geometry with a relative a/b of ~ 0.7 from the two LPG models corresponds to a predicted approximate increase of 20–25 monomers per micelle (37), which agrees with an increase of 25 monomers per micelle determined in this study. As with aggregation number and

core thickness, the radii of gyration vary linearly with the number of carbons in the alkyl chain ($1.55 \pm 0.85 \text{ \AA}$ per carbon added; Table 3.2).

Using the geometric packing approach of Tanford, the calculated aggregation numbers based on chain length (*e.g.* 60, 83, and 110 for $n_c = 10, 12,$ and 14, respectively, for phosphocholine; 47, 58, 70, and 97 for $n_c = 8, 9, 10,$ and 12, respectively, for maltosides; and 105 for $n_c = 14$ and 134 for $n_c = 16$ for LPG) are in good agreement with values determined in this study (Table 3.2). A comparison of the alkyl chain length predicted from the maximum extended chain length determined from the micelle model indicates that the alkyl chains of the model are 80 – 90% of the maximum extension, consistent with a flexible yet closely-packed hydrocarbon core (34).

3.3.3 *Effects of head group steric bulk and electrostatics*

In addition to chain length, a major determinant of micelle aggregation number is the size and charge of the detergent head group. Aggregation numbers for the nonionic series depend on the head group identity, as can be observed with a comparison of the aggregation numbers for a single chain length (Figure 3.3A). Two previously reported data sets for (N-alkylamino)-1-deoxylactitols (35) and sucrose esters (36) are included in Figure 3.3A to provide additional comparisons of head group effects. The observed trend shows an increase in steric bulk (nearest to the alkyl chain) with a decrease in aggregation number. Charged LPGs have smaller aggregation numbers than those extrapolated for nonionic or zwitterionic head groups. Phosphocholine prolate micelles cannot be directly compared by head group to oblate micelles because prolate micelles have a smaller aggregation number (larger surface area per head group) than oblate

micelles for the same chain length and aspect ratio, regardless of the repulsion that likely exists between head groups (37).

3.3.4 *Dependence of head group packing*

Micelle shapes have been debated in the literature (36, 37, 39-41); however, overwhelming evidence indicates that head group properties dictate the ellipticity (aspect ratio; a/b) of the micelle for single chain detergents, where prolate and oblate ellipsoid micelles are observed (15, 21, 35-37). Beyond this simplified treatment of head group interactions, Iyer and Blankschtein (42) and Dupuy *et al.* (35) propose models for nonionic surfactants that predict ellipticity and shape based on the packing and interactions between head groups (and solvent) independent of chain length. Their model predicts that oblate micelles are preferred for small nonionic detergents, but as the head group size increases or electrostatic repulsion occurs, prolate micelles may be preferred. The oblate ellipticity is predicted to approach spherical (aspect ratio of 1) as the head group increases in size or has repulsive electrostatic interactions (larger surface area). This trend is observed in the ellipticities experimentally determined for the glucosides, maltosides, and LPGs (Table 3.2); the electrostatic repulsions between negatively charged head groups in LPG micelles produces a more spherical micelle geometry compared to the uncharged glucosides and maltosides. The zwitterionic phosphocholines form prolate micelles indicating that the head group has significant steric and electrostatic repulsion and has a high surface area. This effect may be exaggerated due to counterion interactions at the surface with the prediction that ellipticity of the phosphocholine prolate micelle would be dependent on ionic strength. Additionally, as predicted by the

Iyer and Blankschtein model, micelle ellipticity remains constant with increasing chain length and aggregation number (Table 3.2).

3.4 Concluding remarks

The detergents investigated form micellar aggregates, which are well described by core-shell ellipsoids with near maximally extended alkyl chains comprising the core, and a compact shell formed by the detergent head groups separating the hydrophobic core from the surrounding aqueous environment. Elliptical geometries provided best fits to the micelle scattering data with dimensions consistent with physical properties of the detergent monomer. Micelle sizes increased linearly with increasing alkyl chain length: approximately 16 ± 3 monomers are added per micelle with each additional carbon atom. The increase in size was accommodated by an increase in the longer axis to maintain similar ellipticities. These results provide a better understanding of the principles of detergent self-assembly, enabling predictions of additional micelle properties based on these principles, as well as establishing a foundation of physical properties important for mixed detergent and PDC systems.

3.5 Materials and methods

The detergents *n*-decyl-phosphocholine (FC10), *n*-dodecyl-phosphocholine (FC12), *n*-tetradecyl-phosphocholine (FC14), *n*-octyl- β -D-glucopyranoside (OG), *n*-nonyl- β -D-glucopyranoside (NG), *n*-decyl- β -D-glucopyranoside (DG), *n*-octyl- β -D-maltopyranoside (OM), *n*-decyl- β -D-maltopyranoside (DM), and *n*-dodecyl- β -D-maltopyranoside (DDM) (Figure 3.1) were purchased from Anatrace. The lysophospholipid detergents 1-myristoyl-2-hydroxy-*sn*-glycero-3-phospho-(1'-*rac*-

glycerol) (14:0 Lyso PG, LMPG) and 1-palmitoyl-2-hydroxy-*sn*-glycero-3-phospho-(1'-*rac*-glycerol) (16:0 Lyso PG, LPPG) were purchased from Avanti Polar Lipids. Deuterium oxide (D₂O) was purchased from Cambridge Isotope Labs. All other chemicals were obtained from Fisher Scientific, unless otherwise noted.

3.5.1 Preparation of detergent micelles

A concentration series up to 200 mM was prepared for each detergent in a final buffer consisting of 20 mM sodium phosphate, pH 6.2, 150 mM NaCl, and 10% v/v D₂O (necessary for NMR deuterium lock). Detergent monomers do not significantly contribute to the observed scattering (15), and all scattering profiles presented are at concentrations well above the CMC (Table 3.1). Detergent concentrations were verified using 1D ¹H-NMR and standards of known concentration.

3.5.2 Micelle size and shape by SAXS

SAXS data were measured at the XOR/BESSRC undulator beam line 12-ID-C,D of the Advanced Photon Source (Argonne, IL), with a sample-to-detector distance of 2 m and a Pilatus 2 M detector. The data were collected at ambient conditions (~25 °C) using a custom-made sample holder (43) and an X-ray energy of 12 keV (corresponding to a wavelength of $\lambda = 1 \text{ \AA}$). The useable range of momentum transfer q was $0.02 < q < 0.3 \text{ \AA}^{-1}$. Additional descriptions of the beamline setup and measurement have been previously published (43-45).

Three proteins were used as molecular weight standards; five exposures of 0.1 s were collected, image corrected, and circularly averaged. For the detergent samples, at least five exposures of 0.5 s each were collected. The absence of radiation damage was

confirmed by comparing subsequent exposures of the same sample with no significant changes in the SAXS profile detected (data not shown). The five resulting profiles for each condition were merged to improve signal quality. Matched buffer profiles were collected using identical procedures and subtracted from the sample scattering for background correction.

3.5.3 Core-shell model fitting

Analysis of the SAXS profiles followed procedures outlined in Chapter 2 and Lipfert, *et al.* (15) for determination of micelle size and shape parameters. One noted exception was the use of a nonlinear, least-square fitting routine implemented in Igor Pro (WaveMetrics) as part of the NCNR analysis toolkit (46) to fit the core-shell models (*i.e.* spheroid, oblate/prolate ellipsoid) to the full scattering profiles. Although this procedure was designed to model fits to small-angle neutron scattering (SANS) data, it was readily adapted to SAXS data by replacing scattering length densities (effective atomic scattering powers in SANS) with electron densities for the micelle core and shell components. Agreement between model-independent and similar model-derived values was used for additional validation of the modeling approach.

3.6 References

1. Oliver, R. C., J. Lipfert, D. A. Fox, R. H. Lo, S. Doniach, and L. Columbus. 2013. Dependence of micelle size and shape on detergent alkyl chain length and head group. *PLoS one* 8:e62488.
2. Wennerström, H. 1979. Micelles. *Physical chemistry of surfactant association*. *Physics Reports* 52:1-86.

3. Columbus, L., J. Lipfert, H. Klock, I. Millett, S. Doniach, and S. A. Lesley. 2006. Expression, purification, and characterization of thermotoga maritima membrane proteins for structure determination. *Protein Science* 15:961-975.
4. Garavito, R. M. 2001. Detergents as tools in membrane biochemistry. *Journal of Biological Chemistry* 276:32403-32406.
5. Sanders, C. R., and F. Sönnichsen. 2006. Solution nmr of membrane proteins: Practice and challenges. *Magnetic Resonance in Chemistry* 44:S24-S40.
6. Seddon, A. M., P. Curnow, and P. J. Booth. 2004. Membrane proteins, lipids and detergents: Not just a soap opera. *Biochimica et Biophysica Acta (BBA) - Biomembranes* 1666:105-117.
7. Denisov, I. G., Y. V. Grinkova, A. A. Lazarides, and S. G. Sligar. 2004. Directed self-assembly of monodisperse phospholipid bilayer nanodiscs with controlled size. *Journal of the American Chemical Society* 126:3477-3487.
8. Sanders, C. R., and R. S. Prosser. 1998. Bicelles: A model membrane system for all seasons? *Structure* 6:1227-1234.
9. Bill, R. M., P. J. F. Henderson, S. Iwata, E. R. S. Kunji, H. Michel, R. Neutze, S. Newstead, B. Poolman, C. G. Tate, and H. Vogel. 2011. Overcoming barriers to membrane protein structure determination. *Nature Biotechnology* 29:335-340.
10. Eshaghi, S. 2005. An efficient strategy for high-throughput expression screening of recombinant integral membrane proteins. *Protein Science* 14:676-683.
11. le Maire, M., P. Champeil, and J. V. Møller. 2000. Interaction of membrane proteins and lipids with solubilizing detergents. *Biochimica et Biophysica Acta (BBA) - Biomembranes* 1508:86-111.

12. Privé, G. G. 2007. Detergents for the stabilization and crystallization of membrane proteins. *Methods* 41:388-397.
13. Raman, P., V. Cherezov, and M. Caffrey. 2006. The membrane protein data bank. *Cellular and molecular life sciences* 63:36-51.
14. Krueger-Koplin, R. D., P. L. Sorgen, S. T. Krueger-Koplin, I. O. Rivera-Torres, S. M. Cahill, D. B. Hicks, L. Grinius, T. A. Krulwich, and M. E. Girvin. 2004. An evaluation of detergents for nmr structural studies of membrane proteins. *Journal of biomolecular NMR* 28:43-57.
15. Lipfert, J., L. Columbus, V. B. Chu, S. A. Lesley, and S. Doniach. 2007. Size and shape of detergent micelles determined by small-angle x-ray scattering. *The Journal of Physical Chemistry B* 111:12427-12438.
16. Lorber, B., J. B. Bishop, and L. J. DeLucas. 1990. Purification of octyl β -d-glucopyranoside and re-estimation of its micellar size. *Biochimica et Biophysica Acta (BBA) - Biomembranes* 1023:254-265.
17. Kameyama, K., and T. Takagi. 1990. Micellar properties of octylglucoside in aqueous solutions. *Journal of colloid and interface science* 137:1-10.
18. Helenius, A., D. R. McCaslin, E. Fries, and C. Tanford. 1979. Properties of detergents. *Methods in enzymology* 56:734.
19. Nilsson, F., O. Söderman, P. Hansson, and I. Johansson. 1998. Physical-chemical properties of c9g1 and c10g1 β -alkylglucosides. Phase diagrams and aggregate size/structure. *Langmuir* 14:4050-4058.
20. He, L., V. M. Garamus, S. S. Funari, M. Malfois, R. Willumeit, and B. Niemeyer. 2002. Comparison of small-angle scattering methods for the structural analysis of

- octyl- β -maltopyranoside micelles. *The Journal of Physical Chemistry B* 106:7596-7604.
21. Dupuy, C., X. Auvray, C. Petipas, I. Rico-Lattes, and A. Lattes. 1997. Anomeric effects on the structure of micelles of alkyl maltosides in water. *Langmuir* 13:3965-3967.
 22. VanAken, T., S. Foxall-VanAken, S. Castleman, and S. Ferguson-Miller. 1986. Alkyl glycoside detergents: Synthesis and applications to the study of membrane proteins. *Methods in enzymology* 125:27.
 23. Strop, P., and A. T. Brunger. 2005. Refractive index-based determination of detergent concentration and its application to the study of membrane proteins. *Protein Science* 14:2207-2211.
 24. Stafford, R. E., T. Fanni, and E. A. Dennis. 1989. Interfacial properties and critical micelle concentration of lysophospholipids. *Biochemistry* 28:5113-5120.
 25. Tian, C., C. G. Vanoye, C. Kang, R. C. Welch, H. J. Kim, A. L. George, and C. R. Sanders. 2007. Preparation, functional characterization, and nmr studies of human *kcne1*, a voltage-gated potassium channel accessory subunit associated with deafness and long qt syndrome. *Biochemistry* 46:11459-11472.
 26. Fernández, C., C. Hilty, G. Wider, and K. Wüthrich. 2002. Lipid-protein interactions in dhpc micelles containing the integral membrane protein ompx investigated by nmr spectroscopy. *Proceedings of the National Academy of Sciences* 99:13533-13537.

27. Columbus, L., J. Lipfert, K. Jambunathan, D. A. Fox, A. Y. Sim, S. Doniach, and S. A. Lesley. 2009. Mixing and matching detergents for membrane protein nmr structure determination. *J Am Chem Soc* 131:7320-6.
28. Santonicola, M. G., A. M. Lenhoff, and E. W. Kaler. 2008. Binding of alkyl polyglucoside surfactants to bacteriorhodopsin and its relation to protein stability. *Biophysical Journal* 94:3647-3658.
29. de Planque, M. R., and J. A. Killian*. 2003. Protein-lipid interactions studied with designed transmembrane peptides: Role of hydrophobic matching and interfacial anchoring (review). *Molecular membrane biology* 20:271-284.
30. Bowie, J. U. 2005. Solving the membrane protein folding problem. *Nature* 438:581-589.
31. Baldwin, P. A., and W. L. Hubbell. 1985. Effects of lipid environment on the light-induced conformational changes of rhodopsin. 2. Roles of lipid chain length, unsaturation, and phase state. *Biochemistry* 24:2633-2639.
32. Lee, A. G. 2004. How lipids affect the activities of integral membrane proteins. *Biochimica et Biophysica Acta (BBA)-Biomembranes* 1666:62-87.
33. Pilot, J. D., J. M. East, and A. G. Lee. 2001. Effects of bilayer thickness on the activity of diacylglycerol kinase of escherichia coli. *Biochemistry* 40:8188-8195.
34. Tanford, C. 1980. *The hydrophobic effect: Formation of micelles and biological membranes* 2d ed editors J. Wiley.
35. Dupuy, C., X. Auvray, C. Petipas, R. Anthore, F. Costes, I. Rico-Lattes, and A. Lattes. 1996. Small angle x-ray and neutron scattering study of the micellization of (n-alkylamino)-1-deoxylactitols in water. *Langmuir* 12:3162-3172.

36. Kawaguchi, T., T. Hamanaka, Y. Kito, and H. Machida. 1991. Structural studies of a homologous series of alkyl sucrose ester micelle by x-ray scattering. *The Journal of Physical Chemistry* 95:3837-3846.
37. Tanford, C. 1972. Micelle shape and size. *The Journal of Physical Chemistry* 76:3020-3024.
38. Dill, K. A., and P. J. Flory. 1981. Molecular organization in micelles and vesicles. *Proceedings of the National Academy of Sciences* 78:676-680.
39. Bogusz, S., R. M. Venable, and R. W. Pastor. 2001. Molecular dynamics simulations of octyl glucoside micelles: Dynamic properties. *The Journal of Physical Chemistry B* 105:8312-8321.
40. Tieleman, D., D. Van der Spoel, and H. Berendsen. 2000. Molecular dynamics simulations of dodecylphosphocholine micelles at three different aggregate sizes: Micellar structure and chain relaxation. *The Journal of Physical Chemistry B* 104:6380-6388.
41. Israelachvili, J. N., D. J. Mitchell, and B. W. Ninham. 1976. Theory of self-assembly of hydrocarbon amphiphiles into micelles and bilayers. *J Chem Soc, Faraday Trans 2* 72:1525-1568.
42. Iyer, J., and D. Blankschtein. 2012. Are ellipsoids feasible micelle shapes? An answer based on a molecular-thermodynamic model of nonionic surfactant micelles. *The Journal of Physical Chemistry B* 116:6443-6454.
43. Lipfert, J., I. S. Millett, S. Seifert, and S. Doniach. 2006. Sample holder for small-angle x-ray scattering static and flow cell measurements. *Review of Scientific Instruments* 77:046108.

44. Beno, M. A., G. Jennings, M. Engbretson, G. S. Knapp, C. Kurtz, B. Zabransky, J. Linton, S. Seifert, C. Wiley, and P. A. Montano. 2001. Basic energy sciences synchrotron radiation center undulator sector at the advanced photon source. Nuclear Instruments and Methods in Physics Research Section A: Accelerators, Spectrometers, Detectors and Associated Equipment 467-468, Part 1:690-693.
45. Seifert, S., R. E. Winans, D. M. Tiede, and P. Thiyagarajan. 2000. Design and performance of a asaxs instrument at the advanced photon source. Journal of Applied Crystallography 33:782-784.
46. Kline, S. R. 2006. Reduction and analysis of sans and usans data using igor pro. Journal of Applied Crystallography 39:895-900.

4. Manipulating micelle dimensions and properties with detergent mixtures

This chapter expands upon the previous by including measurements of micelle solutions containing two miscible detergent components, and investigations of the resulting mixed micelle properties. This work has been prepared for publication, and is in the process of submission to a peer-reviewed journal. Although combinations of detergents have been used in recent membrane protein investigations, the extent of mixing between micelle components and influence on resulting mixed micelle morphology has not been well studied. By investigating micelle size and shape formed at multiple ratios of detergent mixing, this study aims to determine common principles of detergent mixing so that the influence of each detergent, and its relative concentration, is better understood. This information will provide a basis for manipulating micelle dimensions and other relevant micelle features for fine tuning mixed micelles to optimize protein stability in PDCs.

4.1 Overview

Mixtures of detergents provide a means to obtain additional micellar properties; however, the prediction of the properties from detergent mixtures is limited due to a lack of systematic investigations on commonly used detergents. In this study, the shape and size of binary mixtures from ten different detergents frequently used in molecular host-guest systems and membrane protein research were investigated. The data suggests that the combined detergents formed ideally mixed micelles with sizes and shapes different from the pure individual micelles. For most measurements of size, mixtures varied linearly with detergent mole fraction and, hence, can be calculated from the values of the

pure detergents. This dependence on mole fraction allows properties such as geometry, size, and surface charge to be systematically and predictably tuned for specific applications by simply selecting and adjusting detergent concentrations.

4.2 Introduction

Detergent mixtures were selected from previously characterized detergents (Table 4.1), and their significance in membrane protein investigations. Isothermal titration calorimetry (ITC) was used to measure the critical mixed micelle concentrations and to evaluate the extent of detergent mixing for representative mixtures of each type. The results indicate a population of mixed micelles with a critical micelle concentration (CMC) predicted by ideal mixing is formed. In addition, the resulting mixed micelle has a new set of physical properties, dependent upon the mole fraction of each detergent present in the micelle. Small-angle X-ray scattering (SAXS) was used to measure micelle size and shape with systematic variations in micelle composition using binary detergent mixtures. Mixtures of maltosides with different alkyl chain lengths (OM/14M, NM/13M, and DM/DDM) were used to examine nonionic detergent mixing and effects independent of changes in head group. Combinations of phosphocholine and maltoside detergents (OM, DM, and DDM with FC10, FC12, or FC14) were systematically investigated to examine nonionic and zwitterionic detergent mixing at conditions relevant for membrane protein solubilization. In addition, mixtures with an anionic detergent (LPMG with FC10, FC12, DM, or DDM) were selected to investigate the ability to modify the micelle surface potential.

Detergent	Abbr	FW (Da)	CMC ^a (mM)	$V_{\text{mon}}^{\text{b}}$ (\AA^3)	$\rho_{\text{det}}^{\text{c}}$ ($\text{e}/\text{\AA}^3$)	$N_{\text{lit.}}$
<i>n</i> -decylphosphocholine	FC10	323	11	494	0.360	24 ^a , 45-53 (1)
<i>n</i> -dodecylphosphocholine	FC12	351	1.5	548	0.354	54 ^a , 60-80 (1)
<i>n</i> -tetradecylphosphocholine	FC14	380	0.12	602	0.348	108 ^a
<i>n</i> -octyl- β -D-maltopyranoside	OM	454	19.5	590	0.416	6 ^a , 26 (2)
<i>n</i> -nonyl- β -D-maltopyranoside	NM	469	6	617	0.412	25 ^a
<i>n</i> -decyl- β -D-maltopyranoside	DM	483	1.8	644	0.407	69 ^a , 82-90 (1)
<i>n</i> -dodecyl- β -D-maltopyranoside	DDM	511	0.17	698	0.398	78-149 ^a , 135-145 (1, 3)
<i>n</i> -tridecyl- β -D-maltopyranoside	13M	525	0.024	725	0.394	186 ^a
<i>n</i> -tetradecyl- β -D-maltopyranoside	14M	539	0.01	752	0.388	ND
1-myristoyl-2-hydroxy- <i>sn</i> -glycero-3-phosphor-(1'- <i>rac</i> -glycerol)	LMPG	478	0.16	639	0.404	90 ^d

Table 4.1 Properties of detergents used to form mixed micelles. ^aReported by Anatrice. CMCs are reported for conditions of detergent in H₂O, except for the CMC of OM which is reported in 20 mM HEPES, pH 7.5 with 100 mM NaCl. ^bMonomer volumes were calculated from published specific densities, using the Tanford formula ($V_{\text{tail}} = N * (24.7 + 26.9n_c)$) for alkyl chain volumes to adjust for different chain lengths. ^cThe detergent electron density values were computed by summing the number of electrons from the chemical composition and dividing by the molecular volume. ^dA measured value was not found in the literature; although many studies report an aggregation number. However, an estimate can be made from the PDC molecular weight reported by Tian *et al.* of ~60 kD (detergent contribution of 44 kD), which yields an aggregation number of ~90 (4).

4.2.1 Solutions of mixed detergents

In a solution of micelles, the CMC describes the concentration of detergent monomers in equilibrium with detergent micelles. If micelle formation is considered to be a balance of attractive forces between hydrocarbon chains and repulsive interactions between head groups, then the formation of mixed micelles excludes the combination of non-repulsive head groups (*e.g.* oppositely-charged cationic and anionic detergents). However, when two miscible detergent species are present, rather than remaining as discrete micelles, a heterogeneous mixed micelle is energetically preferred and forms readily. Studies of the detergent association and mixed micelle formation (5-8) have yielded the following generalized relationship for critical micelle concentrations of a binary detergent mixture:

$$\frac{1}{CMC_{mix}} = \frac{\chi_A}{CMC_A} + \frac{\chi_B}{CMC_B} \quad (1)$$

where CMC_{mix} is the CMC of the mixture, CMC_A and CMC_B are the CMCs of the two pure components, and χ_A and χ_B are the mole fractions of each micelle-forming detergent.

Ideal mixing is achieved when the micelle composition ratio is equal to the bulk detergent concentration ratio (Figure 4.1). Formation of ideal mixed micelles containing nonionic head groups with different alkyl chain lengths was previously reported (6, 9, 10). However, interactions between different detergent head groups, such as electrostatic interactions, are proposed to hinder ideal mixing of detergents in micelles (11). Deviations from ideal mixing were observed in mixtures of dodecyl sulfate and octyl(oxyethylene) dodecyl ether, in which it was reported that CMC values were lower

than predicted due to weaker repulsive forces between head groups in the mixed micelle as compared to that formed by the pure component (12). With these different reports, the extent of mixing of detergents that are commercially available and commonly used in membrane protein research was investigated with ITC and SAXS.

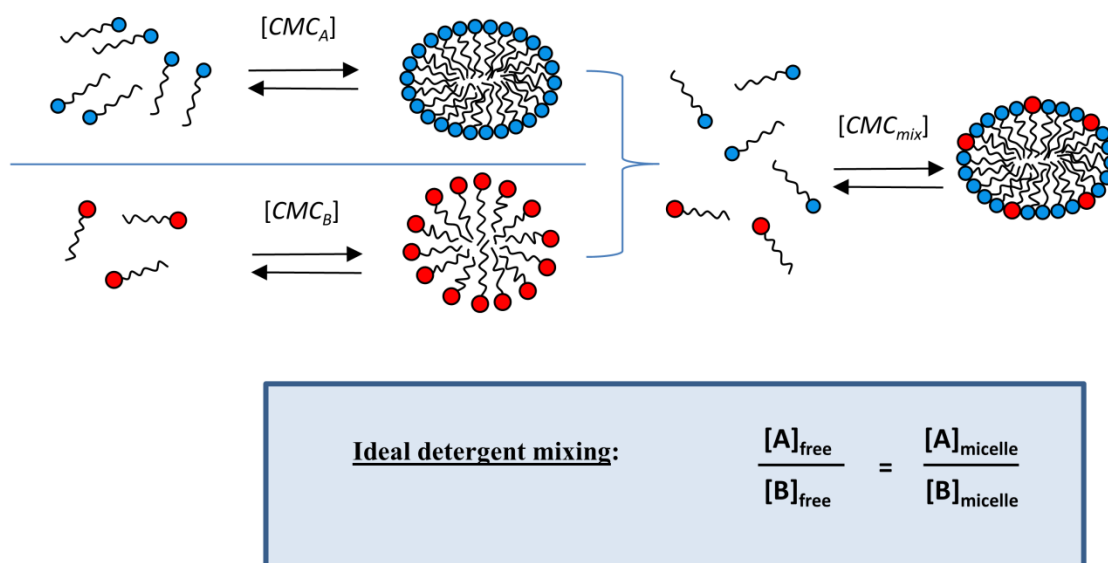


Figure 4.1 Ideal mixing for binary combinations of micelle-forming detergents. Two solutions of micelle forming detergents are represented, existing in equilibrium between those forming the micelle and other free detergent monomers in solution defined by CMC_A (blue) and CMC_B (red). The combination of these two detergents produces mixed micelles with new physical properties and equilibrium between micelle and free detergent (CMC_{mix}). Under ideal mixing conditions, this population of mixed micelles contains the same ratio of detergent as the bulk environment and free detergent monomers.

4.2.2 Mixed micelle size and shape

The size of a micelle can be assessed with different parameters such as aggregation number (N) and micelle geometrical dimensions, which can be determined using SAXS with model-dependent and independent approaches toward interpreting the final data. With respect to geometrical dimensions, the ellipsoidal radii and L_{expt} are two measurements of interest because they correlate with the micelle hydrophobic thickness, which may be of importance for various applications such as stabilizing membrane proteins (13). Additional properties that reflect micelle size and can be measured with SAXS are micelle volume (V_{model}), aggregation numbers (N , N_A , and N_B ; model-dependent and independent measurements), and R_g (model-dependent and independent measurements).

For mixed micelles of two detergents (*e.g.*, detergents A and B), the total aggregation number (N_T) is the sum of all detergent monomers in the micelle. Partial aggregation numbers (N_A , N_B) can be used to describe the populations of each component in the mixed micelle, such that $N_T = N_A + N_B$. If the mole fraction of each component and total aggregation number are known, such that $N_T = \chi_A \cdot N_T + \chi_B \cdot N_T$, partial aggregation numbers can be determined according to eq 2.

$$N_A = \chi_A \cdot N_T \quad \text{or} \quad N_B = \chi_B \cdot N_T \quad (2)$$

Total aggregation numbers were estimated using two methods: first, from a comparison to SAXS measurements of well-characterized molecular weight standards, and alternatively, from the best-fit geometric models. For SAXS measurements of macromolecules, the zero-angle scattering intensity $I(0)$ is related to the number of

macromolecules (n) and the product of a contrast term ($\Delta\rho$) and volume (V) squared (eq 3). The contrast term ($\Delta\rho$) describes the effective scattering power of the macromolecule, and is the measure of electron density difference between particle and solvent in the case of X-ray scattering from electrons. Based on this relationship and using $I(0)$ measurements of well-characterized macromolecules under similar conditions, a standard curve can be used to estimate mixed micelle size.

$$I(0) = n(\Delta\rho \cdot V)^2 \quad (3)$$

Consequently, a micelle of N detergent monomers scatters N -fold more strongly than N monomers, and the micellar aggregation number can be determined from the measured $I(0)$ and that expected for a monomer, described by eq 4.

$$N = \frac{I(0)_{micelle}}{I(0)_{monomer}} = \frac{I(0)}{\kappa(C - CMC_{mix})(\rho_{mix} - \rho_s)^2(V_{mix})^2} \quad (4)$$

κ is the proportionality constant determined from $I(0)$ measurements of three molecular weight standards (described in sample preparation) of known concentration, volume, and electron density. For mixed micelles, C is the total concentration of both detergent monomer components, and CMC_{mix} is the CMC adjusted for the detergents used and ratio of mixing (eq 1). The solvent electron density (ρ_s) was $0.34 \text{ e}/\text{\AA}^3$ in all calculations. For mixed micelle values such as electron densities (ρ_{mix}) and monomer volumes (V_{mix}), a mole-fraction weighted linear combination of the values from each component was used, as demonstrated for mixed micelle volume V_{mix} :

$$V_{mix} = \chi_A \cdot V_A + \chi_B \cdot V_B \quad (5)$$

After calculating a total aggregation number, partial aggregation numbers ($N_{A\text{ expt}}$ and $N_{B\text{ expt}}$) were determined using mixed micelle mole fractions.

Alternatively, aggregation numbers were determined from the best-fit micelle models fit to the experimental data. The total volume of the dry hydrophobic core was divided by the volume per monomer

$$N_{core} = \frac{\frac{4\pi}{3}ab^2}{V_{tail}} \quad (6)$$

where V_{tail} is the volume occupied by a hydrocarbon chain, based on Tanford's formula for alkyl chain volume ($V_{tail} = 27.4 + 26.9*n_c$, where n_c is the number of alkyl chain carbons)(11) and the elliptical core axes (a and b). This approach implies maximum detergent packing to fill the mixed micelle volume. The individual detergent aggregation numbers ($N_{A\text{ model}}$ and $N_{B\text{ model}}$) are extracted from the total aggregation number (N_{core}) using a weighted linear combination for multiple component mixed micelles.

A local maximum between $0.1 < q < 0.3 \text{ \AA}^{-1}$, corresponding to length scales of $20 < d < 60 \text{ \AA}$, is characteristic of x-ray scattering profiles from micelle-forming detergents. The position of this maximum (q_{max}) indicates the most frequently occurring distance of separation among the detergent head groups across the micelle core (L_{expt}), and correlates with the micelle's hydrophobic thickness along the minor elliptical axis. L_{expt} is, therefore, calculated directly from the experimental SAXS profile for each micelle (eq 7).

$$L_{expt} = \frac{2\pi}{q_{max}} \quad (7)$$

An analogous term can be obtained from the geometric model fit to the experimental data (L_{model}), given by eq 8,

$$L_{model} = 2r + t \quad (8)$$

where r is the minor elliptical core axis (a for oblate, b for prolate) and t is the shell thickness. The length of the shorter core axis is constrained by the maximum extended alkyl chain length, as exceeding this limit results in unoccupied volume at the micelle center (11). Using Tanford's formula for maximum extended alkyl chain length (l_c , eq 9), a constraint for the maximum core thickness (L_{max}) of each micelle can be calculated according to eq 10.

$$l_c = (1.5 + 1.265 \cdot n_c) \quad (9)$$

$$L_{max} = 2(1.5 + 1.265 \cdot n_c) + t \quad (10)$$

4.2.3 Surface potential

Another property of micelles that can be modulated using binary mixtures is the surface potential. Detergent head groups can be anionic, cationic, zwitterionic, or neutral; thus, proper mixing ratios can produce micelles with a predictable net surface charge. Micelles containing the anionic detergent LMPG have net negative charge, and an associated surface potential. The surface potentials of these LMPG mixed micelles were calculated using an adaptation for elliptical micelles from the method for spherical ionic micelles described by Luo and Wang (14). The micellar surface charge density (σ_0) was calculated using eq 13,

$$\sigma_0 = \frac{(e \cdot N_{LMPG})}{4\pi ab} \quad (13)$$

where e is the elementary electric charge, N_{LMPG} is the number of LMPG molecules in the mixed micelle, and a and b are the axial dimensions (core and shell) of the elliptical core-shell model fit to the experimental SAXS profile for each mixed micelle condition. The surface charge density may also be defined as:

$$\sigma_0 = \frac{\varepsilon_r \varepsilon_0 \kappa k T}{e I} \quad (14)$$

where $\kappa = (2ne^2 / \varepsilon_0 \varepsilon_r k T)^{1/2}$, n is the number concentration of ions in the bulk solution (0.15 M in this case), ε_r is the relative permittivity of the solution (78.3 for water at 25 °C), ε_0 is the permittivity of a vacuum, k is the Boltzmann constant, and T is the temperature ($T = 298$ K), while I denotes the dimensionless surface charge density.

Using the simple expression for surface charge density for spherical colloidal particles, the generalized expression for surface potential can be written as:

$$\Psi = 2 \ln\left(1 - \frac{4}{\kappa A}\right) \quad (15)$$

where ψ is the normalized surface potential, and A is the distance from micelle center to surface. A geometric mean of the elliptical axes, $A = \sqrt{((a+t)^2 + (b+t)^2)}$, was used to approximate this distance.

4.3 Results and discussion

4.3.1 Ideal mixing of detergents

Isothermal titration calorimetry (ITC) was used to determine the CMC of the three mixtures at different mole fraction ratios (Figure 4.2). Eq 1 predicts the CMC of the mixture assuming ideal mixing and has previously described the mixing of short chain

nonionic binary surfactant systems (6). Similarly, the CMC value dependence on mole fraction for all three binary mixtures in this study was fit with eq 1 and demonstrated ideal mixing. Deviation from the fit was observed at the lowest mole fraction of DDM when mixed with FC10; however, this is the only mixing ratio that deviates from ideal mixing. The SAXS profile for a mixed micelle is not the same as the sum of the individual scattering profiles for each component (Figure 4.3) suggesting that the detergents are mixing. The following sections demonstrate that the geometrical micellar properties of the binary mixtures (without an assumption of ideal mixing, such as L_{expt}) follow trends that are indicative of ideal mixing.

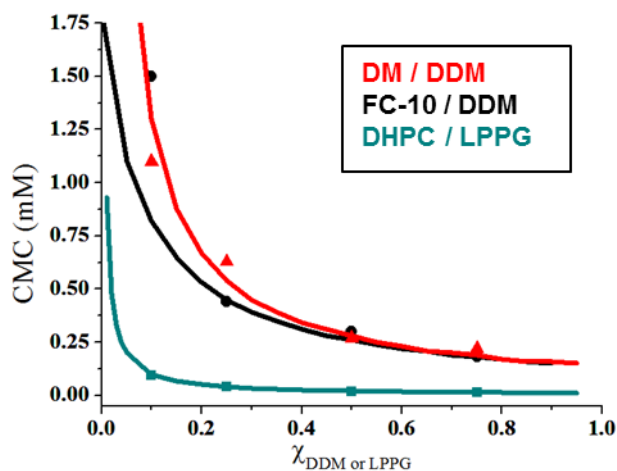


Figure 4.2 CMC of detergent mixtures measured by ITC. Mixtures of two nonionic maltosides with different alkyl chain lengths (DM and DDM, red), a zwitterionic phosphocholine and nonionic maltoside (FC10 and DDM, black) with similar hydrophobic radii but different alkyl chain lengths, and a zwitterionic phosphocholine and anionic phosphatidyl glycerol (DHPC and LPPG, teal) with different length and number of alkyl chains. CMC values are plotted versus mole fraction of either DDM or LPPG in the mixed micelle. The lines represent fits using Eq. 1 and the pure detergent CMC values (Table 4.1; CMC_{DHPC} : 14 – 15 mM, CMC_{LPPG} : 0.6 mM).

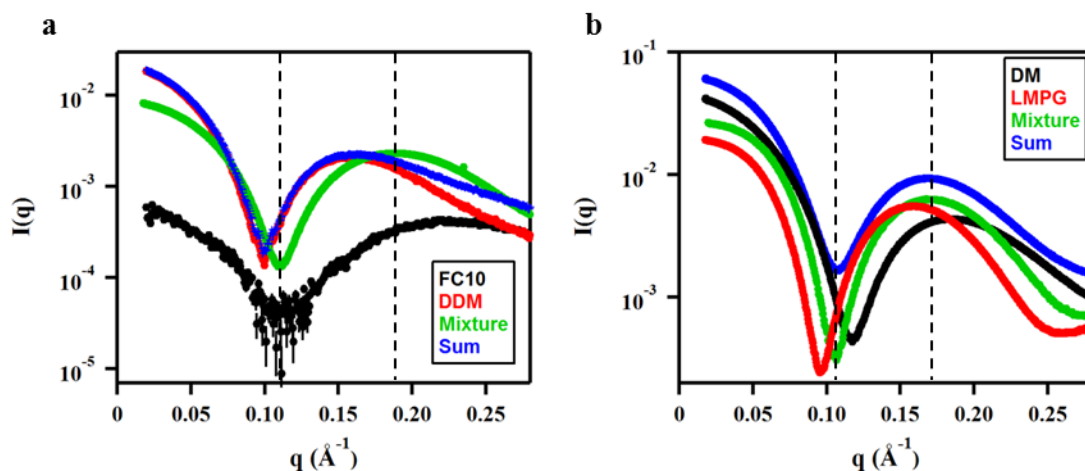


Figure 4.3 Scattering of mixed micelles versus individual and sum components. a.

Scattering profiles are shown for pure detergents FC10 (36 mM, black) and DDM (17 mM, red). The scattering profile from the binary detergent mixture (39 mM FC10 and 19 mM DDM, green) is different than the sum of the two pure detergent scattering profiles (blue) indicating that the micelle is a mixture of both of the detergents. **b.** Scattering profiles are shown for pure detergents DM (58 mM, black) and LMPG (54 mM, red). The scattering profile from the binary detergent mixture (46 mM DM and 39 mM LMPG, green) is different than the sum of the two pure detergent scattering profiles (blue) indicating that the micelle is a mixture of both of the detergents. Dashed lines are added to guide the eye.

4.3.2 *Modulating micelle size*

The model-independent measurement of the micelle short axis (L_{expt} ; the dominant length between two head groups) was determined for several binary detergent mixtures with the same head group (maltosides; Figure 4.4) and different head groups (Figure 4.5; properties of all micelle mixtures are listed in Appendix I: Supplementary Tables S1-S4). The maltoside alkyl chain length mixtures investigated were 10 and 12, 9 and 13, and 8 and 14 carbons. A linear decrease in L_{expt} is observed as the mole fraction of the shorter chain detergent is increased. As expected from the linear dependence, micelles with equimolar ratios have a similar L_{expt} to 11M (dashed line in Figure 4.4). The L_{expt} also varies linearly for mixtures of detergent with different head group properties such as nonionic maltoside with zwitterionic phosphocholine (Figure 4.5a-c) and anionic phosphatidyl glycerol head groups (Figure 4.5d). L_{expt} remains approximately constant for mixtures of detergents with similar L_{expt} (e.g. DM and FC12, Figure 4.5b).

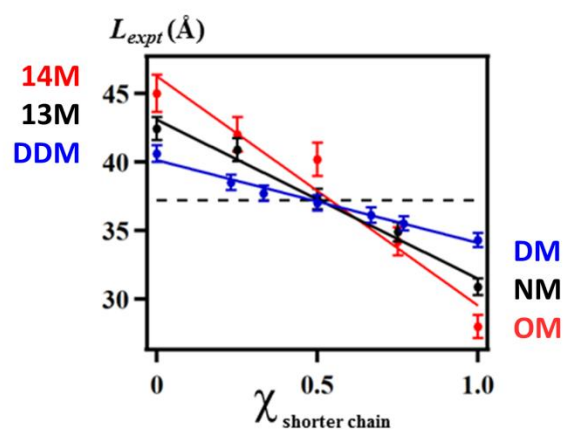


Figure 4.4 Model-independent micelle thicknesses from maltoside mixtures. Micelle thickness described by L_{expt} varies linearly with micellar mole fraction. Measured L_{expt} values from binary maltoside mixtures are plotted as a function of mole fraction of shorter chain maltoside using three pairs of alkyl chain lengths: 8 and 14 carbons (OM and 14M, red), 9 and 13 carbons (NM and 13M, black), and 10 and 12 carbons (DM and DDM, blue). A best fit line is shown for each data set. The dashed line indicates the measured L for a maltoside with 11 alkyl chain carbons.

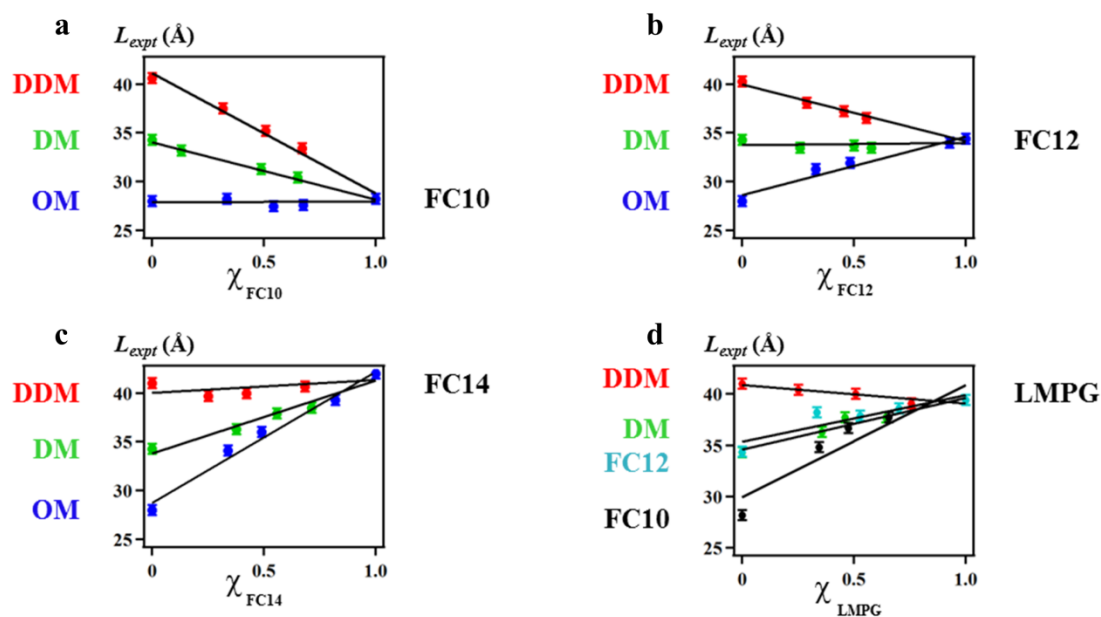


Figure 4.5 Model-independent micelle thicknesses from mixtures of maltosides, phosphocholines, and LMPG. A linear dependence is observed throughout various mixtures of L_{expt} on the micellar mole fraction for binary detergent mixtures. Combinations of maltosides, phosphocholines, and LMPG are plotted as a function of mole fraction of phosphocholine detergent (**a-c**), and LMPG (**d**). Solid lines indicate best linear fits for each data set.

The model-dependent minor inner core radius (a for oblate and b for prolate) are also measurements of the dominant hydrophobic thickness and directly comparable to L_{expt} ($t + 2a$ for oblate and $t + 2b$ for prolate). For all mixtures, a linear trend was observed for the minor radius as a function of micelle mole fraction (an example is shown in Figure 4.6a). However, larger deviations from the linear fit were observed compared to the model-independent L_{expt} measurements and are likely due to the approximation of the shell thickness and electron density of the head group mixture. Nota bene: although DM and FC12 have similar L_{expt} values, DDM and FC12 have similar minor radii because the maltoside head group is larger than the phosphocholine head group which is a component of the L_{expt} measurement.

For mixtures of maltosides (OM, DM, and DDM) and phosphocholines, V_{model} vary approximately linearly with mole fraction (an example for mixtures with FC12 are shown in Figure 4.6b). Since V_{model} is dependent on the radii, which each vary linearly with mole fraction, the linear dependence of the volume is not surprising; however, the plot highlights the volume similarities between prolates and oblates with different dimensions. For instances, OM and FC12 have similar volumes but differ in minor radius length and L_{expt} because they are different shapes (prolate vs. oblate). V_{model} may be an important parameter to consider in terms of membrane protein hydrophobic surface area or maximum load capacity of pharmaceuticals.

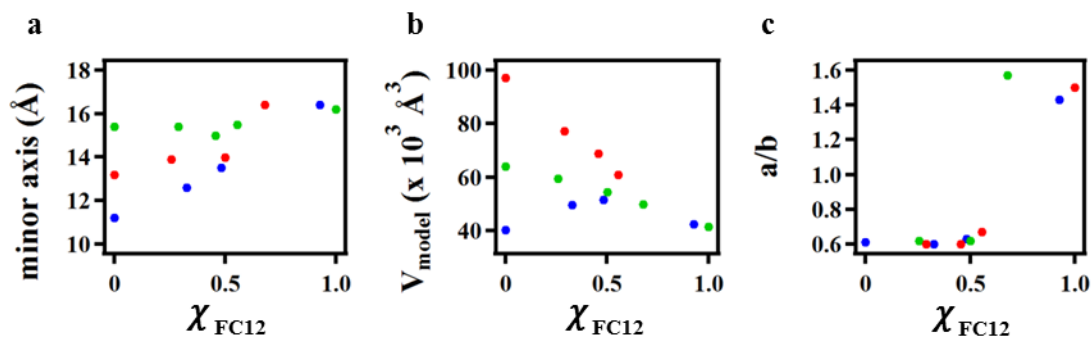


Figure 4.6 Model-dependent measurements of micelle size and shape from mixtures of maltosides with FC12. The minor axis length (a), micelle model volume (b), and axial ratio a/b (c) for binary mixtures containing FC12 with OM (blue), DM (green), or DDM (red) are plotted versus the micellar mole fraction of FC12.

Aggregation numbers are another model-dependent measurement of micelle size, and are extracted from the model volumes using detergent mole fractions and monomer volumes. In most cases, partial (N_{model}) and total (N_{total}) aggregation numbers varied linearly with micelle mole fraction (Figure 4.7). Deviations from linearity were observed for OM and FC12, FC14 with OM and DDM, and LMPG with FC10, FC12, and DM. In each case, the micelles change shape and are mixtures of relatively small and large micelles. Another assessment of micelle size is the radius of gyration, R_g . The dependence of the model-independent $R_{g\text{ }expt}$ with respect to mixed micelle composition is linear for many mixtures (Figure 4.8), but not all. In the cases of longer chain prolate phosphocholine and oblate maltosides micelle mixtures, there appears to be a transition at the higher mole fractions of phosphocholine that deviates from the linear dependence (Figure 4.8b and c). More data is required in this transition region to be able to discuss molecular explanations for this trend.

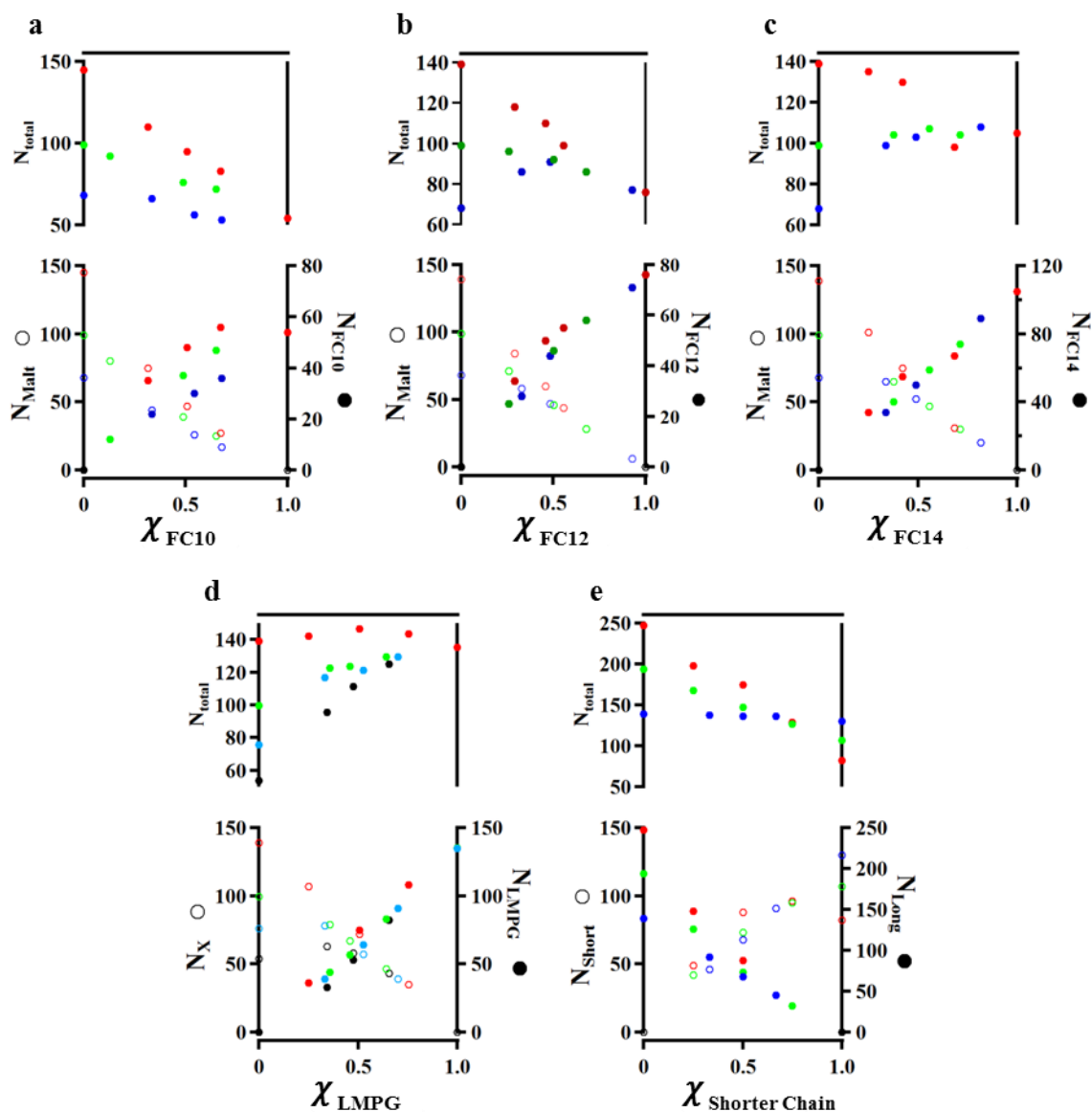


Figure 4.7 Aggregation numbers for detergent mixtures. Total micelle aggregation numbers (N_{total} ; top) and the partial aggregation numbers for each component are plotted as a function of micellar mole fraction of FC10 (a), FC12 (b), FC14 (c), LMPG (d), and the shorter chain maltoside (e). Open circles and filled circles indicate aggregation numbers for maltosides (OM, blue; DM, green; DDM, red) with either FC10 (a), FC12 (b), or FC14 (c); mixed components (FC10, black; FC12, cyan; DM, green; and DDM, red) with LMPG (d); and short and long chain maltosides (OM/14M, red; NM/13M, green; and DM/DDM, blue) (e), respectively.

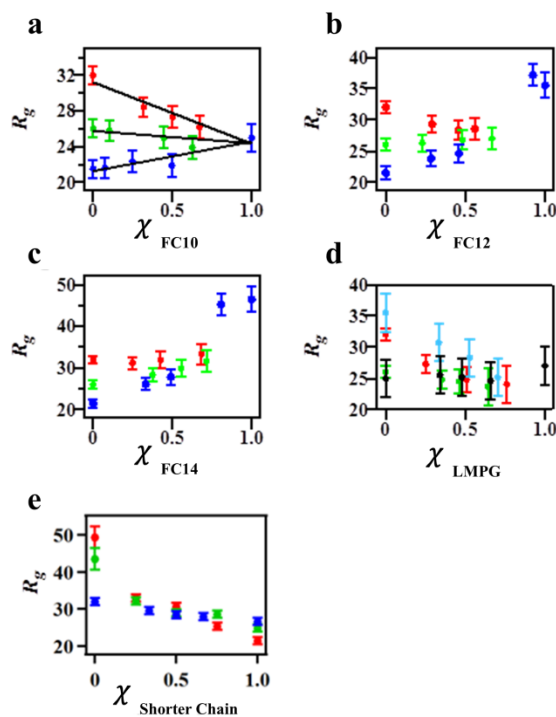


Figure 4.8 Dependence of mixed micelle R_g on mole fraction of detergent in a binary mixed micelle. R_g calculated from the Guinier analysis are plotted as a function of FC12 (a), FC12 (b), FC14 (c), and LMPG (d) micellar mole fraction for mixtures with DDM (red), DM (green), and OM (blue) (a–c), or with FC10 (black), FC12 (cyan), DM (green), and DDM (red) (d). In addition, R_g for maltoside mixtures are plotted for OM and 14M (red), NM and 13M (green), and DM and DDM (blue) as a function of micellar mole fraction of the shorter chain detergent.

These trends in micelle size allow for the rational design of micelles of specific sizes using binary mixtures, which will be useful for many basic science and industrial applications. In each application, if a particular micelle property is hypothesized to be important then mixtures with similar properties can be explored to systematically test the hypothesis. This approach was previously used to investigate the influence of micelle hydrophobic dimensions on membrane protein fold and NMR spectral quality (13).

4.3.3 *Modulating micelle shape*

The micelles in this study are ellipsoids and can vary in the type of ellipsoid (prolate or oblate) and the ellipticity (the extent of deviation from sphere). Although in some cases the oblate and prolate ellipsoid models fit almost equally well to the scattering profiles, the models can be distinguished. A comparison of the core minor axis dimension b to the expected alkyl chain length and a comparison of the experimental and model-derived R_g and L values typically distinguishes the appropriate model (15). The best-fit geometric models indicate that maltosides are oblate, while phosphocholines are prolate (1, 15). The ellipticity of mixed micelles of maltoside (OM, DM, and DDM) and FC12 detergents varies approximately linearly with mole fraction (Figure 4.6c). Above mole fraction of ~ 0.55 , the shape of the micelle changes from oblate to prolate. Thus, shape and ellipticity are tunable properties using binary mixtures. Two micelles of nearly equal volumes but having different shape (high and low aspect ratios) can be mixed to obtain a similar volume mixed micelle with a modulated ellipticity.

4.3.4 *Modulating micelle surface properties*

Another property of micelles that can be modulated using binary mixtures is the surface potential. Detergent head groups can be anionic, cationic, zwitterionic, or neutral; thus, proper mixing ratios can produce micelles with a predictable net surface charge. In this study, the only charged detergent is LMPG and, thus, the surface potentials of binary mixtures with LMPG are reported (Figure 4.9 and Appendix I:Table S4). A mixture of a zwitterionic or neutral detergent and LMPG were mixed at different ratios for a desired charge density. With careful selection of the additional component, the mixed micelle size and shape can be predicted (or controlled) as well (Figure 4.5d, 4.7d, and 4.8d).

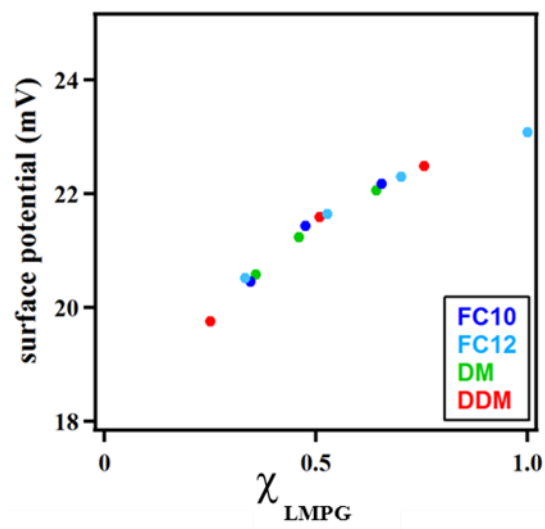


Figure 4.9 Modulation of micelle surface potential with binary mixtures. Measured surface potentials are plotted as a function of LMPG content for mixtures of LMPG with FC10 (blue), FC12 (cyan), DM (green), and DDM (red).

With the knowledge of shape and size of binary mixtures and the head group charge, micelles of specific sizes and shapes can be designed with specific surface potentials. One application for modulating surface properties is for membrane proteins where the interactions of soluble domains with the surface of the micelle or necessary electrostatic membrane protein interactions at the membrane – solvent interface. For example, the addition of ionic detergent increases the specific activity of phospholipase C (16). Other applications could be the enhancement of molecular host – guest interactions or better recapitulating a biological membrane for molecular host investigations (17). Collectively, these properties may be useful not only for mediating interactions between the detergent and membrane proteins or molecular hosts, but interactions between micelles. The effects of surface potential on the interparticle effects between micelles should be considered. For example, if membrane protein instability in a particular micelle is expected to be a result of aggregation between protein-detergent complexes, the addition of a second detergent with negatively charged head groups may be used to increase the net charge of the complex and minimize aggregation.

4.4 Concluding remarks

These investigations of binary detergent solutions at different mole ratios of mixing demonstrate the formation of mixed micelles with a size and shape dependent on micelle composition. The critical micelle concentrations of these micelles behave as predicted by Tanford as indicated by ITC results, and also support the formation of mixed micelles. The size and shape of these mixed micelles are described by a core-shell ellipsoid model fit to small-angle scattering profiles, which previously provided much insight into pure detergent micelle formation. Many properties, such as elliptical axis

lengths (a and b), shell thickness (t), and micelle thickness (L) demonstrate an overall linear dependence on mixing ratio. This observation exists over a broad range of studied detergents, and provides a convenient method for designing mixed micelles with particular dimensions. Additionally, trends in aggregation numbers and radii of gyration appear continuous (if not mostly linear) over the complete range of detergent mixing, and provide additional descriptions of the mixed micelles. These principles of mixed micelle formation are hypothesized to provide a more streamlined approach for optimizing protein stability in PDCs to stabilize the membrane protein for functional and structural studies.

In this streamlined approach, the protein is assumed to be partially soluble in a known detergent, but the PDC is not entirely stable and eventually precipitates after removal from the membrane. Additionally, the native fold and function are often not maintained. A coarse screen for solubility should be performed using detergents with a high rate of success for solubilization, such as DDM or FC12. The following approach seeks to optimize three potential factors of influence on PDC stability in a directed manner. First, a match between the hydrophobic transmembrane region of the protein and hydrophobic core of the mimic is performed. Micelle thickness is systematically varied using a detergent with the same head group as the solubilizing detergent, but having a different alkyl chain length by 1 or 2 carbons. For example, if partial solubility occurs in DDM, then increasing concentrations of DM or 14M can be added to aliquots of the sample, and each monitored for an increase in PDC stability (either by improved persistence to precipitation or an improvement in the quality of NMR spectra) or an increase in functional activity (as determined via assay for native function).

Once the optimum micelle thickness has been determined, influence of changes in head group properties, and related micelle properties (such as aggregation number, volume, and shape), can be systematically investigated. Let us assume that in the above example, optimum stability was observed for a 3:1 mixture of DDM and DM (~38 Å thickness). Micelles with a similar thickness, but with varied head groups, can then be systematically tested for effects on PDC stability or functional activity. For example, a 3:1 mixture of DDM and FC12 produces a mixed micelle with similar thickness. The addition of this zwitterionic detergent may stabilize oppositely-charged residues on the protein surface through favorable electrostatic interactions. In structural investigations using NMR, reducing the molecular weight of the overall complex causes faster rotational correlation times and reduced line broadening resulting in improved spectra. Thus, contributions of the detergent to the overall molecular weight can also be reduced by incorporating detergents which form lower aggregation number micelles.

At this stage considerations must be made based on requirements of the intended technique (such as X-ray crystallography or solution NMR). These requirements can be quite different, such as maintaining non-interacting particles in solution for NMR versus an ordered assembly of particles during crystal formation for crystallography. This third optimization for improved PDC stability aims to modulate the repulsive forces between PDCs by increasing the net micelle surface charge. Since the native membrane contains a net negative charge on the inner leaflet, an anionic detergent is suggested. An increase in the repulsive forces between PDCs is expected to reduce interactions between the protein components which promote aggregation. A similar micelle thickness can be maintained in our example using mixtures containing LMPG.

Finally, some studies indicate that specific lipids may be required for functional activity (18-20) or during crystallization (21-23). At very low concentrations (only a few lipids per micelle), the micelle size and shape are not expected to be significantly perturbed. Thus, PDC stability may be further optimized by combining small amounts of lipid extract – ideally representative of the protein’s native membrane composition – to satisfy these potential requirements. At higher ratios of lipid to detergent, lipid and detergent components separate to form a bicelle structure with a lipid disk surrounded by detergent. A transition from mixed micelles containing solubilized lipids to bicelles is expected to occur in detergent-rich mixtures, but these aggregate structures formed by these mixtures is not well-known and will be the focus of the next chapter.

4.5 Materials and methods

4.5.1 Sample preparation

The detergents n-octyl- β -D-maltopyranoside (OM), n-nonyl- β -D-maltopyranoside (NM), n-decyl- β -D-maltopyranoside (DM), n-undecyl- β -D-maltopyranoside (UM), n-dodecyl- β -D-maltopyranoside (DDM), n-tridecyl- β -D-maltopyranoside (13M), n-tetradecyl- β -D-maltopyranoside (14M), n-decyl-phosphocholine (FC10), n-dodecyl-phosphocholine (FC12), and n-tetradecyl-phosphocholine (FC14) were purchased from Anatrace; and 1-myristoyl-2-hydroxy-sn-glycero-3-phospho-(1'-rac-glycerol) (14:0 Lyso PG, LMPG) was purchased from Avanti Polar Lipids. Relevant physical properties of these detergents used for data interpretation are provided in Table 4.1. Deuterium oxide (D₂O) was purchased from Cambridge Isotope Labs and all other chemicals were obtained from Fisher, unless otherwise noted.

Mixed micelle solutions were prepared by combining and diluting two detergent micelle stock solutions to yield bulk detergent mole ratios of 3:1, 1:1, and 1:3 in a final buffer consisting of 20 mM phosphate buffer, pH 6.2, 150 mM NaCl, and 10% D₂O (necessary for NMR deuterium lock). Detergent concentrations were quantified with ¹H 1D NMR (data not shown). Mixed micelle solutions were prepared with a total micelle concentration of approximately 1 mM.

Hen egg white lysozyme (Fisher: BP535) in 40 mM acetate buffer, pH 3.8 with 150 mM NaCl, horse heart cytochrome c (Sigma: C7150) in 100 mM acetate buffer, pH 4.6 with 0.5 M guanidinium hydrochloride, and bovine serum albumin (Sigma: A8531) in 20 mM HEPES buffer, pH 7.8 with 50 mM NaCl, were used as SAXS molecular weight standards. Five concentrations were measured for each protein standard (up to 10.6 mg/mL lysozyme, 4.2 mg/mL cytochrome c, and 8.6 mg/mL albumin) to determine any concentration-dependent effects on scattering.

4.5.2 *Critical micelle concentrations of mixed micelles*

Isothermal titration calorimetry (ITC) experiments were conducted to examine this relationship between CMC and mixed micelle fraction in select mixed micelles using a VP-ITC MicroCalorimeter (MicroCal) at 30°C with stirring at 300 rpm. The 1.5 mL sample cell contained 20 mM of phosphate buffer at pH 7. The 1.5 mL reference cell contained water. Binary detergent stock solutions were degassed and loaded into the calorimeter syringe. Binary detergent stock solutions containing DM and DDM, FC10 and DDM, and DHPC (1,2-diheptanoyl-sn-glycero-3-phosphocholine, Avanti) and LPPG (16:0 lyso PG, Avanti) in ratios of 1:3, 1:1, 3:1, and 9:1 were prepared in 20 mM

phosphate buffer at pH 7. To observe sufficient baselines before and after phase transitions, stock concentrations needed to be in excess of 20 times the CMC as predicted by eq 1. The titrant was dispensed into the sample cell in 10 μL aliquots for 20 sec per injection, with an equilibration time of 300 sec between injections; the change in total volume after each injection was accounted for in subsequent calculations. A phase transition was usually observed after about 15 injections. Integration of the resulting power versus time plot using yielded an enthalpy versus total detergent concentration plot; the CMC was assumed to be the total detergent concentration at the point of inflection.

4.5.3 SAXS data collection and core-shell model fits

SAXS data were measured at the XOR/BESSRC undulator beam line 12-ID of the Advanced Photon Source (Argonne, IL), with a sample to detector distance of 2 m and a Pilatus 2M detector. The data were collected at 25 $^{\circ}\text{C}$ using a custom-made sample holder (24) and an X-ray energy of 12 keV (corresponding to a wavelength of $\lambda = 1 \text{ \AA}$). The useable range of momentum transfer q was $0.01 < q < 0.28 \text{ \AA}^{-1}$ ($q = 4\pi \sin(\theta)/\lambda$, where 2θ is the scattering angle and λ is the X-ray wavelength). Additional descriptions of the beamline setup and measurement are previously published (1, 15, 25, 26).

Micelle sizes and shapes were determined from ellipsoid core-shell model fits to the SAXS scattering profiles using the NCNR (NIST Center for Neutron Research) analysis toolkit (27), adapted for x-ray scattering as previously described for a comprehensive series of pure detergents relevant to membrane protein investigations (1, 15). For binary mixed micelles, core and shell electron densities were calculated by a

mole-fraction weighted linear combination. Scattering profiles, Guinier plots, and regions of 2nd maxima are included in Appendix I: Figures S1-S3.

4.6 References

1. Lipfert, J., L. Columbus, V. B. Chu, S. A. Lesley, and S. Doniach. 2007. Size and shape of detergent micelles determined by small-angle x-ray scattering. *The Journal of Physical Chemistry B* 111:12427-12438.
2. He, V. M. Garamus, S. S. Funari, M. Malfois, R. Willumeit, and B. Niemeyer. 2002. Comparison of small-angle scattering methods for the structural analysis of octyl- β -maltopyranoside micelles. *The Journal of Physical Chemistry B* 106:7596-7604.
3. Strop, P., and A. T. Brunger. 2005. Refractive index-based determination of detergent concentration and its application to the study of membrane proteins. *Protein Science* 14:2207-2211.
4. Tian, C., C. G. Vanoye, C. Kang, R. C. Welch, H. J. Kim, A. L. George, and C. R. Sanders. 2007. Preparation, functional characterization, and nmr studies of human *kcne1*, a voltage-gated potassium channel accessory subunit associated with deafness and long qt syndrome. *Biochemistry* 46:11459-11472.
5. Holland, P., and D. Rubingh. 1983. Nonideal multicomponent mixed micelle model. *The Journal of Physical Chemistry* 87:1984-1990.
6. Clint, J. H. 1975. Micellization of mixed nonionic surface active agents. *Journal of the Chemical Society, Faraday Transactions 1: Physical Chemistry in Condensed Phases* 71:1327-1334.

7. Hao, L.-S., Y.-T. Deng, L.-S. Zhou, H. Ye, Y.-Q. Nan, and P. Hu. 2012. Mixed micellization and the dissociated margules model for cationic/anionic surfactant systems. *The Journal of Physical Chemistry B* 116:5213-5225.
8. Georgiev, G. 1996. Markov chain model of mixed surfactant systems. *Colloid and Polymer Science* 274:49-58.
9. Harkins, W. D., R. W. Mattoon, and M. L. Corrin. 1946. Structure of soap micelles as indicated by x-rays and interpreted by the theory of molecular orientation: Ii. The solubilization of hydrocarbons and other oils in aqueous soap solutions. *Journal of colloid science* 1:105-126.
10. Puvvada, S., and D. Blankshtein. 1992. Theoretical and experimental investigations of micellar properties of aqueous solutions containing binary mixtures of nonionic surfactants. *The Journal of Physical Chemistry* 96:5579-5592.
11. Tanford, C. 1980. *The hydrophobic effect: Formation of micelles and biological membranes* 2d ed editors J. Wiley.
12. Lange, Y., and C. M. Gary-Bobo. 1973. Ion diffusion in lecithin-water lamellar phases. *Nat New Biol* 246:150-1.
13. Columbus, L., J. Lipfert, K. Jambunathan, D. A. Fox, A. Y. Sim, S. Doniach, and S. A. Lesley. 2009. Mixing and matching detergents for membrane protein nmr structure determination. *Journal of the American Chemical Society* 131:7320-7326.
14. Luo, G., and H. Wang. 2007. The calculation of surface potential for spherical ionic micelles. *Journal of Dispersion Science and Technology* 28:1108-1111.

15. Oliver, R. C., J. Lipfert, D. A. Fox, R. H. Lo, S. Doniach, and L. Columbus. 2013. Dependence of micelle size and shape on detergent alkyl chain length and head group. *PLoS ONE* 8:e62488.
16. El-Sayed, M. Y., and M. F. Roberts. 1985. Charged detergents enhance the activity of phospholipase c (*Bacillus cereus*) towards micellar short-chain phosphatidylcholine. *Biochimica et Biophysica Acta (BBA) - Protein Structure and Molecular Enzymology* 831:133-141.
17. Javor, S., and J. Rebek. 2011. Activation of a water-soluble resorcinarene cavitand at the water-phosphocholine micelle interface. *Journal of the American Chemical Society* 133:17473-17478.
18. Walsh, J. P., and R. M. Bell. 1986. Sn-1, 2-diacylglycerol kinase of *Escherichia coli*. Mixed micellar analysis of the phospholipid cofactor requirement and divalent cation dependence. *Journal of Biological Chemistry* 261:6239-6247.
19. Zimmer, J., and D. A. Doyle. 2006. Phospholipid requirement and pH optimum for the in vitro enzymatic activity of the *E. coli* p-type ATPase ZntA. *Biochimica et Biophysica Acta (BBA)-Biomembranes* 1758:645-652.
20. Shanmugavadivu, B., H.-J. Apell, T. Meins, K. Zeth, and J. H. Kleinschmidt. 2007. Correct folding of the β -barrel of the human membrane protein VDAC requires a lipid bilayer. *Journal of Molecular Biology* 368:66-78.
21. Zhang, H., G. Kurisu, J. L. Smith, and W. A. Cramer. 2003. A defined protein-detergent-lipid complex for crystallization of integral membrane proteins: The cytochrome b₆f complex of oxygenic photosynthesis. *Proceedings of the National Academy of Sciences* 100:5160-5163.

22. Jidenko, M., R. C. Nielsen, T. L.-M. Sørensen, J. V. Møller, M. le Maire, P. Nissen, and C. Jaxel. 2005. Crystallization of a mammalian membrane protein overexpressed in *saccharomyces cerevisiae*. *Proceedings of the National Academy of Sciences of the United States of America* 102:11687-11691.
23. Guan, L., I. N. Smirnova, G. Verner, S. Nagamori, and H. R. Kaback. 2006. Manipulating phospholipids for crystallization of a membrane transport protein. *Proceedings of the National Academy of Sciences of the United States of America* 103:1723-1726.
24. Lipfert, J., I. S. Millett, S. n. Seifert, and S. Doniach. 2006. Sample holder for small-angle x-ray scattering static and flow cell measurements. *Review of Scientific Instruments* 77:046108.
25. Beno, M. A., G. Jennings, M. Engbretson, G. S. Knapp, C. Kurtz, B. Zabransky, J. Linton, S. Seifert, C. Wiley, and P. A. Montano. 2001. Basic energy sciences synchrotron radiation center undulator sector at the advanced photon source. *Nuclear Instruments and Methods in Physics Research Section A: Accelerators, Spectrometers, Detectors and Associated Equipment* 467-468:690-693.
26. Seifert, S., R. E. Winans, D. M. Tiede, and P. Thiyagarajan. 2000. Design and performance of a asaxs instrument at the advanced photon source. *Journal of Applied Crystallography* 33:782-784.
27. Kline, S. R. 2006. Reduction and analysis of sans and usans data using igor pro. *Journal of Applied Crystallography* 39:895-900.

5. Contrast variation studies of bicelle organization

According to the idealized bicelle model, lipid and detergent partition into distinct domains: lipids comprising the central disk with detergents encircling the disk edge. However, the extent of separation between these two domains remains largely unknown, particularly at increasing mole ratios of micelle-forming detergent. Such combinations of detergent and lipid also exist during membrane solubilization. The aim of this investigation is to determine the overall size and shape, as well as internal organization, of two detergent-rich solutions of bicelles using neutron scattering and contrast variation experiments. This information will aid membrane protein studies and solubilization efforts by increasing our understanding of lipid-detergent interactions.

5.1 Overview

In this chapter, small-angle X-ray and neutron scattering (SAXS/SANS) data are presented on aggregate structures (*e.g.* micelle or bicelle) formed by mixtures of DMPC and DHPC. The SAXS data indicated these overall structures were best represented by a core-shell ellipsoid model, but short and long chain components were unresolved. Commercially available amphiphiles with deuterated acyl chains provide the necessary contrast between these components for neutron scattering contrast variation experiments. Scattering data was obtained at multiple solvent deuteration levels for a variety of DMPC/DHPC bicelles with specifically deuterated acyl chains of DMPC. Physical properties of these amphiphiles are given in Table 5.1. Different concentrations of total amphiphile ($c_L = 6$ and 1.5 % w/v) and the ratio of short to long chain amphiphile ($Q = 0.3$ and 0.7; capital Q is used in this work so that the values are not confused with

momentum transfer q) were investigated with neutron scattering. These data were also collected at two temperatures, 25 and 40°C. Interpretation of the contrast variation data is dependent upon the arrangement of the lipids within the bicelle, and approaches for determining the basic scattering functions for the deuterated and non-deuterated components from each contrast series will be discussed. These data will provide structural information for membrane mimics that will facilitate an understanding of membrane protein and detergent/lipid interactions.

Amphiphile	Mol. Wt. (Da)	V_{mon} (\AA^3)	$\rho_{X\text{-ray}}$ ($\text{e}/\text{\AA}^3$)	ρ_{neutron} (10^{10} cm^{-2})
DHPC	453.5	677.2	0.363	0.720
DMPC	677.9	1108	0.338	7.13
DMPC-D54	732.3	1113	0.385	3.95

Table 5.1 Physical properties of amphiphiles used to prepare bicelles for scattering experiments. Monomer volumes (V_{mon}) were determined from published specific densities (1), using the Tanford formula for alkyl chain volume to correct for different chain lengths (2). Scattering length densities, $\rho_{X\text{-ray}}$ and ρ_{neutron} , were determined by summing the number of electrons or scattering lengths of nuclei, respectively, from the chemical composition by the molecular volume.

5.2 Introduction

5.2.1 *The ideal bicelle model*

In the regime at which mixtures of detergent (DHPC) and lipid (DMPC or DMPC-D54) form isotropic bicelles, a central disk of lipids is depicted in a bilayer arrangement encircled by a torus of detergent molecules (Figure 5.1). This central lipid bilayer-like disk is expected to provide a more native-like mimic for membrane protein conditions, as opposed to micelles for example, which have a more curved surface. Studies of bicelles have determined that the resulting morphology is dependent upon total phospholipid concentration, the ratio of components, and temperature (3, 4). The liquid-crystalline counterparts occurring at higher ratios of DMPC:DHPC ($2.5 < Q < 5.0$) have been identified as having a bicelle morphology with a lipid core surface area increasing as the ratio of lipid to detergent is increased. Results from several complementary techniques suggest that bicelles at lower ratios ($Q = 0.05 - 5$) retain this overall morphology and lipid organization. However, the propensity of the detergent to form mixed micelles in detergent-rich conditions and miscibility of amphiphiles suggest that some degree of mixing may occur between detergent and lipid components (rf. Chapter 1.4). That is, the central lipid disk may contain detergent molecules and/or lipid molecules may be contained in the outer rim in a mixed bicelle arrangement as opposed to the ideal bicelle (Figure 5.1).

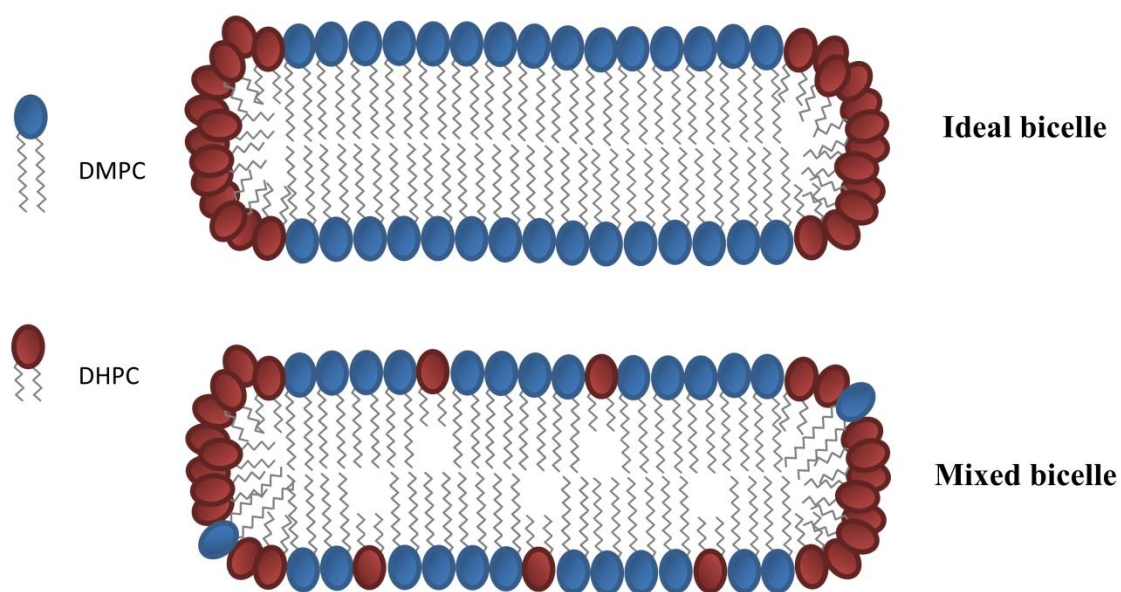


Figure 5.1 Comparison of ideal and mixed bicelle models. The cross-sections of both bicelle models are depicted using the same representations for DMPC and DHPC. In the ideal bicelle model, lipid and detergent components remain isolated, whereas in the mixed bicelle model, components are allowed to exchange between core and rim regions.

5.2.2 *Morphology of lipid-detergent mixtures*

The size and shape of isotropic, low- Q bicelle structure has been previously investigated using a variety of complementary techniques: fluorescence spectroscopy, dynamic light scattering, and electron microscopy (5). Fluorescence spectroscopy revealed a significant increase in aggregate size (attributed to a larger surface area of the planar lipid region) as c_L was decreased from 5% to 1% w/v ($Q = 0.5$). This information supported the dependence of bicelle morphology on total amphiphile concentration, and indicated that bicelle dilution does not simply reduce the number of bicelle aggregates in solution. Dynamic light scattering experiments revealed consistent increases in the mean hydrodynamic radii with narrow size distributions as lipid:detergent ratio was increased from $Q = 0.4$ to 2. In addition, electron microscopy results confirmed the presence of disk-shaped particles in DMPC/DHPC mixtures at $Q = 0.5$ and $c_L = 20\%$ w/v. These results indicated that a bicelle-like structure exists at $Q = 0.5$ (but reveal little about $Q < 0.5$), and that the aggregate structure of lipid-detergent mixtures varied as a result of relative concentration between these two components, as well as with their total concentration.

5.2.3 *Evidence of internal bicelle organization*

Internal organization of the bicelle lipid and detergent components was also investigated using solution NMR in the same study (5). ^{31}P NMR studies demonstrated that the DMPC and DHPC components were highly segregated over a wide range of DMPC/DHPC ratios ($0.05 < Q < 0.5$) and temperatures (15°C and 37°C). A trivalent paramagnetic lanthanide ion (Pr^{3+}) induces a chemical shift perturbation dependent upon

the organization of the phospholipid. The resulting chemical shifts yielded two interesting results. First, larger changes in DMPC chemical shift perturbations implied the presence of a bicellar model in which DMPC in the planar region chelates the lanthanide ion more effectively than DHPC on the rim. Second, the DHPC chemical shifts corresponded closely with micellar rather than monomer values, suggesting that the bicelle rim is micelle-like in organization.

Although the majority of studies suggest that bicelle-like organization is maintained even in detergent-rich conditions, “mixed bicelle” models have also been proposed to account for DHPC miscibility in the bilayer domain (6-9). The challenge of trying to distinguish between these two models requires the ability to resolve lipid and detergent components of the bicelle, which is below the detection limit of most methods but may be accomplished using small-angle neutron scattering contrast variation experiments. This study seeks to investigate the overall structure and internal organization of low- Q bicelles using this approach.

5.3 Results and discussion

5.3.1 X-ray scattering of DMPC and DHPC mixtures

To determine the occurrence of any structural transitions in the regime of detergent-rich bicelles, we investigated mixtures of DMPC and DHPC ranging in Q (ratio of lipid:detergent) from 0.1 to 1.0 in 0.1 increments (Figure 5.2). Concentrations of 1.5, 3, 6, 9, 12, and 15 % total amphiphile weight per volume and temperatures of 6, 25, and 40 °C were also recorded. The concentration series was used to assess the presence of concentration-dependent effects on the measured scattering profiles, such as interparticle

interference or bicelle aggregation at high concentrations. These SAXS data provided a basis for establishing overall bicelle size and shape, and optimization of conditions for neutron scattering contrast variation experiments.

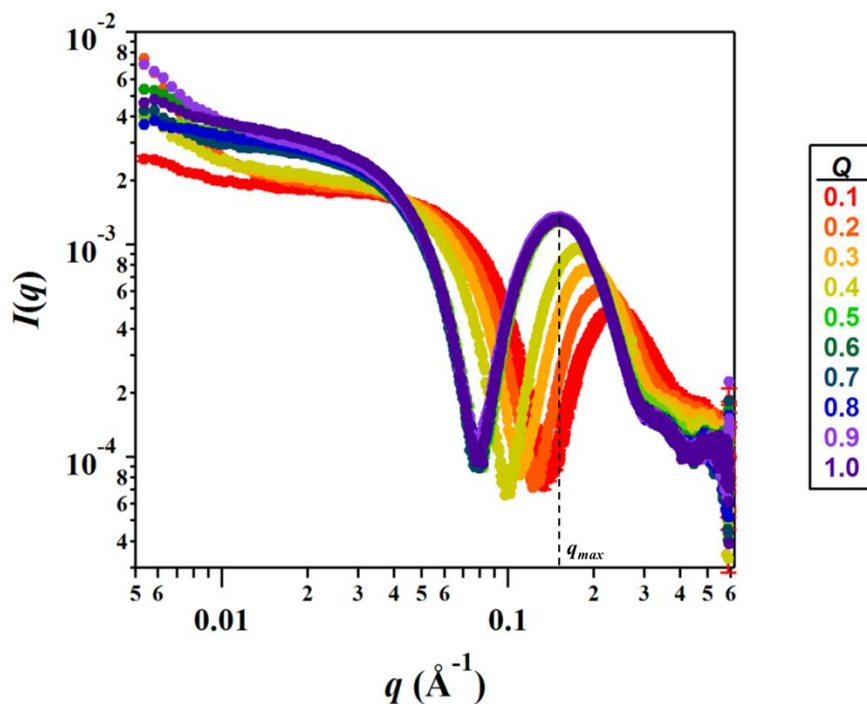


Figure 5.2 SAXS profiles of mixtures with different ratios of lipid and detergent.

Scattering data collected at room temperature (25°C) from bicelles at 6 % total amphiphile weight per volume with systematic variations in ratio of lipid:detergent denoted by Q (color coded according to the provided legend). The dominant real-space distances of separation between opposing head groups determine the position of the second maximum and can be calculated according to $2\pi/q_{max}$ (L). The peak position and corresponding q_{max} for $Q = 1.0$ is shown as an example by the dashed line and is used to calculate the L in Table 5.2.

From initial inspection of the SAXS profiles, two observations are readily apparent that support the hypothesis of lipid-detergent mixing and structural transitions as lipid to detergent ratio increases. First, significant changes in the scattering profile are observed as lipid concentration is increased from $Q = 0.1$ to 0.5, indicating that lipid-detergent components are well-mixed and form new aggregate structures that are dependent on the ratio of lipid-detergent mixing. Second, scattering profiles from $Q = 0.5$ to 1.0 display only minor differences, indicating that the overall size and shape formed by these aggregates is similar. To investigate structural differences in the lipid and detergent domains of these two regimes and lipid-detergent mixing, one condition from each regime ($Q = 0.3$ and 0.7) was selected for neutron scattering contrast variation experiments. Additional descriptions of these mixtures can be obtained from further analysis of the SAXS data.

The position of the second maximum in the SAXS profiles of bicelles studied shifts to lower q as Q is increased from 0.1 to 0.5. This peak position remains relatively constant above $Q = 0.5$. Using peak position as an indicator of the minor axial dimension, or bicelle thickness, this shift to lower- q indicates the formation of a thicker (possibly bilayer-like) arrangement as concentration of DMPC is increased (Table 5.2). These values agree well with thicknesses predicted by the maximum extension of lipid/detergent alkyl chains. For comparison, the maximum extended chain lengths (l_{max}) for DMPC and DHPC are 19.2 Å and 9.1 Å, respectively. Thus, if the headgroup contributes roughly 6 Å to the distance measured across the shorter axis, the expected distance between head groups across two maximally-extended, opposing chains is ~44.4 Å for a pure DMPC bilayer and ~24.2 Å for a pure DHPC micelle.

Q	R_g (Å)	L (Å)
0.1	18.0	26.2
0.2	19.7	29.5
0.3	22.8	33.3
0.4	27.1	36.0
0.5	33.5	41.6
0.6	33.2	41.8
0.7	33.9	42.1
0.8	32.5	41.6
0.9	34.5	41.8
1.0	34.3	41.7

Table 5.2 Radii of gyration and dominant lengths of separation (thicknesses) for bicelles at different mole ratios of lipid:detergent from Guinier analysis of SAXS profiles. Data are presented at conditions of 6% w/v and 25°C. Radii of gyration were measured from Guinier analysis of low-angle data, and values of L determined from the position of the second maximum in the SAXS profile (Figure 5.2).

Extrapolation of the dominant distance of separation (L) from $Q = 0.5$ to 0 reveals a thickness within error to that observed for pure DHPC micelles. The shift in peak position is accompanied by an increase in measured radius of gyration as lipid ratio is increased to $Q = 0.5$, and indicates that the macromolecular assembly is undergoing significant changes in size and/or overall structure in this regime, which should also be indicated by the radius of gyration of the bicelle. Additionally, the changes in L as measured by peak position appear to be the linear combination of the two components, similar to those changes measured for binary detergent mixtures.

A Guinier analysis of the scattering profiles shown in Figure 5.2 was used to calculate a radius of gyration for each mixture (Table 5.2). The radius of gyration values correspond well with the trends observed in L . Above $Q = 0.5$, the measured R_g values remain mostly constant, although a slight increase is noted between 0.5 and 1.0. However, below $Q = 0.5$, a gradual increase is observed in R_g values. These data indicate that a transition occurs from the aggregate structure of detergent micelles to mixed lipid-detergent bicelles, and that aggregate structures in this transition likely do not contain a bilayer arrangement or central lipid disk.

Solutions of micelles formed by DHPC have been previously investigated using SAXS, and were determined to form prolate core-shell ellipsoids with $a = 20.5 - 22.5$ Å and $b = 9.5 - 10$ Å with a shell thickness of $3.0 - 4.0$ Å (10). The corresponding radius of gyration for the ellipsoid model is 20 Å with a thickness ($2b + t$), corresponding to L , of about 23 Å (consistent with y-intercept (22 Å) of a linear fit ($R^2 = 0.99$) to the dependence of L on Q for the data range of $0.1 < Q < 0.5$). This extrapolation to micelle-

like conditions supports the hypothesis that lipid-detergent aggregates undergo structural transitions from a micellar to bicellar state.

5.3.2 Comparison of lipid:detergent composition

Two ratios of lipid to detergent, total amphiphile concentrations, and temperatures were investigated in the detergent-rich bicelle regime ($Q = 0.3, 0.7$; $c_L = 1.5, 6\%$ w/v; and $T = 25, 40\text{ }^\circ\text{C}$) to investigate potential differences in the internal organization of lipid and detergent components. Since neutron scattering is sensitive to hydrogen and deuterium content, bicelles prepared from lipids with deuterated tails (in this case DMPC-D54) and detergents with tails that are not specifically deuterated (*e.g.* DHPC) can be used to measure the relative abundance of each component in these regions. This sensitivity is depicted in Figure 5.3, a schematic of the expected differences in observed scattering based on either the ideal or mixed bicelle model. The scattering length density of the core (or rim) is based on chemical composition, thus this value can be measured and compared to the expected scattering length densities for different degrees of mixing. Two eleven-point contrast series for bicelles at $Q = 0.3$ and 0.7 were collected (Figure 5.4) to investigate potential changes in partitioning in addition to structural changes observed via SAXS.

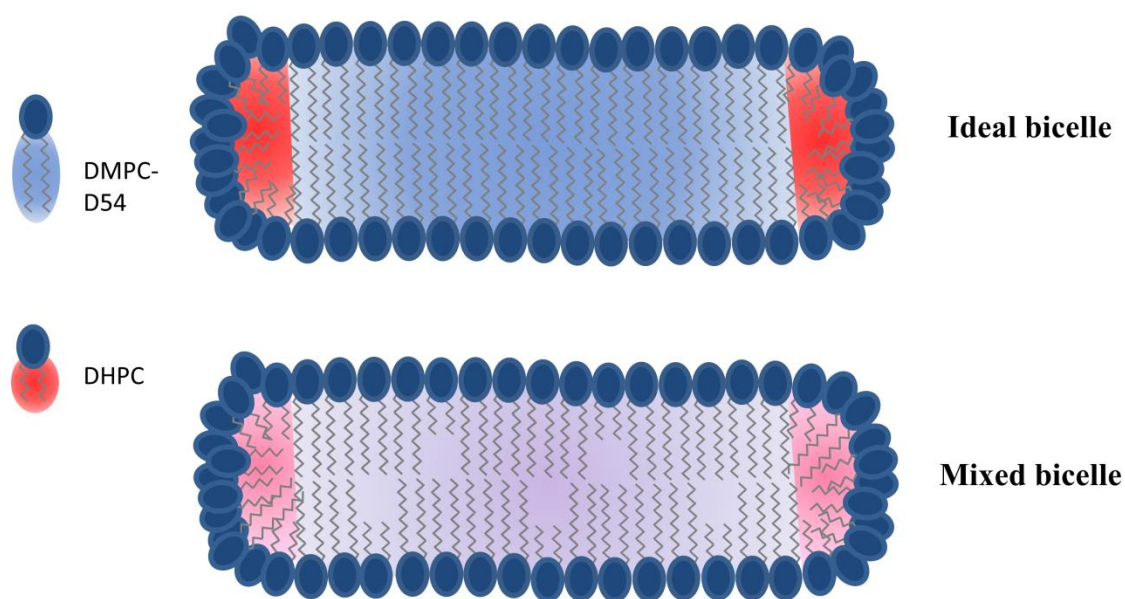


Figure 5.3 Observed contrast in neutron scattering using deuterated and natural alkyl chain tails with and without lipid-detergent mixing. Ideal and mixed bicelle models are depicted as in Figure 5.1, but with contrast and relative scattering length densities of deuterated lipid tails and non-deuterated detergent tails depicted by blue and red shading, respectively. In the ideal bicelle model where components remain isolated, contrast is maximized between the core and rim regions. When lipid-detergent mixing is present, the scattering length densities of core and rim are altered and contrast is weakened since these properties result from an average of all atoms in the region.

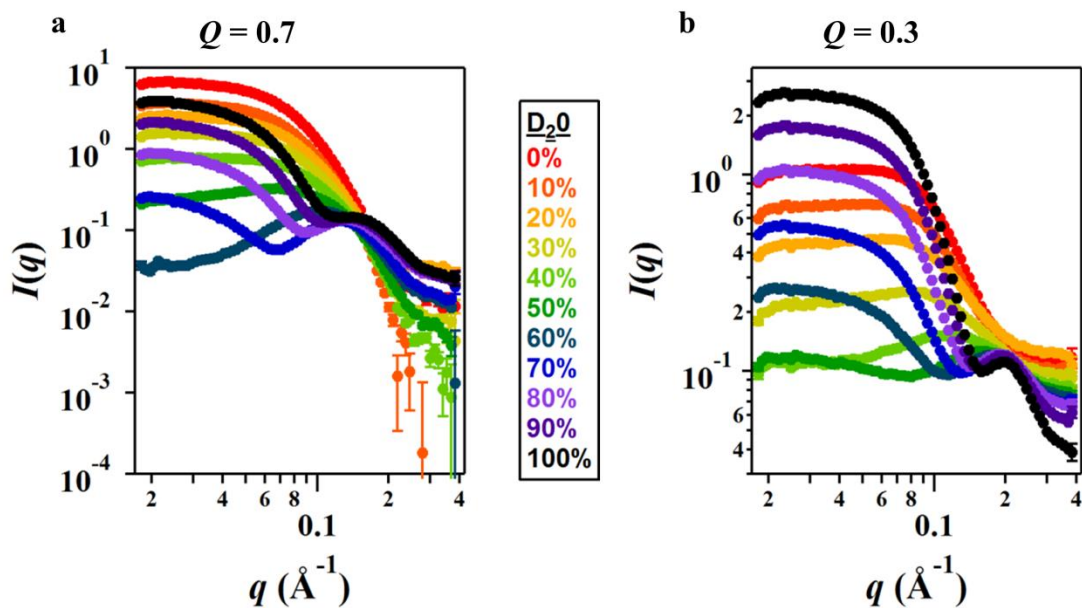


Figure 5.4 Contrast variation series for DMPC-D54:DHPC bicelles at $Q = 0.7$ or 0.3 and 6 % w/v at 25°C. **a.** Neutron scattering contrast variation data for DMPC-D54:DHPC bicelles at $Q = 0.7$ and 6% w/v in buffer with incremental changes in D_2O buffer composition colored according to legend. **b.** Neutron scattering contrast variation data for DMPC-D54:DHPC bicelles at $Q = 0.3$ and 6% w/v with D_2O content indicated by the same coloring scheme.

The forward scattering $I(0)$ and radius of gyration R_g are measured from a Guinier analysis of the low angle scattering data identical to the treatment of SAXS data (Table 5.3), and provide an initial analysis of the contrast variation series and overall size of each scattering subunit (detergent or deuterated lipid). Detergent tails are contrast matched at low concentrations of D_2O (0-40%), thus scattering is the primary result of the lipid core. At high concentrations of D_2O (65-100%) the lipid tails are matched and scattering results mostly from the detergent components. A match point for the total complex can be determined from the x-intercept of a 2nd order polynomial fit to $I(0)/c$ vs. fraction of D_2O in the solvent or a linear fit to the square root of $I(0)/c$ vs. D_2O fraction. The total match was determined to occur at 55.9% and 56.1% D_2O , respectively, for the $Q = 0.7$ bicelle sample, and at 40.5% and 40.3% D_2O for the $Q = 0.3$ sample. At solvent D_2O concentrations near the total match point, the scattering length density from the complex approximates that of the buffer (low contrast, or contrast matched), thus only weak scattering is observed, which often prevents successful Guinier analysis. The match point for each component and the total match point can also be calculated directly from the chemical composition of scattering components. Scattering length densities and contrasts for each component and the total assembly at all fractions of D_2O were determined with the MULCh analysis toolkit (section 5.5.4). The calculated match points from this method for a ratio of $Q = 0.7$ were 18.4% for the detergent match, 64.8% for the lipid match, and 43.6% D_2O for the total match point. For a ratio of $Q = 0.3$, component contrast match points remain the same while the total match shifts to 34.1% D_2O .

Contrast point (%D ₂ O)	$Q = 0.7$		$Q = 0.3$	
	$I(0)$	R_g (Å)	$I(0)$	R_g (Å)
0%	7.24	19.9	1.20	ND
10%	3.97	18.4	0.13	ND
20%	2.74	17.1	0.58	ND
30%	1.63	13.7	0.31	ND
40%	0.79	7.5	ND	ND
50%	ND	ND	ND	ND
60%	ND	ND	0.28	18.2
70%	0.32	39.7	0.58	16.8
80%	1.06	33.7	1.11	15.7
90%	2.48	30.7	1.84	14.9
100%	4.48	29.7	2.72	14.1

Table 5.3 Measured $I(0)$ and R_g from Guinier analysis of contrast series data (6 % w/v and 25°C). Weak scattering observed near solvent match points at 50-60% in the $Q = 0.7$ sample and 40-50% in the $Q = 0.3$ sample prevented successful Guinier analysis (indicated by ND). A decrease in scattering intensity approaching zero-scattering angle also prevents an accurate determination of the radius of gyration for $Q = 0.3$ samples at low D₂O concentrations (also indicated by ND).

The experimental determination of match points is difficult due to the errors in extrapolating $I(0)$, but calculated contrast match points are in agreement with the values measured from forward scattering. However, discrepancies between the two methods may be attributed to the discrete separation of these components during the calculation of contrast match points. Mixing between the detergent and lipid components would have significant effects on the resulting neutron scattering length densities of the core and rim (as indicated by Figure 5.3). Scattering length densities are calculated from the atomic composition and volume of core or rim, and are highly sensitive to hydrogen and deuterium content, and thus the presence of either detergent with hydrogenated tails or lipid with deuterated tails. Therefore, calculated match points could be refined by systematically varying the contrast of these components to account for lipid-detergent mixing.

Successful match point determination needs to be investigated further and is required to extract the basic scattering functions that contain more precise information about the size and shape of the assembly formed by each component. Nonetheless, a Stuhrmann analysis can be performed to approximate additional relationships between the scattering components based on measured radii of gyration at each fraction of solvent D₂O (11). More specifically, this analysis provides a radius of gyration for each component and their distance of separation (12). Due to the absence of R_g information in the $Q = 0.3$ samples at low solvent deuteration, these parameters could only be extracted from the $Q = 0.7$ contrast series. The radii of gyration measured for the lipid core and detergent rim based on this analysis with no lipid-detergent mixing implied is 16.8 ± 1.8 Å and 43.0 ± 3.0 Å, respectively. A meaningful value of the distance of separation is not

obtained because the detergent rim encircles the lipid core, thus the center of masses of these components overlap and not separate. However, the sign of the value obtained indicates that the position of the component with lower scattering length density (DHPC) is located at the periphery of the assembly.

5.3.3 *Effects of temperature*

To investigate potential effects from increased temperature on the internal structure of lipid-detergent aggregates, scattering from these mixtures was also investigated at an increased temperature of 40 °C (Figure 5.5), a temperature often used for NMR membrane protein investigations. The mixing between detergent rim and lipid core domains is expected to increase as a result of the increased kinetic energy and dynamic motions of molecules. However, phase transitions are also present at higher temperatures, which can complicate the structure or internal organization adopted by such aggregates.

The contrast series at increased temperature (40°C) is highly similar to that at room temperature (25°C), and includes many of the same trends at each lipid:detergent ratio discussed for the room temperature condition. Calculated match points are not temperature-dependent, and thus are expected to be the same as those determined previously for samples at 25°C. Unfortunately the trends in $I(0)$ for the $Q = 0.3$ sample, and limited availability of contrast points in the series for $Q = 0.7$, were insufficient to determine accurate experimental match points. Nevertheless, the low solvent R_g values match the detergent and can be compared. The size of the lipid disk for $Q = 0.7$ at increased temperature appears to be larger in size compared to 25°C as indicated by a

larger R_g at low solvent D_2O fractions corresponding to the match point region of the detergent (Table 5.4).

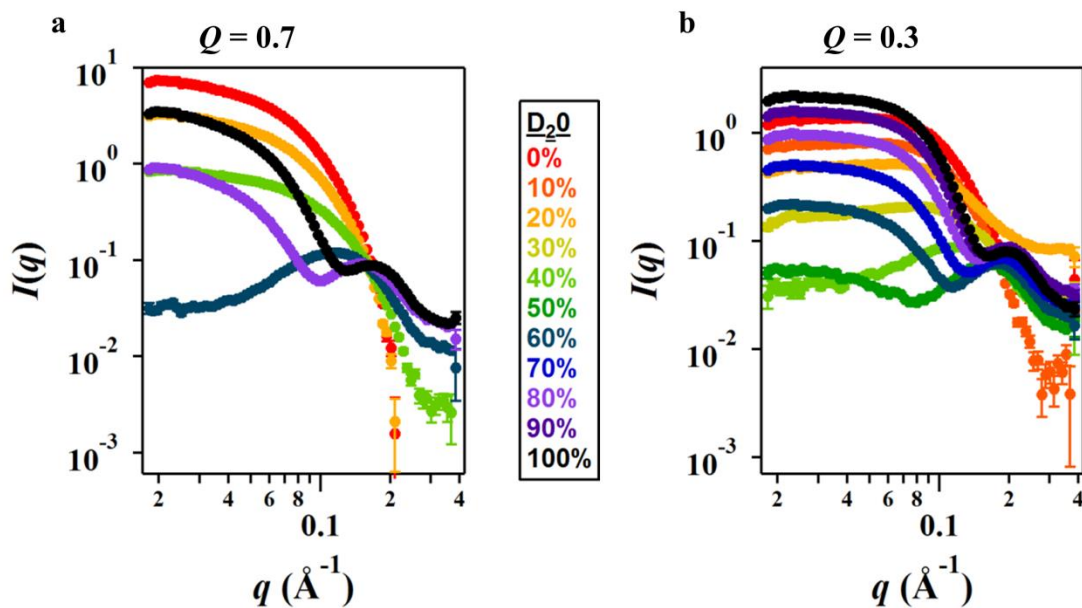


Figure 5.5 Contrast variation data for bicelles at increased temperature (40°C). **a.** Neutron scattering contrast variation data for DMPC-D54:DHPC bicelles at $Q = 0.7$ and 6% w/v at 40°C with incremental changes in D_2O buffer composition colored according to legend. **b.** Neutron scattering contrast variation data for DMPC-D54:DHPC bicelles at $Q = 0.3$ and 6% w/v at 40°C with D_2O content indicated by the same coloring scheme.

Contrast point (%D ₂ O)	$Q = 0.7$		$Q = 0.3$	
	$I(0)$	R_g (Å)	$I(0)$	R_g (Å)
0%	8.20	27.6	1.4	5.9
10%	--	--	0.87	9.1
20%	3.35	22.3	0.12	3.2
30%	--	--	0.05	3.5
40%	0.85	16.8	0.13	8.0
50%	--	--	ND*	ND*
60%	ND*	ND*	0.24	21.0
70%	--	--	0.54	17.4
80%	1.11	37.5	1.02	15.6
90%	--	--	1.66	14.7
100%	4.12	34.5	2.27	13.8

Table 5.4 Measured $I(0)$ and R_g from Guinier analysis of contrast series data at increased temperature (40°C). Weak scattering observed near solvent match points at 60% in the $Q = 0.7$ sample and 50% in the $Q = 0.3$ sample prevented successful Guinier analysis (indicated by ND). A decrease in scattering intensity approaching zero-scattering angle also prevents an accurate determination of the radius of gyration for $Q = 0.3$ samples at low D₂O concentrations, however best approximations are given. Dashes indicate that scattering at the given contrast point was not measured due to sample and beamtime constraints.

5.3.4 Effects of concentration

Lipid-detergent mixtures were also recorded at more dilute concentrations of total amphiphile (1.5 % w/v) to determine the presence of any concentration-dependent effects on the observed scattering (Figure 5.6). If the aggregate structure remains unchanged, and only the concentration of aggregate structures is affected, then the resulting scattering profiles should be directly proportional (and offset by a factor of their dilution). The forward scattering intensity $I(0)$ is also directly proportional to concentration under these same assumptions. Contrast match points and scattering length densities of components are independent of concentration, as long as the ratio of detergent and lipid molecules in the aggregate structure remains unchanged.

A Guinier analysis was performed on these scattering profiles to approximate $I(0)$ and R_g where possible (Table 5.5). Since a dilution factor of four was used, measured values for $I(0)$ at a concentration of 1.5 % w/v should be one-quarter of the measured values at 6% w/v (Table 5.3). In both cases ($Q = 0.3$ and 0.7), measured values at the dilute concentration are higher than expected, except perhaps the D₂O-free condition for $Q = 0.7$. If aggregate structures are maintained under dilute conditions, no changes should be observed in measured radii of gyration. However, measured R_g values are greater, indicating an increase in size of the aggregate structures formed, at more dilute conditions. This observation is consistent with the observations from fluorescence spectroscopy mentioned previously (section 5.2.2). The $I(0)$ proportionality assumes that aggregate size and lipid-detergent ratio remain constant, which is incorrect according to the comparison of measured R_g values. Thus, measured values of $I(0)$ will also be directly proportional to aggregate size (molecular weight), which can account for the higher than

expected $I(0)$ values for larger aggregates formed at a lower total concentration of amphiphile.

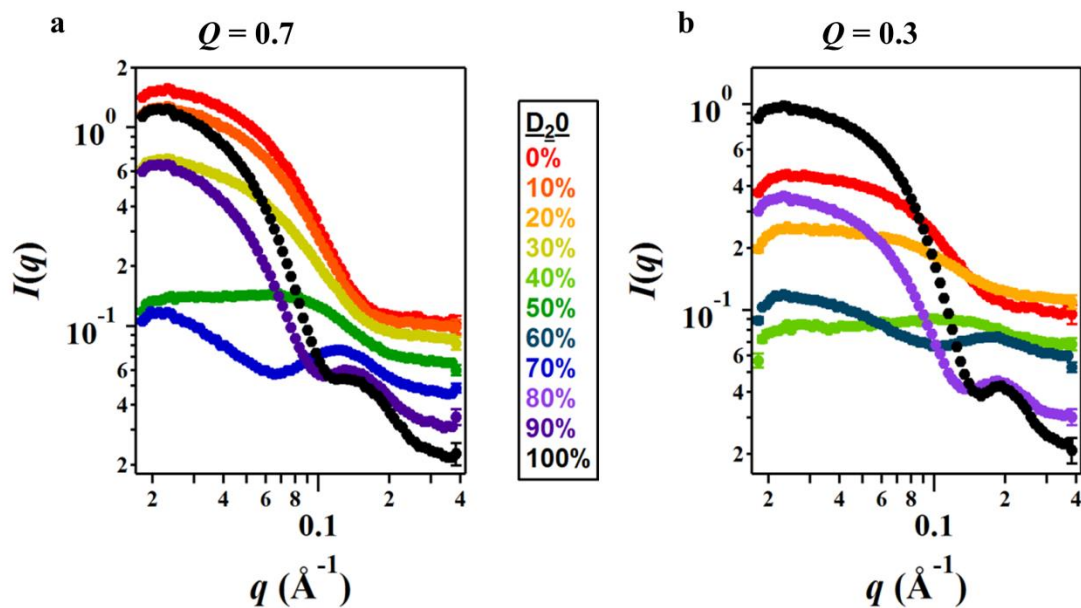


Figure 5.6 Contrast variation data for bicelles at dilute concentration (1.5% w/v). **a.** Neutron scattering contrast variation data for DMPC-D54:DHPC bicelles at $Q = 0.7$, $T = 25^\circ\text{C}$, and 1.5% w/v in buffer with incremental changes in D_2O buffer composition colored according to legend. **b.** Neutron scattering contrast variation data for DMPC-D54:DHPC bicelles at $Q = 0.3$, $T = 25^\circ\text{C}$, and 1.5% w/v with D_2O content indicated by the same coloring scheme.

Contrast point (%D ₂ O)	$Q = 0.7$		$Q = 0.3$	
	$I(0)$	R_g (Å)	$I(0)$	R_g (Å)
0%	1.71	24.1	0.47	14.3
10%	1.38	24.1	--	--
20%	--	--	0.25	9.8
30%	0.72	21.4	--	--
40%	--	--	0.10*	4.0*
50%	0.17*	9.5*	--	--
60%	--	--	ND	ND
70%	0.09*	6.4*	--	--
80%	--	--	0.39	22.6
90%	0.80	34.8	--	--
100%	1.51	34.3	1.06	22.3

Table 5.5 Measured $I(0)$ and R_g from Guinier analysis of contrast series data at dilute conditions (1.5 % w/v). Weak scattering observed near solvent match points at 50 and 70% in the $Q = 0.7$ sample and 40 and 60% in the $Q = 0.3$ sample prevented successful Guinier analysis (indicated by ND or asterisks). However, best approximations were given where possible. Dashes indicate that scattering at the given contrast point was not measured due to sample and beamtime limitations.

5.4 Concluding remarks and future directions

Based on a preliminary analysis of the scattering data collected from lipid-detergent mixtures, a few predictions can be made about the aggregate structures formed in the detergent-rich regime ($Q = 0.1 - 1.0$). First, these mixtures form aggregates whose size and shape are dependent on lipid-detergent ratio up to ~ 0.5 , but remains mostly uniform at the higher ratios studied. A bicelle-like structure with lipid bilayer arrangement does not appear to be formed until above this transition at ratios above ~ 0.5 , as indicated by the position of the second maximum in the SAXS profiles corresponding to the dominant micelle/bicelle thickness. These results contradict common assumptions in the literature that the bicelle-like architecture extends well into the detergent-rich regime (13, 14), and suggest the formation of aggregates with a more mixed micelle-like structure. Neutron scattering data support these observations of aggregate structures, and reveal structural differences between lipid-detergent ratios of 0.7 and 0.3 (above and below the mixed micelle/bicelle transition). Additionally, the degree of mixing between core and rim regions can be more rigorously investigated by extracting basic scattering functions for each component, but requires a more precise determination of contrast match points and characterization of overall aggregate sizes and shapes.

Thus far, our interpretation has considered the two scattering components to be the entire lipid molecule containing deuterated tails and the entire detergent containing non-deuterated tails. However, these two molecules can be further split into head group and tail regions. Fortunately, the head groups of the lipid and detergent are identical and can be treated similarly, reducing the total number of components to three. Although defining three scattering components instead of two complicates interpretation of the

contrast series and match points, this separation of head group and tail regions more accurately describes the aggregate core-shell structure and may be necessary to resolve potential segregation of lipid and detergent tails as expected in the bicelle model.

The lack of bicelle structure and lipid bilayer-like arrangement at $Q < 0.5$ has interesting implications for studies performed in this detergent-rich regime. Enhanced protein stability reported in these mixtures was proposed to be a result of the more native-like bilayer arrangement of lipids. However, another possible explanation is that specific lipids, or properties of the aggregate assembly not yet understood, may promote protein activity and stability. For example, Smr (*Staphylococcal* multidrug-resistance) protein was studied in a variety of membrane mimic environments, but supported ligand binding only in DDM micelles (with partial binding observed in DM micelles) and DMPC/DHPC bicelles between $Q = 0.25$ and 0.5 (15). NMR spectra of similar quality and identifiable peaks were also collected in these conditions; while spectra collected in less stabilizing detergents (LPPG and DPC) appear unable to support the native, functional fold. These results have also been discussed in a few reviews on the topic (13, 16, 17). This improved stability may simply be attributed to a better matching of the protein's hydrophobic transmembrane region and the hydrophobic core of the membrane mimic. The thickness of DM and DDM micelles is about 37.5 and 40 Å, respectively. The thickness observed for low Q lipid-detergent mixtures is similar to these micelle thicknesses, and thus produce similar activity.

Another similar protein involved in multidrug resistance EmrE, demonstrated a similar sensitivity to its surrounding environment (18). In this study by Morrison and Henzler-Wildman, reconstitution methods for EmrE into $Q = 0.33$ bicelles were

compared using either detergent exchange or via addition of detergent to liposomes. Long-term stability and NMR spectra were much improved using reconstitution from liposomes, which the authors attribute to maintaining a more native-like environment during preparation. However, other possible explanations include the kinetic “trapping” of a lipid bilayer-like arrangement or incomplete removal of detergent during the detergent exchange method, leading to a difference between final mimic structures. Further systematic investigations are needed to determine the factors that stabilize the functional protein fold, and the effects of lipid-detergent environments on protein structure. Additionally, more information is needed about the structures formed by these detergent-rich mixtures.

5.5 Materials and methods

5.5.1 Sample preparation

The detergent 1,2-dihexanoyl-*sn*-glycero-3-phosphocholine (06:0 PC, DHPC) and lipids 1,2-dimyristoyl-*sn*-glycero-3-phosphocholine (14:0 PC, DMPC) and 1,2-dimyristoyl-d54-*sn*-glycero-3-phosphocholine (14:0 PC-d54, DMPC-D54) were purchased from Avanti Polar Lipids. DMPC-D54 contains deuterated alkyl chain tails. Physical properties of these amphiphiles used for interpretation of the scattering data are provided in Table 5.1. Deuterium oxide (D₂O) was purchased from Cambridge Isotope Labs and all other chemicals were obtained from Fisher, unless otherwise noted.

Bicelle formulations of DMPC-D54:DHPC were prepared by resuspending the dry deuterated-tail lipids with phosphate buffer containing DHPC to a total amphiphile concentration of 6% w/v. Two ratios of lipid:detergent (Q) were used: 0.7 and 0.3.

Freeze-thaw cycles were performed until solutions were clear at room temperature. Each sample was divided and dialysis (3,500 MWCO) was performed using phosphate buffer containing 7 mM DHPC and either 99% D₂O or water, and post-exchange buffer reserved for matched buffer subtraction. These solutions were diluted with the same buffer to produce additional samples at a total amphiphile concentration of 1.5% w/v. Intermediate ratios of D₂O/H₂O needed for contrast variation were prepared by mixing samples or buffers from dialysis under either condition. Final buffers for all samples consisted of 10 mM phosphate buffer, pH 6.6, and ratio of H₂O/D₂O adjusted as required for contrast variation.

5.5.2 SAXS data collection

SAXS data were measured at the XOR/BESSRC undulator beam line 12-ID of the Advanced Photon Source (Argonne, IL), with a sample to detector distance of 2 m and a Pilatus 2M detector. The data were collected using a custom-made sample holder and an X-ray energy of 12 keV (corresponding to a wavelength of $\lambda = 1 \text{ \AA}$). Using a detector offset from the incident beam, the useable range of momentum transfer q was $0.0053 < q < 0.59 \text{ \AA}^{-1}$.

5.5.3 SANS data collection

SANS data were measured at the Center for Structural Molecular Biology (CSMB) on instrument CG-3 Bio-SANS in the High Flux Isotope Reactor (HFIR) facility of Oak Ridge National Laboratory (ORNL; Oak Ridge, TN). A $1 \times 1 \text{ m}^2$ 2-D linear position-sensitive detector with 192×256 pixel resolution and neutron wavelength of 6 \AA was used with a sample to detector distance of 1.7 m. Data were collected at 25 and 40 °C

using a custom-made sample holder for 1 mm quartz banjo cells. Exposure times ranged from 300 to 12000 sec based on the concentration and solvent D₂O content. The usable q -range was 0.018 to 0.43 Å⁻¹.

5.5.4 Contrast variation experiments

Sizes and shapes of lipid-detergent assemblies were determined from Guinier analysis, position of second maximum, and core-shell model fits to the scattering profiles as previously described. Contrast variation experiments were planned and interpreted using ModULes for the analysis of Contrast variation data (MULCh) (19). These modules include three specific applications: *Contrast*, *Rg*, and *COMPOST*. *Contrast* is used to determine the contrast (or “scattering power” relative to the solvent) for each subunit in the complex at different fractions of solvent D₂O. *Rg* is used to determine the dependence of the radius of gyration on contrast, allowing the R_g of each subunit, as well as their distance of separation, to be determined. *COMPOST* is used to extract the basic scattering functions corresponding to each subunit and a cross-term between the two from all scattering profiles in the contrast series.

5.6 References

1. le Maire, M., P. Champeil, and J. V. Møller. 2000. Interaction of membrane proteins and lipids with solubilizing detergents. *Biochimica et Biophysica Acta (BBA)-Biomembranes* 1508:86-111.
2. Tanford, C. 1980. *The hydrophobic effect: Formation of micelles and biological membranes* 2d ed editors J. Wiley.

3. Gabriel, N. E., and M. F. Roberts. 1984. Spontaneous formation of stable unilamellar vesicles. *Biochemistry* 23:4011-4015.
4. Sanders II, C. R., B. J. Hare, K. P. Howard, and J. H. Prestegard. 1994. Magnetically-oriented phospholipid micelles as a tool for the study of membrane-associated molecules. *Progress in Nuclear Magnetic Resonance Spectroscopy* 26:421-444.
5. Glover, K. J., J. A. Whiles, G. Wu, N.-j. Yu, R. Deems, J. O. Struppe, R. E. Stark, E. A. Komives, and R. R. Vold. 2001. Structural evaluation of phospholipid bicelles for solution-state studies of membrane-associated biomolecules. *Biophysical Journal* 81:2163-2171.
6. Triba, M. N., D. E. Warschawski, and P. F. Devaux. 2005. Reinvestigation by phosphorus nmr of lipid distribution in bicelles. *Biophysical Journal* 88:1887-1901.
7. Bian, J., and M. F. Roberts. 1990. Phase separation in short-chain lecithin/gel-state long chain lecithin aggregates. *Biochemistry* 29:7928-7935.
8. Sanders, C. R., and J. P. Schwonek. 1992. Characterization of magnetically orientable bilayers in mixtures of dihexanoylphosphatidylcholine and dimyristoylphosphatidylcholine by solid-state nmr. *Biochemistry* 31:8898-8905.
9. van Dam, L., G. Karlsson, and K. Edwards. 2004. Direct observation and characterization of dmPC/dhPC aggregates under conditions relevant for biological solution nmr. *Biochimica et Biophysica Acta (BBA)-Biomembranes* 1664:241-256.

10. Lipfert, J., L. Columbus, V. B. Chu, S. A. Lesley, and S. Doniach. 2007. Size and shape of detergent micelles determined by small-angle x-ray scattering. *The Journal of Physical Chemistry B* 111:12427-12438.
11. Ibel, K., and H. Stuhrmann. 1975. Comparison of neutron and x-ray scattering of dilute myoglobin solutions. *Journal of molecular biology* 93:255-265.
12. Olah, G. A., S. E. Rokop, C.-L. A. Wang, S. L. Blechner, and J. Trewella. 1994. Troponin i encompasses an extended troponin c in the Ca^{2+} -bound complex: A small-angle x-ray and neutron scattering study. *Biochemistry* 33:8233-8239.
13. Poget, S. F., and M. E. Girvin. 2007. Solution nmr of membrane proteins in bilayer mimics: Small is beautiful, but sometimes bigger is better. *Biochimica et Biophysica Acta (BBA) - Biomembranes* 1768:3098-3106.
14. Luchette, P. A., T. N. Vetman, R. S. Prosser, R. E. Hancock, M.-P. Nieh, C. J. Glinka, S. Krueger, and J. Katsaras. 2001. Morphology of fast-tumbling bicelles: A small angle neutron scattering and nmr study. *Biochimica et Biophysica Acta (BBA)-Biomembranes* 1513:83-94.
15. Poget, S. F., S. M. Cahill, and M. E. Girvin. 2007. Isotropic bicelles stabilize the functional form of a small multidrug-resistance pump for nmr structural studies. *Journal of the American Chemical Society* 129:2432-2433.
16. Prosser, R. S., F. Evanics, J. L. Kitevski, and M. S. Al-Abdul-Wahid. 2006. Current applications of bicelles in nmr studies of membrane-associated amphiphiles and proteins^{†,‡}. *Biochemistry* 45:8453-8465.
17. Sanders, C. R., and G. C. Landis. 1995. Reconstitution of membrane proteins into lipid-rich bilayered mixed micelles for nmr studies. *Biochemistry* 34:4030-4040.

18. Morrison, E. A., and K. A. Henzler-Wildman. 2012. Reconstitution of integral membrane proteins into isotropic bicelles with improved sample stability and expanded lipid composition profile. *Biochimica et Biophysica Acta (BBA) - Biomembranes* 1818:814-820.
19. Whitten, A. E., S. Cai, and J. Trehwella. 2008. Mulch: Modules for the analysis of small-angle neutron contrast variation data from biomolecular assemblies. *Journal of Applied Crystallography* 41:222-226.

Appendix I.

Table S1. Model-independent geometric properties for detergent mixtures of maltoside and phosphocholine detergents.

Detergents	[A] (mM)	[B] (mM)	X_A	Rg_{expt} (Å)	L_{expt} (Å)	N_{Aexpt}	N_{Bexpt}
DDM	0	57	0.000	32.0	40.6	0	118
DM/DDM-1	25	50	0.333	29.9	37.7	25	49
DM/DDM-2	50	50	0.500	28.5	37.0	33	33
DM/DDM-3	50	25	0.667	27.6	36.1	45	22
DM	58	0	1.000	26.7	34.3	74	0
13M	0	40	0.000	43.5	42.4	0	77
NM/13M-1	10	30	0.250	32.2	40.9	12	35
NM/13M-2	20	20	0.500	28.9	37.3	18	18
NM/13M-3	30	10	0.749	28.6	34.9	26	9
NM	46	0	1.000	24.8	30.9	24	0
14M	0	40	0.000	49.4	45.0	0	129
OM/14M-1	10	30	0.250	33.0	42.0	14	41
OM/14M-2	20	20	0.500	30.7	40.2	31	31
OM/14M-3	30	10	0.750	25.3	34.2	20	7
OM	60	0	1.000	21.5	28.0	44	0
OM	0	56	0.000	21.5	28.0	0	44
FC10/OM-1	19	38	0.333	21.6	28.2	14	28
FC10/OM-2	19	16	0.543	22.3	27.5	25	21
FC10/OM-3	25	12	0.676	21.9	27.6	29	14
FC10	59	0	1.000	25.0	28.2	33	0
DM	0	58	0.000	26.7	34.3	0	74
FC10/DM-1	7	47	0.130	25.8	33.2	9	58
FC10/DM-2	20	21	0.488	25.0	31.3	34	36
FC10/DM-3	39	21	0.650	23.9	30.4	40	21
FC10	59	0	1.000	25.0	28.2	33	0
DDM	0	57	0.000	32.0	40.6	0	118
FC10/DDM-1	18	39	0.316	28.4	37.5	30	65
FC10/DDM-2	30	29	0.508	27.3	35.2	43	42

FC10/DDM-3	39	19	0.672	26.2	33.4	50	25
FC10	59	0	1.000	25.0	28.2	33	0
OM	0	56	0.000	22.0	28.0	0	44
FC12/OM-1	19	39	0.328	23.9	31.3	12	24
FC12/OM-2	27	29	0.482	24.6	31.9	19	20
FC12/OM-3	38	3	0.927	29.2	34.0	45	4
FC12	58	0	1.000	31.8	34.4	47	0
DM	0	58	0.000	26.0	34.3	0	74
FC12/DM-1	16	46	0.258	26.3	33.5	14	40
FC12/DM-2	30	30	0.500	26.8	33.7	34	34
FC12/DM-3	38	18	0.679	27.0	33.5	35	17
FC12	59	0	1.000	31.8	34.4	47	0
DDM	0	57	0.000	32.8	40.3	0	118
FC12/DDM-1	24	59	0.289	29.3	38.1	20	50
FC12/DDM-2	31	37	0.456	28.3	37.2	31	37
FC12/DDM-3	35	28	0.556	28.6	36.5	35	28
FC12	58	0	1.000	31.8	34.4	47	0
OM	0	56	0.000	21.5	28.0	0	44
FC14/OM-1	20	39	0.339	26.1	34.1	14	27
FC14/OM-2	28	29	0.491	27.8	36.0	22	23
FC14/OM-3	18	4	0.818	45.3	39.3	56	12
FC14	58	0	1.000	46.5	42.0	78	0
DM	0	58	0.000	26.7	34.3	0	74
FC14/DM-1	28	46	0.378	28.4	36.3	20	33
FC14/DM-2	44	35	0.557	29.9	37.9	29	23
FC14/DM-3	57	23	0.713	31.6	38.5	35	14
FC14	58	0	1.000	46.5	42.0	78	0
DDM	0	57	0.000	32.0	41.0	0	118
FC14/DDM-1	26	78	0.250	31.2	39.7	17	52
FC14/DDM-2	43	59	0.422	31.9	40.0	30	42
FC14/DDM-3	65	30	0.684	33.3	40.7	41	19
FC14	58	0	1.000	46.5	42.0	75	0

[A] and [B] represent total detergent concentrations in solution. The mole fraction of detergent A comprising mixed micelles, X_A , assumes complete detergent mixing and was calculated using the total detergent concentration adjusted by the cmc for the mixed micelle. R_g was determined from Guinier analysis, L_{expt} from the position of the second peak maximum, aggregation numbers for each component according to eq 4.

Table S2. Model-independent geometric properties for detergent mixtures with LMPG.

Detergents	[A] (mM)	[B] (mM)	X_A	Rg_{expt} (Å)	L_{expt} (Å)	N_{Aexpt}	N_{Bexpt}	Ψ (mV)
DM	0	58	0.000	26.8	34.3	74	0	0
LMPG/DM-1	30	54	0.357	24.8	36.3	25	14	16.4
LMPG/DM-2	39	46	0.459	24.5	37.7	20	17	17.4
LMPG/DM-3	61	34	0.642	23.7	37.7	11	19	18.0
LMPG	54	0	1.000	27.7	39.4	0	42	20.4
DDM	0	58	0.000	33.1	41.0	118	0	0
LMPG/DDM-1	29	87	0.250	27.3	40.4	39	13	15.2
LMPG/DDM-2	60	58	0.508	24.8	40.0	17	18	17.3
LMPG/DDM-3	90	29	0.756	24.1	39.1	7	20	18.0
LMPG	54	0	1.000	27.7	39.4	0	42	20.4
FC10	0	59	0.000	25.0	28.2	33	0	0
LMPG/FC10-1	20	38	0.345	25.8	34.8	28	15	17.7
LMPG/FC10-2	28	31	0.475	25.7	36.7	23	21	18.9
LMPG/FC10-3	38	20	0.655	25.7	37.7	16	29	19.6
LMPG	54	0	1.000	27.7	39.4	0	42	20.4
FC12	0	58	0.000	31.8	34.4	47	0	0
LMPG/FC12-1	20	40	0.333	30.7	38.2	28	14	16.9
LMPG/FC12-2	39	35	0.527	28.3	37.9	16	17	17.8
LMPG/FC12-3	61	26	0.701	25.1	38.6	8	19	18.0
LMPG	54	0	1.000	27.7	39.4	0	42	20.4

[A] and [B] represent total detergent concentrations in solution. The mole fraction of detergent A comprising mixed micelles, X_A , assumes complete detergent mixing and was calculated using the total detergent concentration adjusted by the cmc for the mixed micelle. Rg was determined from Guinier analysis, L_{expt} from the position of the second peak maximum, and aggregation numbers for each component according to eq 4, and surface potential according to eq 11.

Table S3. Model-dependent geometric properties for detergent mixtures of maltoside and phosphocholine detergents.

Detergents	ρ_1 (e/Å ³)	ρ_2 (e/Å ³)	shape	a (Å)	b (Å)	t (Å)	N_A	N_B	Rg_{model} (Å)	L_{model} (Å)
DDM	0.277	0.520	oblate	15.9	28.1	5.5	0	142	30.4	36.3
DM/DDM-1	0.276	0.520	oblate	15.0	26.3	5.5	44	87	29.0	35.5
DM/DDM-2	0.275	0.520	oblate	14.4	25.7	5.5	62	62	28.2	34.3
DM/DDM-3	0.274	0.520	oblate	13.9	25.2	5.5	78	39	27.6	33.3
DM	0.273	0.520	oblate	13.2	23.1	5.5	100	0	25.5	31.9
13M	0.278	0.520	oblate	16.0	31.7	5.5	0	179	34.0	37.5
NM/13M-1	0.277	0.520	oblate	15.5	28.5	5.5	38	113	31.1	36.5
NM/13M-2	0.274	0.520	oblate	14.5	26.1	5.5	64	64	28.7	34.5
NM/13M-3	0.271	0.520	oblate	13.1	24.0	5.5	80	27	26.3	31.7
NM	0.270	0.520	oblate	11.8	21.5	5.5	85	0	23.7	29.1
14M	0.280	0.520	oblate	17.5	33.4	5.5	0	202	36.3	40.5
OM/14M-1	0.277	0.520	oblate	17.0	28.6	5.7	40	120	31.9	39.7
OM/14M-2	0.274	0.520	oblate	16.1	26.9	5.5	75	75	30.3	37.7
OM/14M-3	0.271	0.520	oblate	14.0	22.2	6.0	77	26	25.3	34
OM	0.268	0.520	oblate	11.2	18.5	5.5	66	0	21.0	27.9
OM	0.268	0.520	oblate	11.2	18.5	5.5	0	68	21.0	27.9
FC10/OM-1	0.268	0.518	oblate	10.9	19.3	4.5	22	44	21.6	26.3
FC10/OM-2	0.269	0.513	oblate	11.0	18.8	3.5	31	26	21.9	25.5
FC10/OM-3	0.270	0.505	prolate	21.7	13.1	3.3	36	17	22.1	29.5
FC10	0.273	0.490	prolate	21.0	13.4	2.9	54	0	24.3	29.7
DM	0.273	0.520	oblate	13.2	23.1	5.5	0	99	25.5	31.9
FC10/DM-1	0.273	0.517	oblate	13.1	22.3	5.1	12	80	24.9	31.3
FC10/DM-2	0.273	0.507	oblate	12.8	20.6	4.2	37	39	24.0	29.8

FC10/DM-3	0.273	0.501	oblate	12.4	20.1	3.9	47	25	23.8	28.7
FC10	0.273	0.490	prolate	21.0	13.4	2.9	54	0	24.3	29.7
DDM	0.277	0.520	oblate	15.9	28.1	5.5	0	145	31.0	37.3
FC10/DDM-1	0.276	0.511	oblate	14.8	24.6	4.6	35	75	28.3	34.2
FC10/DDM-2	0.275	0.505	oblate	14.0	23.4	4.0	48	47	27.8	32.0
FC10/DDM-3	0.274	0.500	oblate	13.5	21.5	3.8	56	27	26.1	30.8
FC10	0.273	0.490	prolate	21.0	13.4	2.9	54	0	24.3	29.7
OM	0.268	0.520	oblate	11.2	18.5	5.5	0	68	21.0	27.9
FC12/OM-1	0.271	0.511	oblate	12.6	21.1	4.9	28	58	24.0	30.1
FC12/OM-2	0.272	0.506	oblate	13.5	21.3	4.7	44	47	24.8	31.7
FC12/OM-3	0.276	0.492	prolate	23.5	16.4	3.1	71	6	29.9	35.9
FC12	0.277	0.490	prolate	24.3	16.2	2.9	76	0	32.1	35.3
DM	0.273	0.520	oblate	13.2	23.1	5.5	0	99	25.5	31.9
FC12/DM-1	0.274	0.512	oblate	13.9	22.6	4.9	25	71	25.8	32.7
FC12/DM-2	0.275	0.505	oblate	14.0	22.5	4.2	46	46	26.5	32.2
FC12/DM-3	0.276	0.500	prolate	25.7	16.4	3.7	58	28	27.5	36.5
FC12	0.277	0.490	prolate	24.3	16.2	2.9	76	0	32.1	35.3
DDM	0.277	0.520	oblate	15.4	27.8	5.5	0	139	30.4	36.3
FC12/DDM-1	0.277	0.511	oblate	15.4	25.6	4.7	34	84	29.3	35.5
FC12/DDM-2	0.277	0.506	oblate	15.0	24.9	4.3	50	60	29.1	34.3
FC12/DDM-3	0.277	0.503	oblate	15.5	23.3	4.0	55	44	28.6	35.0
FC12	0.277	0.490	prolate	24.3	16.2	2.9	76	0	32.1	35.3
OM	0.268	0.520	oblate	11.2	18.5	5.5	0	68	21.0	27.9
FC14/OM-1	0.272	0.510	oblate	15.0	22.0	4.7	34	65	26.2	34.7
FC14/OM-2	0.274	0.505	oblate	15.1	23.3	4.2	50	52	28.2	34.4
FC14/OM-3	0.278	0.495	prolate	30.3	18.2	3.3	89	20	36.2	39.7

FC14	0.280	0.490	prolate	29.3	18.7	2.9	105	0	46.2	40.3
DM	0.273	0.520	oblate	13.2	23.1	5.5	0	99	25.5	31.9
FC14/DM-1	0.276	0.509	oblate	15.4	23.9	4.3	40	65	28.4	35.1
FC14/DM-2	0.277	0.503	oblate	15.7	24.5	3.9	59	47	30.4	35.3
FC14/DM-3	0.278	0.499	oblate	15.9	24.5	3.5	74	30	32.6	35.3
FC14	0.280	0.490	prolate	29.3	18.7	2.9	105	0	46.2	40.3
DDM	0.277	0.520	oblate	15.4	27.8	5.5	0	139	30.4	36.3
FC14/DDM-1	0.278	0.513	oblate	15.2	28.1	4.8	34	101	31.3	35.2
FC14/DDM-2	0.278	0.507	oblate	16.0	27.2	4.4	55	75	31.8	36.4
FC14/DDM-3	0.279	0.499	prolate	28.5	18.0	3.5	67	31	31.7	39.5
FC14	0.280	0.490	prolate	29.3	18.7	2.9	105	0	46.2	40.3

ρ_1 and ρ_2 are calculated electron densities for head group and tail portions of the detergent using the Tanford formula to adjust for alkyl chain length, the shape is determined by the best-fit comparison of oblate, prolate, and sphere core-shell models, a and b are dimensions of the ellipsoid having thickness t , N_A and N_B are calculated from the model according to eq 6, Rg , and L from eq 8.

Table S4. Geometric properties for detergent mixtures with LMPG as determined from core-shell ellipsoid model fits to the mixed micelle SAXS profiles.

Detergents	ρ_1 (e/Å ³)	ρ_2 (e/Å ³)	shape	a (Å)	b (Å)	t (Å)	N_A	N_B	Rg_{model} (Å)	L_{model} (Å)
LMPG	0.280	0.470	oblate	15.9	24.7	6.0	0	135	29.4	37.8
DM/LMPG-1	0.277	0.488	oblate	15.9	24.4	5.8	46	83	28.7	37.6
DM/LMPG-2	0.276	0.497	oblate	15.5	24.2	5.7	67	57	28.1	36.7
DM/LMPG-3	0.275	0.502	oblate	15.9	23.8	5.7	79	44	27.9	37.5
DM	0.273	0.520	oblate	13.2	23.1	5.5	100	0	25.5	31.9
LMPG	0.280	0.470	oblate	15.9	24.7	6.0	0	135	29.4	37.8
DDM/LMPG-1	0.279	0.482	oblate	16.5	25.7	5.9	35	108	30.3	38.9
DDM/LMPG-2	0.279	0.495	oblate	16.6	26.5	5.8	72	75	30.5	39.0
DDM/LMPG-3	0.278	0.507	oblate	16.5	26.8	5.6	107	36	30.5	38.6
DDM	0.277	0.520	oblate	15.4	27.8	5.5	139	0	30.4	36.3
LMPG	0.280	0.470	oblate	15.9	24.7	6.0	0	135	29.4	37.8
FC10/LMPG-1	0.278	0.477	oblate	16.3	23.9	4.9	43	82	29.9	37.5
FC10/LMPG-2	0.276	0.480	oblate	14.8	23.5	4.4	58	53	29.2	34.0
FC10/LMPG-3	0.275	0.483	oblate	15.1	21.5	4.0	63	33	28.1	34.2
FC10	0.273	0.490	prolate	21.0	13.4	2.9	54	0	24.3	29.7
LMPG	0.280	0.470	oblate	15.9	24.7	6.0	0	135	29.4	37.8
FC12/LMPG-1	0.279	0.476	oblate	16.9	24.4	5.0	39	91	30.5	38.8
FC12/LMPG-2	0.279	0.479	oblate	16.3	24.3	4.5	57	64	30.7	37.1
FC12/LMPG-3	0.278	0.483	oblate	16.4	24.1	4.0	78	39	32.1	36.8
FC12	0.277	0.490	prolate	24.3	16.2	2.9	76	0	32.1	35.3

ρ_1 and ρ_2 are calculated electron densities for head group and tail portions of the detergent using the Tanford formula to adjust for alkyl chain length, the shape is determined by the best-fit comparison of oblate, prolate, and sphere core-shell models, a and b are dimensions of the ellipsoid having thickness t , N_A and N_B are calculated from the model according to eq 6, Rg , and L from Equ 8.

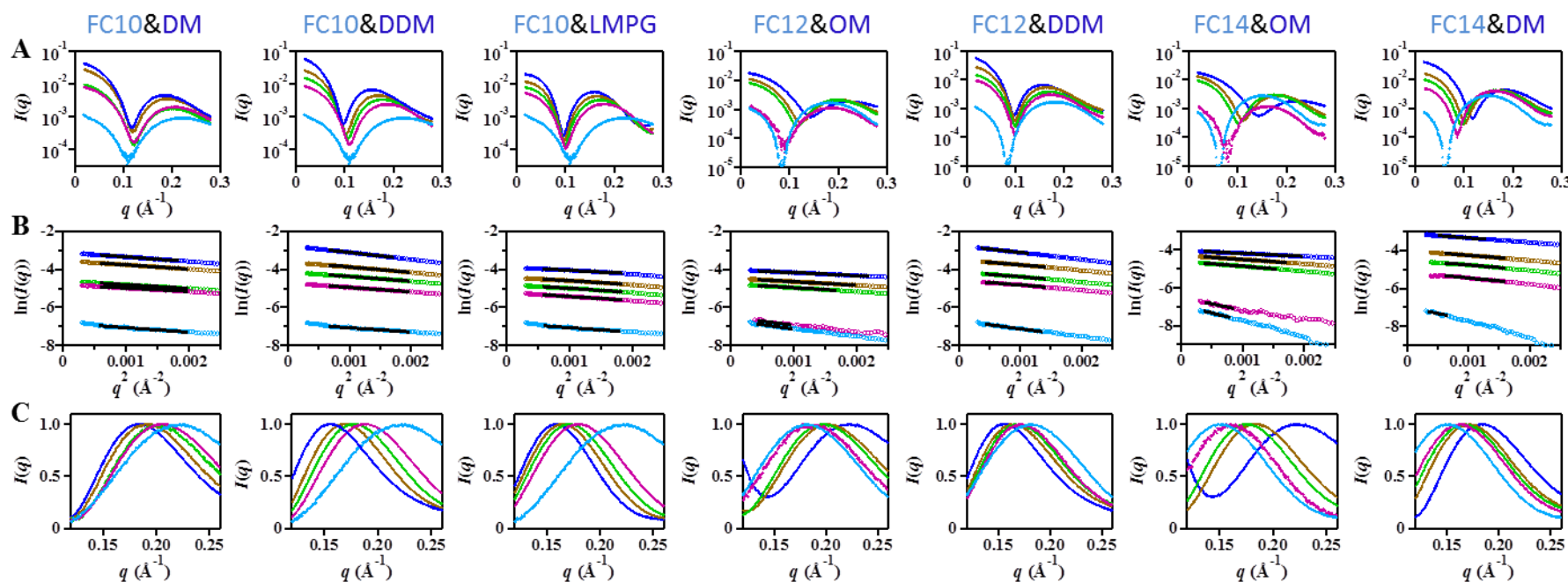


Figure S1. Small-angle X-ray scattering profiles, Guinier plots ($\ln(I)$ vs q^2) of low angle scattering, and second maxima normalized by peak height for binary detergent mixtures. A) SAXS scattering profiles of binary mixtures comprised of the two detergents listed above the plot. B) Guinier plots of the low angle scattering data shown in panel A. Linear fits are shown (black lines), and the slope of these lines was used to determine R_g . C) Normalized plots of the second maximum observed at intermediate scattering angles the maximum is used to calculate L_{expt} .

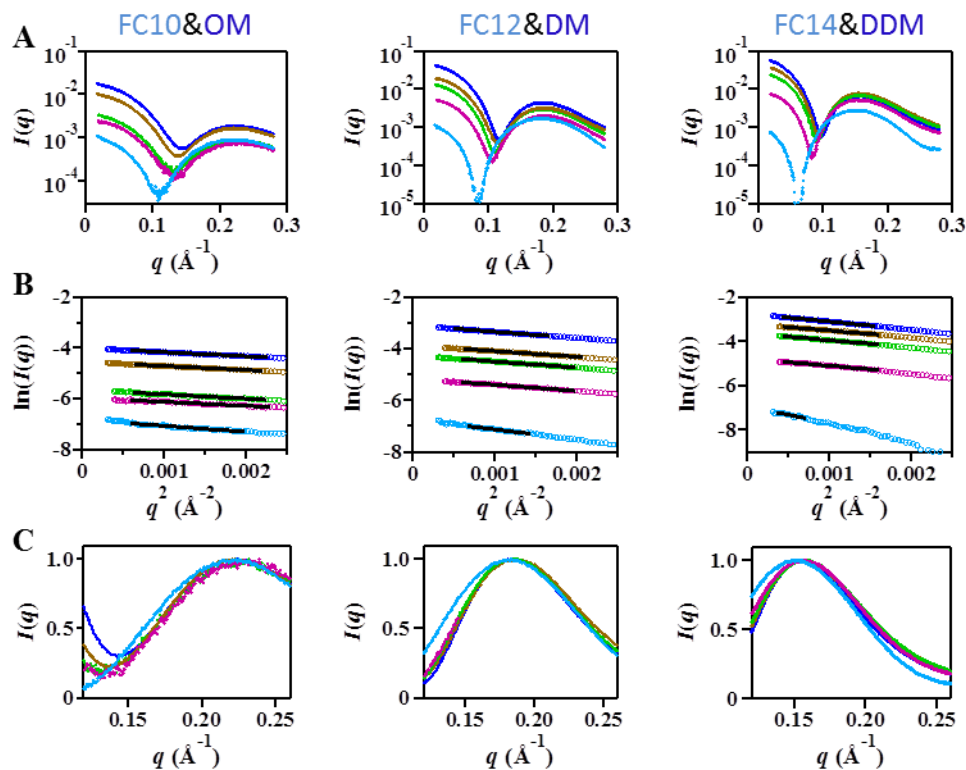


Figure S2. Small-angle X-ray scattering profiles, Guinier plots ($\ln(I)$ vs q^2) of low angle scattering, and second maxima normalized by peak height for binary mixtures. A) SAXS scattering profiles of binary mixtures comprised of the two detergents listed above the plot. B) Guinier plots of the low angle scattering data shown in panel A. Linear fits are shown (black lines), and the slope of these lines was used to determine R_g . C) Normalized plots of the second maximum observed at intermediate scattering angles the maximum is used to calculate L_{expt} .

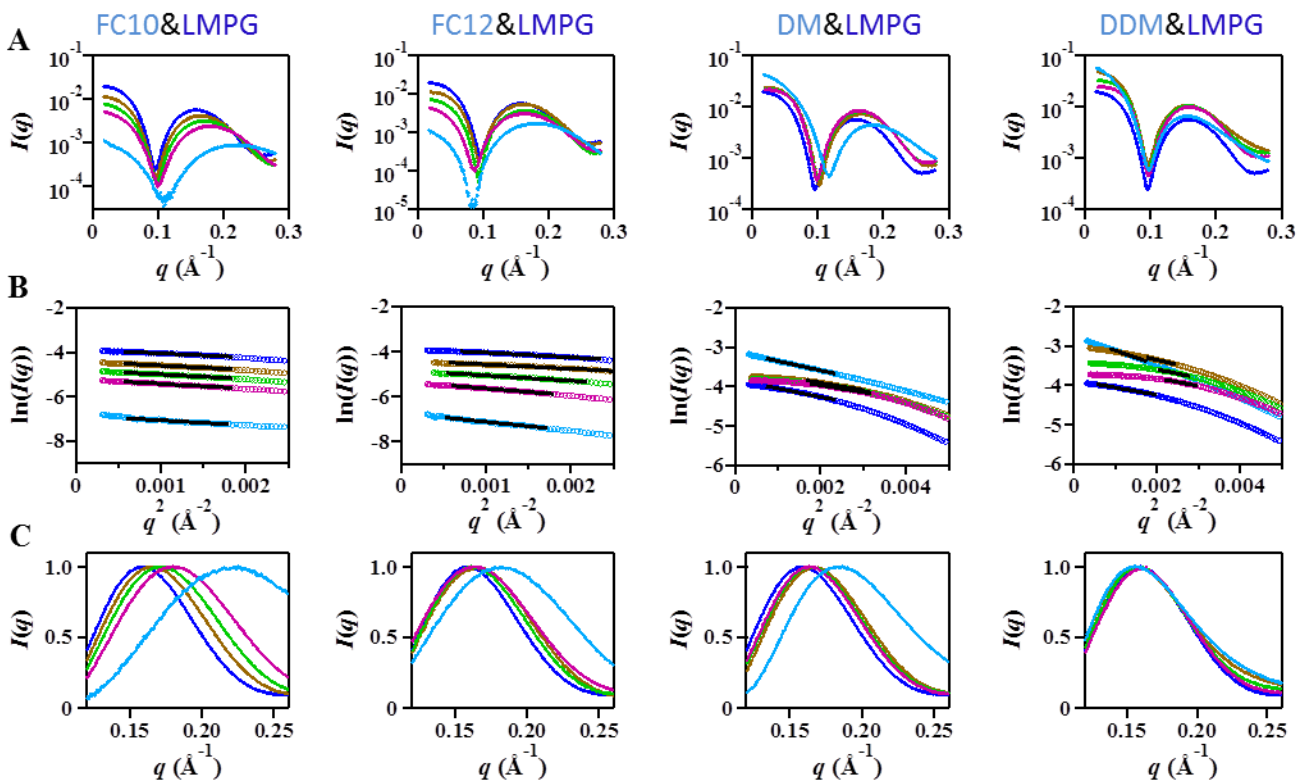


Figure S3. Small-angle X-ray scattering profiles, Guinier plots ($\ln(I)$ vs q^2) of low angle scattering, and second maxima normalized by peak height for binary mixtures. A) SAXS scattering profiles of binary mixtures comprised of the two detergents listed above the plot. B) Guinier plots of the low angle scattering data shown in panel A. Linear fits are shown (black lines), and the slope of these lines was used to determine R_g . C) Normalized plots of the second maximum observed at intermediate scattering angles the maximum is used to calculate L_{expt} .